Sedimentology, Ichnology and Biogenic Permeability of the upper Montney Formation, northeast British Columbia

by

Aimée Elizabeth Gegolick

A thesis submitted in partial fulfillment of the requirements for the degree of

Master of Science

Department of Earth and Atmospheric Science
University of Alberta

© Aimée Elizabeth Gegolick, 2017

ABSTRACT

The upper Montney Formation is a tight gas reservoir that consists of silt and very fine-grained sandstone in its entirety. Despite its limited variation in grain-size, this formation is highly heterogeneous and the distribution of facies is complex, both vertically and laterally. Subtle changes in characteristics affect reservoir properties, resulting in compartmentalization of resources. These changes include frequently interbedded facies and sporadically distributed bioturbation. A detailed analysis of the subsurface reservoir was conducted in order to provide insight into these subtle heterogeneities.

Fourteen cores within the upper Montney Formation of northeast British Columbia were studied in order to interpret depositional processes and assess bioturbated fabrics and their relationship with permeability and porosity. Five facies were identified, representing deposition within the distal offshore to offshore transition zone. Sediment was sourced from low-density turbidity currents. Varying velocity within the boundary layer of turbulent flow was likely the mechanism for the physical separation of coarser and finer silt components. This mechanical separation resulted in the development of pinstripe laminae that dominate the formation.

Permeability was assessed with a Core Laboratories Pressure Decay Profile Permeameter (PDPK-400) to characterize the effects of bioturbation on permeability and assess its utility for fine-grained rocks. Spot permeametry provides the most discrete measurement that can be obtained and the bulk permeability provides a representative value for a given fabric. Results from the permeability testing demonstrate that pervasively bioturbated fabrics locally enhance permeability relative to non-biotubated fabrics. Bioturbation needs to be pervasive in order to significantly adjust pore aperture sizes. Permeability anisotropy was tested, however, spot-permeametry is unable to characterize anisotropy and the results were repeatedly more homogenous vertically.

PREFACE

This thesis is an original work by Aimée Elizabeth Gegolick. No part of this thesis has been previously published.

DEDICATION

This work is dedicated to my best friend, my partner in crime, and the love of my life Tim Barnett.

You are my rock.

ACKNOWLEDGEMENTS

Five years ago, I joined the Ichnology Research Group at the University of Alberta. Being part of this group has provided me with so many opportunities and I am grateful for all the people that have been part of my journey as an undergraduate and a graduate student. Firstly, I cannot thank Dr. J.P. Zonneveld enough for all of his support for the several years we have known each other. I am grateful for the numerous opportunities for field research, and wouldn't have had so many experiences if it weren't for you. Not only have you been a remarkable mentor, but also you have become a friend. Thank you Dr. Murray Gingras for your guidance and expertise relating to permeability and many other things. Thank you for your patience and understanding during my panicked moments. Thank you Dr. Jeff Kavanaugh for being part of my defending committee. A final thanks to Dr Nikrityuk for additional help relating to permeability.

Thank you Shivangi Sharma (Shay) for all your help with the permeability data. You went above and beyond in every way. You are incredibly smart and you amaze me with the magic you perform on computers. I couldn't have done this without you and your encouragement was always enlightening. I would like to thank Scott Botterill for his kindness and patience as he endured many painful hours with early versions of my writing. You are a great friend and a role model for chasing your dreams. Carolyn Furlong, where do I begin? We've been through a lot, and have shared so many experiences. The joys of Fort St. John (Roustabouts) with some killer playlists and endless amounts of siltstone. You've been my go-to for so many of my problems and concerns, discussions, tears of joy and your advice is invaluable. As well as other members of the IRG for all having positively influenced my last three years: Eric Timmer, Dave Herbers, Donald Prenoslo, Patricia Gonzalez Hernandez, Derek Hayes, Brette Harris, Calla Knudson, Olga Kovalchuck, Maya LaGrange, Reed Myers, Tiffany Playter, Alina Shchepetkina, Nabilah Adani, and Matthew Sommers.

From the Department of Earth and Atmospheric Sciences at the University of Alberta I would like to thank Mark Labbe for all of his time and effort for working with the permeameter. Also Igor Jakab for answering many questions and always printing posters on short notice. Thank you Shyra Craig for always being a friendly face and being there for me.

I'd like to thank Ryan Olson, Sung-Eun Kim and John Ross from the British Columbia Oil and Gas Commission. You were incredibly kind, helpful and accommodating during many weeks of core logging.

I would like to sincerely thank the following companies for financial assistance: Birchcliff Energy Ltd., Canbriam Energy Inc., Progress Energy Canada Ltd., Sasol Canada, Shell Canada Ltd., and TAQA North Ltd. I would like to acknowledge the following individuals for their additional support and guidance throughout my research endeavours: from Sasol: John Cole and Craig Smith; from Progress Energy: Gerald Nyberg, Wayne Hovdebo, Stavros Michailides and Audrey Whitlock; and finally David Kelly from Canbriam.

Lastly I would like to thank my parents Ward and Sheelagh. I am thankful for your never-ending love, support and encouragement during university and providing the foundation to reach this academic level. I am grateful to move on to the next chapter with a strong education behind me. Thank you Tim for graciously handling everyday life with me. Your positivity, charisma, and humour kept me going everyday. No matter what, you made me smile and laugh everyday. You have been a constant source of support and encouragement during all my challenges as a grad student. You never let me give up on myself and I couldn't have done this without you.

TABLE OF CONTENTS

CHAPTER 1: INTRODUCTION 1

CHAPTER 2: FACIES DESCRIPTIONS AND INTERPRETATIONS OF THE UPPER MONTNEY FORMATION, NORTHEAST BRITISH COLUMBIA 5

2.1 Introduction 5
2.2 Previous work 6
2.3 Tectonic Setting 7
2.4 Stratigraphic Framework 10
2.5 Palaeoenvironmental Setting 11
2.6 Age of the Montney 13
2.7 Project Area 14
2.8 Upper Montney 15
2.9 Methods 16
2.9.1 Core Analysis 16
2.10 Results and Interpretations 17
2.10.1 Facies 1 (F1): Pinstripe laminated siltstone 17
Description 17
Interpretation 18
2.10.2 Facies 2 (F2): Pinstriped and rippled laminated siltstone 19
Description 19
Interpretation 20
2.10.3 Facies 3 (F3): Calcite cemented concretions and beds 22
Description 22
Interpretation 22
2.10.4 Facies 4 (F4): Bioclastic packstone beds 23
Description 23
Interpretation 23
2.10.5 Facies 5 (F5): Bioturbated siltstone 24
Description 24
Interpretation 25
2.11 Discussion 39
2.11.1 Deposition of the Upper Montney and Significance of the Pinstripe Laminae 39
2.11.2 Sequence Stratigraphy 45
2.12 Conclusions 48

CHAPTER 3: THE RELATIONSHIP BETWEEN BIOTURBATION AND PERMEABILITY IN FINE-GRAINED DEPOSITS, AN EXAMPLE FROM THE UPPER MONTNEY FORMATION, NORTHEAST BRITISH COLUMBIA 49
3.1 Introduction 49
3.2 Background 50
3.3 Previous Research 51
3.4 Methods 52
3.4.1 Facies Selection 52
3.4.2 Spot-Permeametry 55
3.4.3 Scoring Permeability Matrices – Vertical and Horizontal 56
3.4.4 Bulk Permeability – Double Integral Technique 57
3.4.5 Global Matrix 57
3.4.6 High-Pressure Mercury Injection Porosimetry 58
3.5 Results and Discussion 59
3.5.1 Spot permeability 59
3.5.2 Scoring Matrices 65
3.5.3 Bulk Permeability and Relationship to Core Data 68
3.5.4 Global Matrix 70
3.5.5 High Pressure Mercury Injection Porosimetry 71
3.6 Conclusions 74
CHAPTER 4: SUMMARY AND CONCLUSIONS 75
REFERENCES 77
APPENDIX I – BIOTURBATION INDEX 87
APPENDIX II – DOUBLE INTEGRAL SAMPLE CALCULATION FOR SAMPLE 4 88
APPENDIX IV – LITHOLOGY LOGS OF CORED INTERVALS 90

LIST OF FIGURES

Figure 1.1: Study area map 3
Figure 1.2: Representative lithology log of the upper Montney Fm 3
Figure 2.1: Map of the PRB 9
Figure 2.2: Lithostratigraphic divisions 11
Figure 2.3: Palaeogeographic map 13
Figure 2.4: Study area 15
Figure 2.5: Montney subdivisions 16
Figure 2.6: Facies 1A 27
Figure 2.7: Facies 1B 27
Figure 2.8: Facies 1C. 30
Figure 2.9: Facies 2A 30
Figure 2.10: Facies 2B 33
Figure 2.11: Facies 2C 33
Figure 2.12: Facies 3 36
Figure 2.13: Facies 4 36
Figure 2.14: Facies 5 39
Figure 2.15: Depositional model 41
Figure 2.16: Example silt turbidites 43
Figure 2.17: Representative lithology log of the well d-48-A/94-B-9 45
Figure 2.18: Cross section 48
Figure 3.1: Litholog of the core d-66-I/94-B-16 53
Figure 3.2: PDPK – 400. 56
Figure 3.3: Scoring matrix example. 57
Figure 3.4: Global matrix schematic 58
Figure 3.5: Hg-injection samples 59
Figure 3.6: Spot permeability samples and results 59
Figure 3.7: Box and whisker graph 64
Figure 3.8 Vertical and horizontal permeability 67
Figure 3.9: Addition scoring matrix test 68
Figure 3.10: PDPK-400 and core data 69
Figure 3.11: Permeability ranges. 70
Figure 3.12: Global matrix results. 71
Figure 3.13: Hg-injection results. 72

LIST OF TABLES

Table 2.1: Summary table of wells with upper Montney core logged for the study 16
Table 2.2: Summary of facies 25
Table 3.1: Summary table of the samples for high-pressure mercury injection..... 59
Table 3.2: Summary of spot-permeability samples arranged by depth. 64
Table 3.3: Summary table of the score matrices 66

CHAPTER 1: INTRODUCTION

Energy demand is poised to rise in the upcoming decades with developing countries such as China, India, Malaysia and Indonesia requiring ever increasing petroleum imports to fuel their expanding economies. A major part of this energy solution will be found in the clean and prolific natural gas resources found within unconventional reservoirs that occur in tight siltstone and shale successions. The Montney Formation ('Montney') of northeast British Columbia is a world-class unconventional hydrocarbon reservoir where the resource occurs within tight siltstone, and to a lesser extent, very fine-grained sandstone. However, exploitation of unconventional tight reservoirs has not been without environmental scrutiny as a result of hydraulic fracturing ('fracking') consuming large amounts of freshwater resources. It is becoming increasingly important to characterize the Montney reservoirs and develop predictive models. These models will result in decreased risk in exploration and will allow higher resolution well pad planning and spacing. Properly placed horizontal wells will require fewer hydraulic fractures and will allow maximum hydrocarbon recovery while reducing the overall environmental footprint. Improved exploration practices in this major unconventional gas play are crucial to maintain and develop Western Canada as a leader in environmentally responsible resource exploration.

Over the past decade, advances in horizontal drilling and multistage hydraulic fracturing made it possible to exploit hydrocarbons from this unconventional siltstone reservoir (National Energy Board et al., 2013). As a result, British Columbia has become a leading province in the exploration and development of unconventional gas resources (Hayes, 2012). The Montney Formation is the foremost gas-producing formation in British Columbia and is estimated to house 449 tcf of marketable natural gas along with high volumes of gas liquids and condensate (National Energy Board et al., 2013). Despite the relatively restricted grain-sizes, the sedimentary facies of the Montney are very heterogeneous. This refers to the several sedimentological and ichnological factors that result in variability in reservoir characteristics, particularly porosity and permeability. Subtle changes in the rock fabric both laterally and vertically results in the compartmentalization of resources within zones of distinctly different porosity and permeability values.

Another factor affecting reservoir properties is the effect of bioturbation. The variation and distribution and its effects have not been extensively studied to date, and thus the goal of this study is to quantify these effects. Biogenic permeability has the ability to either enhance or reduce permeability or porosity (Gingras et al., 2012; Baniak et al., 2015). Bioturbation can influence the porosity and permeability by changing the distribution of grains and affect the geochemistry, thus altering diagenetic processes (Gingras et al., 2012). The restriction of grain size within the Montney adds additional interest since there is little variation between the trace fossils and the surrounding rock. Trace fossils in the Montney Formation also provide invaluable information

about biota during the recovery interval after the end-Permian mass extinction and palaeoenvironmental conditions (Zonneveld, 2011a).

This study focuses on the sedimentology and ichnology of the upper Montney Formation in northeast British Columbia. This area is within the Townships 82 to 84, between Ranges 24W6 to 26W6, and includes areas on NTS 094A and 094B. This area is commonly referred to as the Northern Montney within the Montney Play Trend and is part of the dry gas fairway (OGC Report, 2011). Upper Montney cores from fourteen wells have been described in detail and provide the primary data for this project. The cores are from natural gas producing pools such as Farrell Creek, Graham/Altares, Blueberry and Cypress. The Montney extending into this northern region has not been extensively studied and facies predictions in relation to the rest of the basin are not well understood (Figure 1.1).

Chapter 2 provides detailed background information associated with the Montney Formation. An extensive literary review summarizes previous work including the tectonic setting, the stratigraphic framework, palaeoenvironmental conditions and dating the Montney Formation. The lithostratigraphic framework defined within British Columbia is used in this study. Detailed examination of core focussed on grain size, physical and biogenic structures, and provided the fundamental information for the development of five facies (Figure 1.2). The study area described in Chapter 2 is referenced in Chapter 3 and all the cores examined within the study are found within this area.

Chapter 3 focuses on the utility of a spot-permeameter (PDPK-400) in fine-grained reservoirs and its use for measuring small-scale heterogeneities relating to varying degrees of laminated, rippled, and bioturbated fabrics. Eleven samples were chosen from an upper Montney core (d-66-I/94-B-16) and permeability measurements were obtained in a grid pattern across the surface of the core. A new technique was designed to characterize permeability anisotropy. The spot-permeameter provides the most discrete measurement that can be obtained and the grid method is successful at characterizing bulk-permeability for a given fabric. However, is it unable to effectively characterize anisotropy as the order in which points were measured influenced the results.

In summary, this thesis aims to characterize the upper Montney Formation in northeast British Columbia. The data obtained within this study will help expand the overall understanding of the subtle heterogeneities observed in the upper Montney Formation. As well it will provide a greater understanding of the use of a spot-permeameter and its effectiveness and limitations within this fine-grained reservoir.

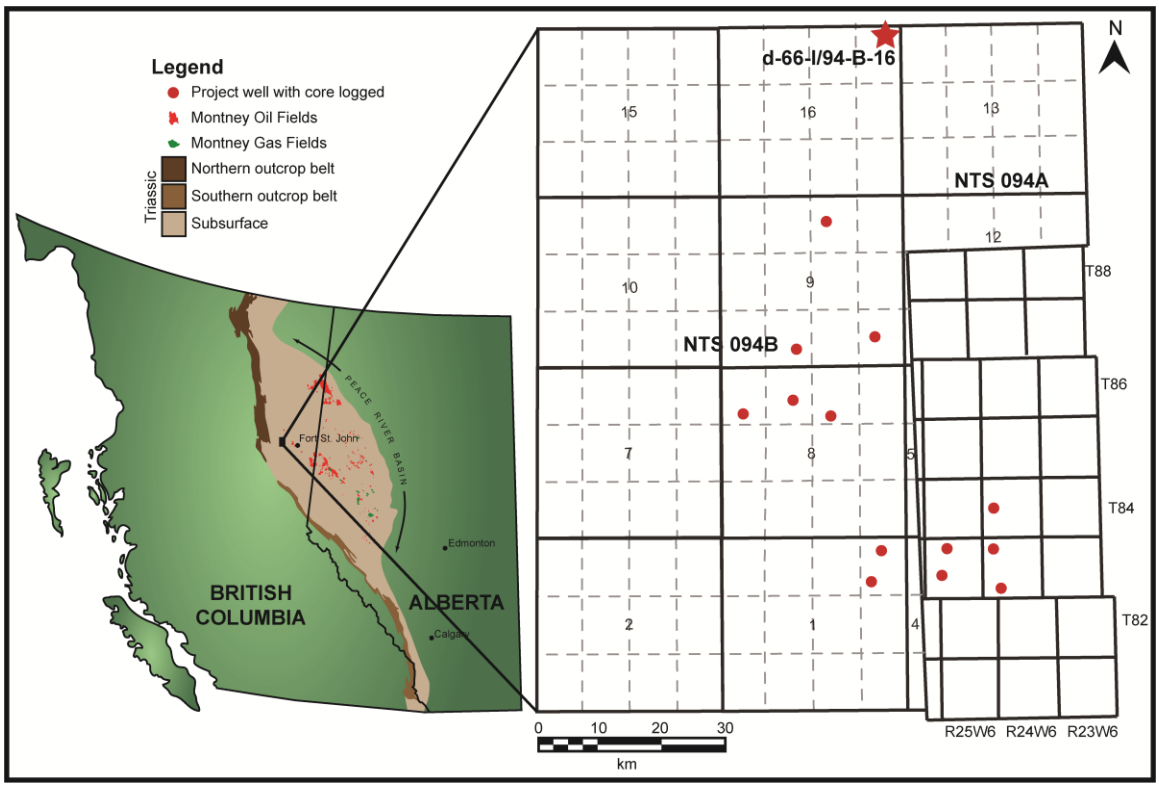

Figure 1.1: The study area is located in northeast British Columbia and the red dots represent the wells logged for this study. The smaller map indicates the extent of the Montney Formation within the Peace River Basin (modified from Zonneveld, 2011b).

Figure 1.2 (next page): Representative lithology log of the upper Montney Formation, well d-66-I/94-B-16. This well is a complete section of the upper Montney from the Smithian-Spathian Boundary to the base of the Anisian wedge. Samples from this well were used for spot-permeametry analysis.

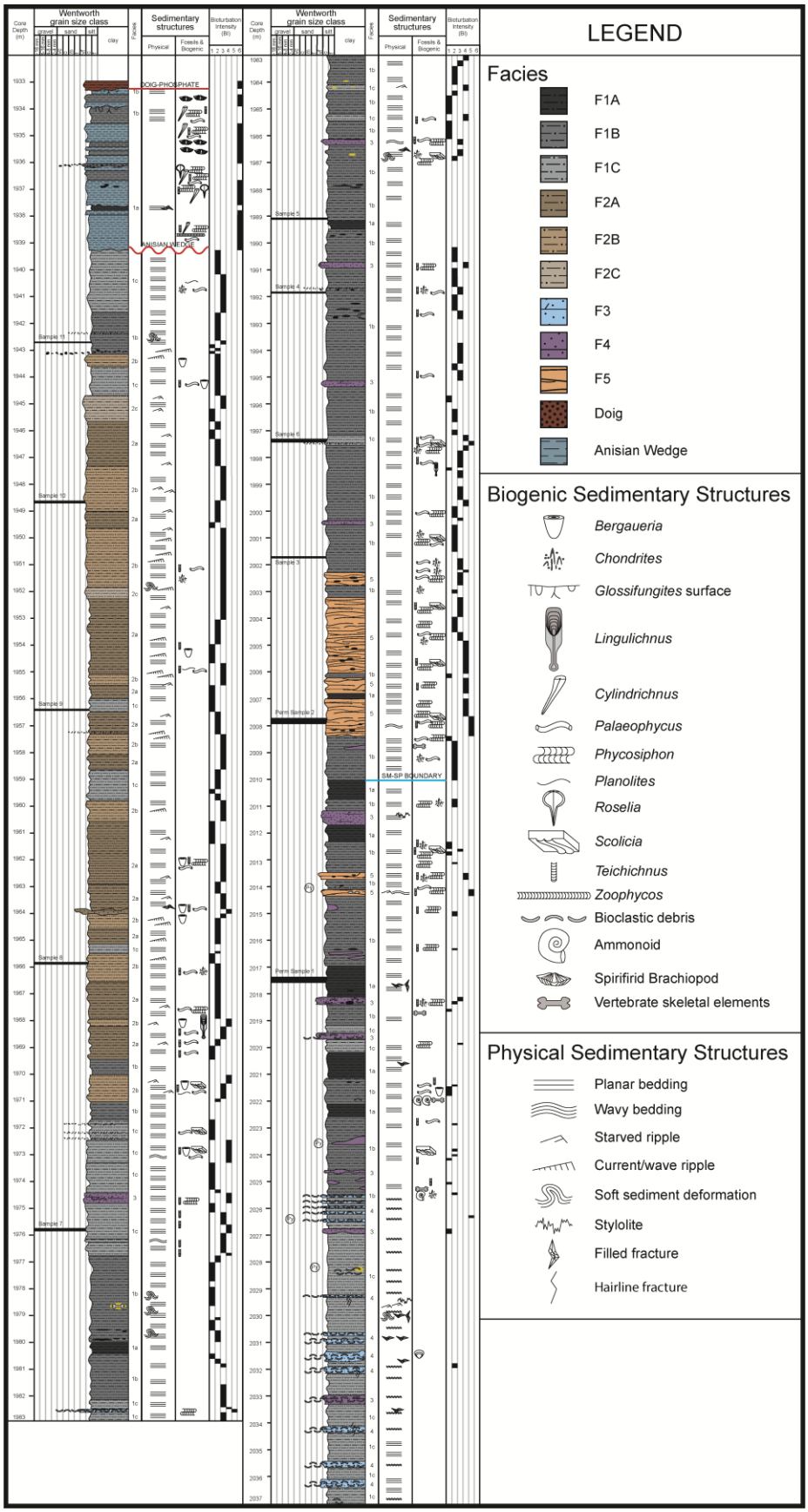
Wentworth grain size class
Sedimentary structures
Physical
Fossils & Biogenic
Bioturbation Intensity (BI)
Facies
Core Depth (m)
gravel
sand
silt
clay
DOIG-PHOSPHATE
ANISIAN WEDGE
Sample 10
Sample 9
Sample 8
Sample 7
Sample 6
Sample 5
Sample 4
Sample 3
Perm Sample 2
Perm Sample 1
SM-SP BOUNDARY
LEGEND
Facies
F1A
F1B
F1C
F2A
F2B
F2C
F3
F4
F5
Doig
Anisian Wedge
Biogenic Sedimentary Structures
Bergaueria
Chondrites
Glossifungites surface
Lingulichnus
Cylindrichnus
Palaeophycus
Phycosiphon
Planolites
Roselia
Scolicia
Teichichnus
Zoophycos
Bioclastic debris
Ammonoid
Spirifirid Brachiopod
Vertebrate skeletal elements
Physical Sedimentary Structures
Planar bedding
Wavy bedding
Starved ripple
Current/wave ripple
Soft sediment deformation
Stylolite
Filled fracture
Hairline fracture

CHAPTER 2: FACIES DESCRIPTIONS AND INTERPRETATIONS OF THE UPPER MONTNEY FORMATION, NORTHEAST BRITISH COLUMBIA

2.1 Introduction

The Lower Triassic Montney Formation is a world-class unconventional hydrocarbon reservoir hosted primarily in low-permeability siltstone, and to a lesser extent, very fine-grained sandstone. The Montney Formation is the primary gas-producing formation in British Columbia and is estimated to house 449 tcf of marketable natural gas along with high volumes of natural gas liquids and condensate (National Energy Board et al., 2013). Despite the economic importance, the fine-grained siltstone that dominates the Montney was largely overlooked prior to the past decade (Zonneveld et al., 2011).

The Montney Formation was originally believed to be deposited along a passive margin of Pangaea (Gibson and Barclay, 1989; Davies, 1997). Recent geochemical studies have revealed two sediment sources into the basin, and the margin of Pangaea has been reinterpreted to be tectonically active and in a period of transition towards a back-arc basin (Ferri and Zonneveld, 2008; Beranek and Mortensen, 2011; Golding et al., 2016). The Montney low-permeability siltstone units have been largely overlooked, likely as a result of its minimal grain size variation. Subtle sedimentological and ichnological characteristics result in the compartmentalization of resources, and characterizing these features is difficult. The Montney Formation is geographically vast, and with changing tectonic regimes, facies distribution is highly complex both vertically and laterally.

The integration of sedimentology and ichnology is key to interpreting depositional settings and understanding physical and biological processes that affect the distribution of facies. This study focuses on the upper Montney Formation in northeast British Columbia. It provides a detailed core study focussed on sedimentological and ichnological properties such as grain size, primary sedimentary structures, trace fossil identification and bioturbation intensity. Following facies definitions, deposition was interpreted to occur within a narrow environmental range from the distal offshore through to the offshore transition zone. Sediment was sourced into the basin from low-density currents and produced the pinstripe laminae that dominate in this formation. Ichnological assessment reveals a sporadic distribution of bioturbation, vertically and laterally, and is highly variable within the same facies. A highly bioturbated interval within an offshore environment was observed within the upper Montney (F5). It is *Phycosiphon*-dominated, with diminutive trace fossils of *Palaeophycus*, *Planolites*, *Scolicia* and *Teichichnus*. This interval is the most pervasively bioturbated interval within the study area, which has implications relating to palaeoenvironmental conditions within the western part of the upper Montney Formation.

The purpose of this study is to characterize the upper Montney Formation based on sedimentological, ichnological and petrographic observations. Cores from fourteen wells were

described and analysed, and five facies were identified (summarised in Table 2.2). This study provides insight into the subtle heterogeneities association with the upper Montney Formation

2.2 Previous work

The Montney Formation ('Montney') was first described from the type section core from the Texaco N.F.A. Buick Creek No. 7 well 6-26-87-21W6 in northeast British Columbia (Armitage, 1962). Early subdivisions of the Montney were based on observations that the lower strata is composed of dark grey dolomitic siltstone, which grades upwards to interbedded blocky brown siltstone and fine-grained sandstone (Armitage 1962; Davies et al., 1997; Dixon, 2000).

Initial conventional development focussed on the Montney Subcrop play, which consists of shallow marine sandstone and porous coquina units (Bird et al., 1994; Zonneveld et al., 2010a). This play developed throughout the 1950s and was primarily a secondary pay zone during drilling of the Devonian Leduc reef (Bird et al., 1994; Zonneveld et al., 2010a). Major fields for the Subcrop play included Kaybob South, Sturgeon Lake, and Sunset in Alberta and Pedigree/Ring Border field in British Columbia (Mederos, 1995; Zonneveld et al., 2010a).

Throughout the 1990s, exploration focused on the Turbidite play (or 'Montney Distal Shelf' play) (Bird et al., 1994; Moslow and Davies 1997; Moslow, 2000). Moslow and Davies (1997) produced the first detailed core study on this play, using data from the Valhalla, La Glace and Glacier fields in Alberta. Moslow (2000) provided the foundation for the facies associations that are key to understanding reservoir characteristics and building predictive models within this play. These studies concluded that the Cindy Graben ("satellite" graben in the Dawson Creek Graben Complex) was a conduit for sediment and mass wasting at a ramp edge, resulting in turbidity currents transporting and depositing thick turbidite sands (Moslow and Davies, 1997; Moslow, 2000). As well, underlying grabens caused over-thickening of turbidite channel facies as a result of syn-depositional subsidence / fault movement (Moslow and Davies, 1997; Moslow, 2000).

In 2005, in a well drilled near Dawson Creek, the first multistage hydraulic fracturing in a Montney horizontal well resulted in a drastic increase in production, allowing exploration to focus on the "shale" gas resource play (Hayes, 2012; Zonneveld and Moslow, 2015a). Although the Montney play was originally considered to be a thick, homogeneous 'basin-centered' resource play, subsequent research has shown that significant lithological and textural differences exist both within and between different field areas (Zonneveld and Moslow, 2015a). The first full-diameter core penetrating the entirety of the Montney was the Talisman Altares 16-17-83-25W6 well (approximately 270 meters recovered), which was drilled in 2009 (Golding et al., 2014). This core provides >90% coverage of the Montney, from the upper Permian Belloy Formation into the lower Doig Formation (Golding et al., 2014). Since then, many other long cores have been drilled in attempts to understand vertical and lateral heterogeneities in the Montney Formation. At

present, the Montney Formation is targeted for natural gas, natural gas liquids (NGLs) and oil (Hayes, 2012).

2.3 Tectonic Setting

Basin terminology for the Triassic within the Peace River region remains poorly defined and a brief summary of important features that directly or indirectly affected Triassic deposition are described below. The oldest structural anomaly affecting Triassic sedimentation is the Peace River Arch (PRA). The PRA is a large structure in which the Precambrian basement in northwestern Alberta and northeastern British Columbia was uplifted during the early Cambrian (Cant, 1988; O'Connell, 1994). Starting in the Mississippian, the Arch began to subside and invert, an event often referred to as the collapse of the PRA (Barclay et al., 1990; Gibson and Edward, 1990; Cant, 1988). Subsequently, the PRA evolved into a series of grabens known as the Dawson Creek Graben Complex (DCGC) (Barclay et al., 1990). The DCGC has three major elements: the Fort St John Graben (FSJG), the Hudson Hope Low (HHL), and satellite grabens named the Hines Creek, Whitelaw and Cindy Graben (Barclay et al., 1990; O'Connell, 1994). This graben complex represents the core of the Peace River Embayment (PRE) that formed a major depocentre during the Carboniferous, Permian and Triassic (Barclay et al., 1990; O'Connell, 1994). The PRE confined the Stoddart Group, Belloy Formation and Triassic strata within its boundaries, thus increasing in size throughout deposition of these formations (Barclay et al., 1990). Davies (1997) differentiated the Peace River Basin (PRB) as a basin centered on the DCGC but was broader in area than the PRE. It extended 900 kilometres in length (NNW-SSE), at least 350 kilometres east to west and extended past the margins of the underlying Permian strata (Davies, 1997). Despite this differentiation, boundary definitions of the PRB are unclear and it is thought that the basin represents the extent of Triassic strata. The original outline of the PRE defined by Barclay et al., (1990) has been adopted by others (O'Connell, 1994; Henderson et al., 1994; Richards et al., 1994) but terminology between the PRE and the PRB has been interchanged over time (see Figure 2.1 for boundary definitions).

It was previously believed that during the Triassic, the Alberta-British Columbia part of northwestern Pangaea was a tectonically stable passive margin with a single northeast derived sediment source (i.e. 'Triassic stable craton' of Gibson and Barclay, 1989; Davies, 1997). It was postulated that offshore of the margin of Pangaea, subduction and collisions of island arcs occurred in the Panthalassa Ocean, distant from the coast of Pangaea (Gibson and Barclay, 1989; Davies, 1997). Terrane accretion was inferred to occur only during the latest Jurassic and Early Cretaceous, and thus these western tectonic elements did not affect deposition in the Triassic of the study region (Gibson and Barclay, 1989; Davies, 1997). A growing body of evidence, based on stratigraphic architecture, geochemical models, and zircon dating, suggests that the basin architecture and concomitant sediment provenance is more complex than previous

interpretations indicated (e.g. Ferri and Zonneveld, 2008; Berenak et al., 2010; Golding et al., 2016; Rohais et al., in press). Detrital zircon provenance studies revealed that sediment was deposited into the WCSB from two directions: the Laurentian craton to the east and the Arctic to the north (Golding et al., 2016). Geochronological studies in the Yukon provide strong evidence that the Yukon-Tanana terrane accreted onto the North American continental margin during the early Triassic (Beranek and Mortensen, 2011). Paleozoic zircons derived from this terrane occur in Olenekian-aged sediments in the WCSB (Golding et al., 2016). As a result of terrane accretion in the west, the long evolution, from a passive margin basin to a foreland basin, started in the Early Triassic (Ferri and Zonneveld, 2008; Rohais et al., in press). Ideas regarding Early Triassic evolution in basin architecture and its implications relating to basin circulation, depositional gradients and sedimentary processes remain in a state of flux.

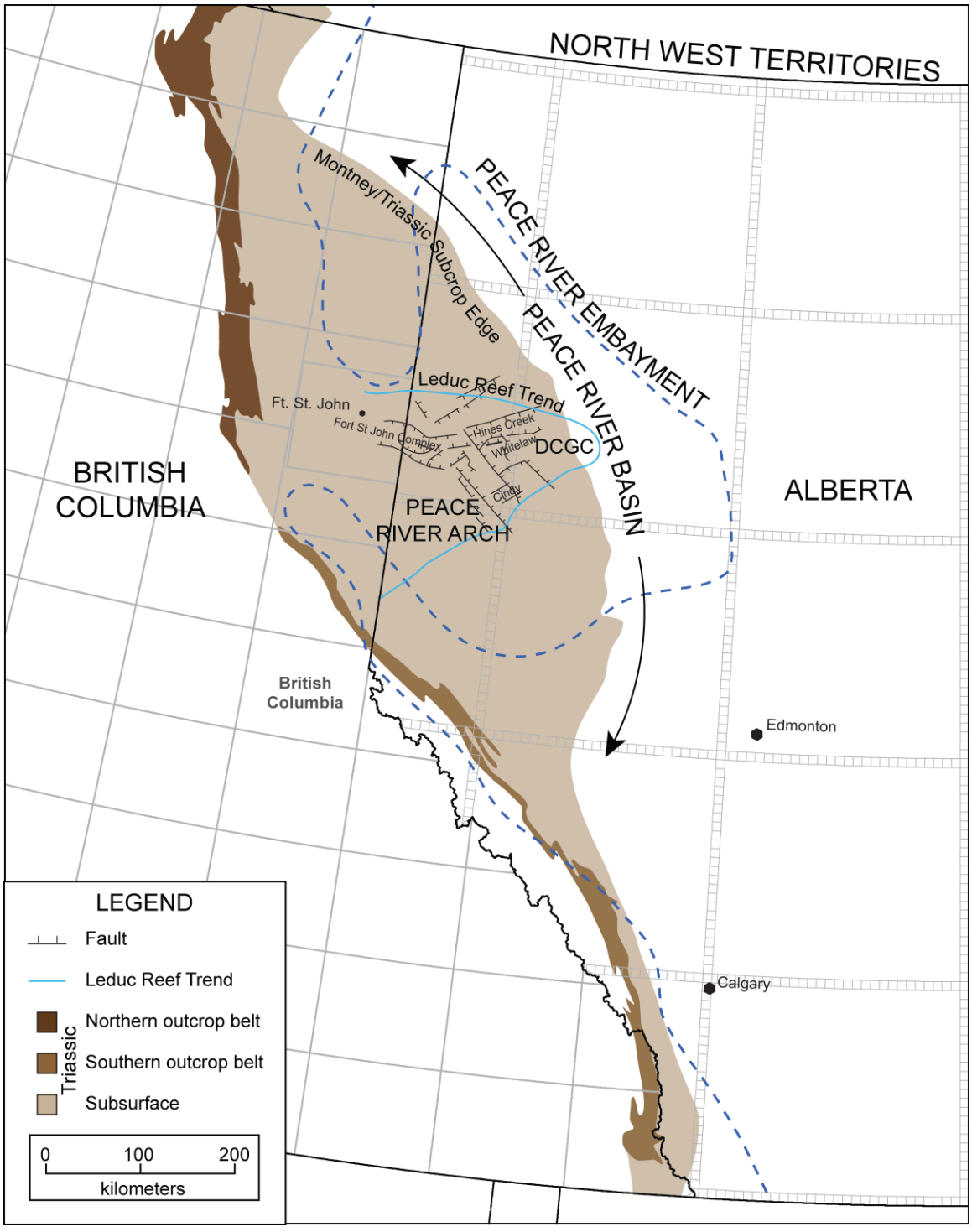

Figure 2.1: Map of the original Peace River Embayment defined by Barclay et al., (1990) and the Peace River Basin represents the extent of the Triassic within the Western Canada Sedimentary Basin (Davies, 1997). Modified from Zonneveld et al. (2011b).

2.4 Stratigraphic Framework

Embry (1997) inferred twelve high-order sequence boundaries in Triassic successions in Arctic Canada, Svalbard, Italy, Siberia, the Himalayas and the USA. Embry (1997) recognized six second-order sequence boundaries of global extent and inferred their occurrence in the Triassic of the Western Canada Sedimentary Basin (WCSB). However, available biostratigraphic / chronostratigraphic evidence for the exact temporal occurrence of these unconformities remains sparse. What evidence is available clearly indicates that the stratigraphic architecture of Embry (1997) is erroneous (Zonneveld et al., in press).

The Montney Formation was initially divided into three informal members: the Lower member (Griesbachian to Dienerian), the Coquinal Dolomite Middle member (CDM) (Dienerian to Smithian) and the Upper member (Smithian to Spathian) (Davies et al., 1997; Markhasin, 1997; Kendall, 1999). The Davies et al. (1997) lithostratigraphic scheme is most applicable in west-central Alberta where the CDM is present (Davies et al., 1997). The Montney Formation in most areas is bound by significant unconformities. Both the basal contact with the Belloy Formation and the upper contact with the Doig Phosphate zone are commonly characterized by *Glossifungites*- and / or *Trypanites*-demarcated discontinuity surfaces.

Dixon (2000) proposed an alternative lithostratigraphic classification scheme in an attempt to rectify problems from the previous scheme. He proposed that the Lower member becomes the Sandstone member, the Coquinal Dolomite Middle member becomes the Coquinal Dolomite member, and the Upper member becomes the Siltstone member. A fourth member named the Siltstone-sandstone member was added where the Sandstone and Siltstone member are hard to differentiate in the absence of the Coquina Dolomite member (Dixon, 2000). These subdivisions have not been accepted by the geological community, due in part to the fact that the lithology-based lithostratigraphic nomenclature fails to reflect the fact that siltstone and sandstone dominate the entirety of the Montney Formation.

Recent revisions, summarized by Zonneveld et al. (2015c) and Davies and Hume (2016), separated the clastic component of the Montney Formation in Alberta into informal lower, middle and upper members (Davies and Hume, 2016, fig. 2). The lower member is bounded on top by the Dienerian-Smithian sequence boundary, determined by conodont biostratigraphy, and is essentially identical to the mid-Montney sequence boundary identified previously (Markhasin, 1994; Mederos, 1995; Davies et al., 1997; Davies and Hume, 2016). Previously, the upper Montney included everything from the top of the lower Montney to the base of the Doig Phosphate Zone (Davies et al., 1997). At some point the Alberta government (AER), based on an unpublished consulting report, shifted the economic Montney-Doig boundary to the base of a unit referred to as the lower Doig siltstone (Davies and Hume, 2016). Although some industry users follow this practice, many do not (Zonneveld et al., 2010a; 2015b; Wilson et al., 2012) and it is inconsistent with the formal Montney-Doig lithostratigraphic definition. In practice, the upper

Montney Formation (Davies et al., 1997) has been subdivided into the middle Montney and the upper Montney, separated by a regional unconformity that approximates the Smithian-Spathian (Induan-Olenekian) boundary (Wilson et al., 2012; Zonneveld et al., 2015b; 2017; Davies and Hume, 2016) (Figure 2.2).

The outcrop equivalent of the Montney Formation, south of the Pine River, includes the Phroso and Vega Members of the Sulphur Mountain Formation (Gibson, 1974; Gibson and Barclay, 1989; Gibson and Edwards, 1990; Davies et al., 1997). The northern equivalents (north of the Pine River in northeast British Columbia) are the Grayling and Toad Formations (Gibson, 1974; Davies et al., 1997; Orchard and Zonneveld, 2009). A well-sorted sandstone unit, the Meosin Mountain Member, occurs in the greater Wapiti Lake area between the Phroso and Vega members (Orchard and Zonneveld, 2009). This unit is depositionally equivalent to the "turbidite zone" of the lower Montney but is younger and stratigraphically higher (Orchard and Zonneveld, 2009). In the Mackenzie Gap – Cadomin area, the dolomitic coquina named the Mackenzie Dolomite Lentil is unconformity bound and separates the Phroso and Vega Members (Gibson, 1974; Davies et al., 1997).

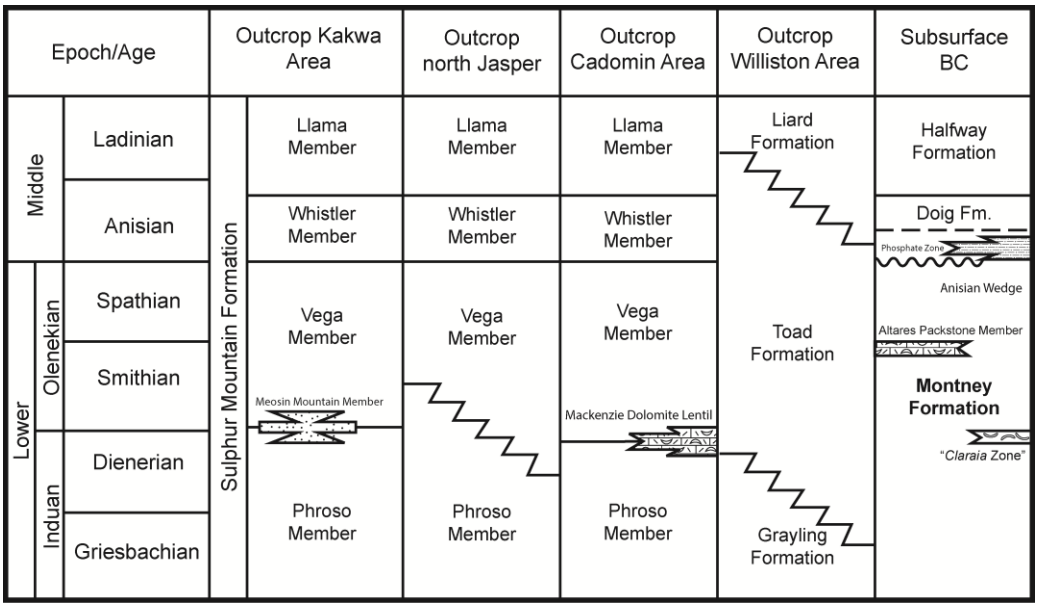

Figure 2.2: Lithostratigraphic divisions for the Lower and Middle Triassic. Note that the nomenclature changes in different locations and changes from outcrop to subsurface. Modified from Orchard and Zonneveld (2009), Zonneveld et al. (2010b), and Zonneveld (2011a).

2.5 Palaeoenvironmental Setting

During the Triassic the Western Canada Sedimentary Basin (WCSB) was located in a mid-latitudinal setting on the western margin of the supercontinent Pangaea (Davies, 1997). This setting experienced an arid climate, mixed siliciclastic and carbonate deposition and extensive dolomite and evaporate formation (Gibson and Barclay, 1989; Gibson and Edwards, 1990; Davies, 1997). These lithologies represent a wide range of deposition from deep shelf to upper

shoreface, through peritidal, and into sabkha environments (e.g. Gibson and Barclay, 1989; Mederos, 1995; Markhasin, 1997; Davies et al., 1997; Kendall, 1999; Moslow, 2000; Panek, 2000; Zonneveld et al., 2010a; 2010b). Sediment delivery to the coastline included aeolian input, but was dominated by fluvial sediment delivery (Zonneveld and Moslow, 2014). Seasonal storms contributed to river flooding and the generation of low-density turbidity currents (Davies et al., 1997). Wave-generated structures resulted from a combination of normal and storm wave conditions (Davies et al., 1997). During the summer northeast trade winds likely prevailed, while onshore storms in the winter may have promoted cold-water upwelling (Davies et al., 1997).

The Lower Triassic Montney Formation records the interval during which marine faunas struggled to recover in northwestern Pangaea in the aftermath of the end-Permian mass extinction (Zonneveld et al., 2010b). This extinction was the most severe in the marine record, resulting in the loss of 54% of late Permian marine families, 68% of genera, and up to 92% of species (Sepkoski, 1992; Knoll et al., 2007). The extinction was due, in part, to wide-spread oceanic anoxic conditions that continued into the Middle Triassic (Wignall and Hallam, 1992; Twitchett and Wignall, 1996; Hayes et al., 2007; Zonneveld et al., 2010b) as well as acidic water conditions in the world's oceans due to massive marine volcanism in the Siberian Traps (Benton and Twitchett, 2003; Zonneveld, 2011a; Lau et al., 2016). Geochemical and ichnologic studies provide significant evidence supporting pervasive anoxic conditions in early Triassic successions in Western Canada, United States, and Italy (i.e. Wignall and Hallam, 1992; Twitchett and Wignall, 1996; Hayes et al., 2007; Beatty et al., 2008; Zonneveld et al., 2010b). Ichnologic studies have shown that discrete and isolated lower Triassic intervals were intensely bioturbated despite the widespread anoxia (Beatty et al., 2008; Zonneveld et al., 2010b). As a result of frequent storms affecting the margin of Pangaea, waves aerated a zone from the shoreface under fair-weather conditions to the offshore transition during storm-weather conditions, resulting in the formation of the 'habitable zone' (Beatty et al., 2008; Zonneveld et al., 2010b). This bioturbated zone is characterized by high trace fossil diversity, and moderate to high bioturbation intensities (Beatty et al., 2008; Zonneveld et al., 2010b). Trace fossils from the Kahntah River field in northeast British Columbia include: *Asterosoma*, *Cylindrichnus*, *Cruziana*, *Diplocraterion*, *Lockeia*, *Palaeophycus*, *Phycodes*, *Planolites*, *Rhizocorallium*, *Rosselia*, *Skolithos*, *Spongeliomorpha*, *Teichichnus* and *Thalassinoides* as well as other, less common forms (Zonneveld et al., 2010b).

Oceanic acidity had a strong affect on the occurrence and preservation of marine invertebrates, particularly those with calcareous tests or shells (Wignall and Hallam, 1992; Woods and Bottjer, 2000; Wignall and Newton, 2003; Hayes et al., 2007; Knoll et al., 2007; Zonneveld, 2011a). The loss of abundant shell-secreting taxa changed the nature of the sediments along the northwestern Pangaean coast. The Permian Belloy Formation was deposited in a carbonate-dominated ramp succession that changed abruptly to a shallow siliciclastic ramp in the aftermath of the extinction and the sudden loss in biomass of shelled organisms.

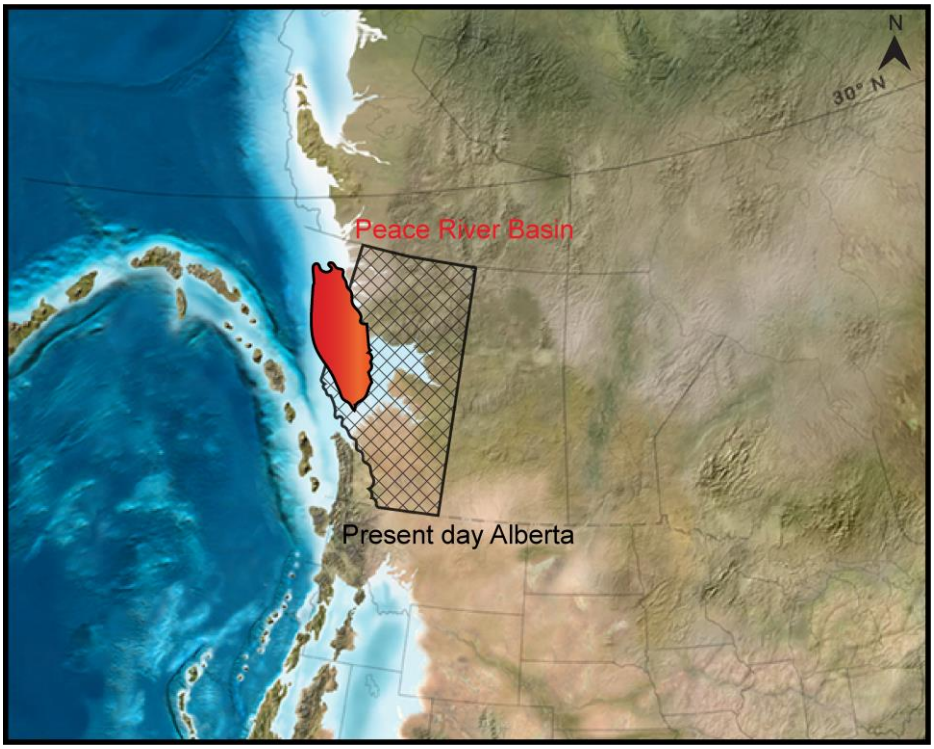

Figure 2.3: Palaeogeographic map of North America during the Early Triassic (~245 Ma). Modified from Blakey (2013).

2.6 Age of the Montney

The Montney Formation was initially divided into three informal members: the Lower member (Griesbachian to Dienerian), the Coquinal Dolomite Middle member (CDM) (Dienerian to Smithian) and the Upper member (Smithian to Spathian) (Davies et al., 1997). Initial dating of these members was done using palynology (Davies et al., 1997), however long-lasting forms dominate the palynomorph taxa cited by these authors (Davies et al., 1997) and additional work is needed to refine the stratigraphy. Conodont analyses, which are far more accurate than palynology in dating Triassic marine sediments, have been conducted by a variety of authors in various parts of the basin (eg. Markhasin, 1997; Paull et al., 1997; Kendall, 1999; Panek, 2000; Orchard and Zonneveld, 2009; Golding et al., 2014; 2015), however this data needs to be amalgamated and placed within an updated biostratigraphic framework.

The Sulphur Mountain Formation, the outcrop equivalent of the Montney Formation, has been dated using conodonts (Paull et al., 1997; Orchard and Zonneveld, 2009). In the Wapiti Lake area, the Phroso Member spans from the Griesbachian to the early Smithian (Orchard and Zonneveld, 2009). The Vega Member spans from the remaining Smithian and extends the entire Spathian interval (Orchard and Zonneveld, 2009). In this region, the Meosin Mountain Member is observed between the Phroso and Vega members, whereas, in the Cadomin area the Mackenzie Dolomite Lentil also occurs between the Phroso and Vega members (Paull et al., 1997; Orchard

and Zonneveld, 2009). Conodonts have dated the Mackenzie Dolomite Lentil as latest Dienerian to earliest Smithian in age (Paull et al., 1997) and thus, it is older, at least in part, than the Meosin Mountain Member (Orchard and Zonneveld, 2009).

Conodont data from the Talisman Altares long core (270 metres recovered) 16-17-083-25W6, verified ages of important boundaries within the Montney Formation (Golding et al., 2014). The top of the middle Montney is marked by a stratal surface that is easily correlated throughout the basin and marks the Smithian-Spathian boundary (Golding et al., 2014). As well, the Montney-Doig boundary, as currently defined, ranges from Spathian to Middle Anisian in age, which is older than previous inferences (Golding et al., 2014). The age of this boundary varies geographically and is highly diachronous (Golding et al., 2015). Table 2.1 provides the ages of the Montney – Doig (M – D) boundary for wells used in this study from Golding et al. (2015) as well as inferred ages. This core occurs in the present study area and is the most useful dataset for providing age constraints on units described herein. It should be noted that the Montney-Doig boundary interval is currently under review, with the likely occurrence of an intervening stratigraphic unit (the 'Anisian Wedge') separating the two formations in some areas (Furlong et al., 2016; 2017; Zonneveld and Moslow, 2015a,b; Zonneveld et al., 2015c; 2016).

2.7 Project Area

The study area is commonly referred to as the northern Montney within the Montney play trend and is part of the dry gas fairway (Hayes, 2012). The area of interest lies within Townships 82 to 84, Ranges 24 to 26W6M, and includes parts of NTS 094A and 094B blocks. There are approximately 2000 wells that penetrate the top of the Montney Formation over this 10,300 square kilometre area. Within the upper Montney Formation, there are 86 wells that have full-diameter cores preserved and stored at the BC Oil and Gas Commission Core Research Facility in Fort St. John. A detailed sedimentological description of core from fourteen wells provides the primary data for facies analysis and interpretations for this project (see Table 1 for core list and intervals).

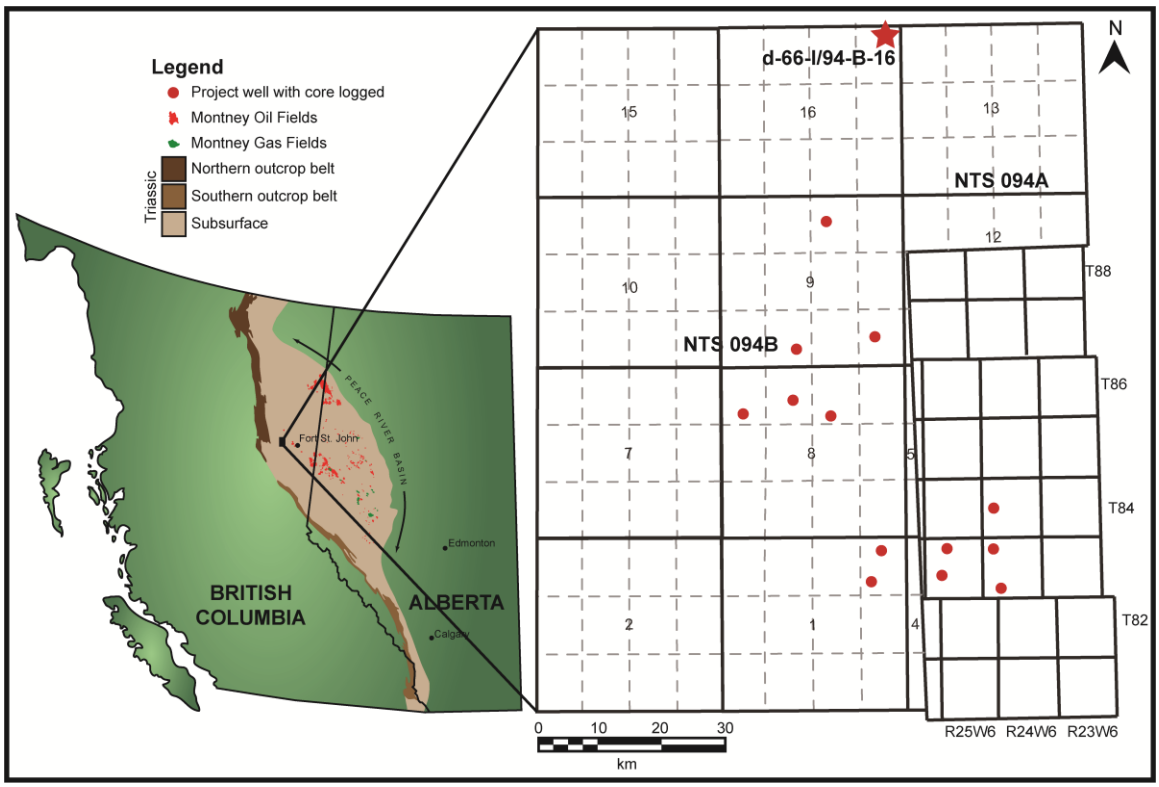

Figure 2.4: The study area is located in northeast British Columbia and the red dots represent the wells logged for this study. The smaller map indicates the extent of the Montney Formation within the Peace River Basin (modified from Zonneveld, 2011b).

2.8 Upper Montney

An issue with Montney stratigraphy is that terminology has not remained consistent between various academic, industrial and governmental Montney workers; furthermore formal terminology differs between Alberta and British Columbia. The British Columbia terminology is used within this study. This paradigm is the more conservative of the frameworks (see Edwards et al., 1994) and defines the Montney Formation as a thick siltstone and very fine-grained sandstone succession between the sandy, commonly silicified carbonate beds of the underlying Permian Belloy Formation and the overlying phosphatic beds of the Doig Phosphate Zone or of the 'Anisian Wedge' where the latter is present (Furlong et al., 2016; 2017; Zonneveld and Moslow, 2015a,b; Zonneveld et al., 2015c; 2016). The upper Montney Formation, as discussed herein, ranges from an abrupt contact to the base of the Doig Phosphate Zone. The basal contact, commonly referred to as the mid-Montney Marker, is characterized by a shift in grain size and interpreted as an intraformational sequence boundary and is interpreted to demarcate a major transgression. In core a phosphatic lag is observed at this contact in proximal settings, whereas in more distal settings this surface is sometimes difficult to identify (Golding et al., 2014). The mid-Montney boundary corresponds approximately to the Smithian-Spathian boundary and

will be referred to as the Sm-Sp boundary herein to avoid confusion with Alberta notation (Golding et al., 2014).

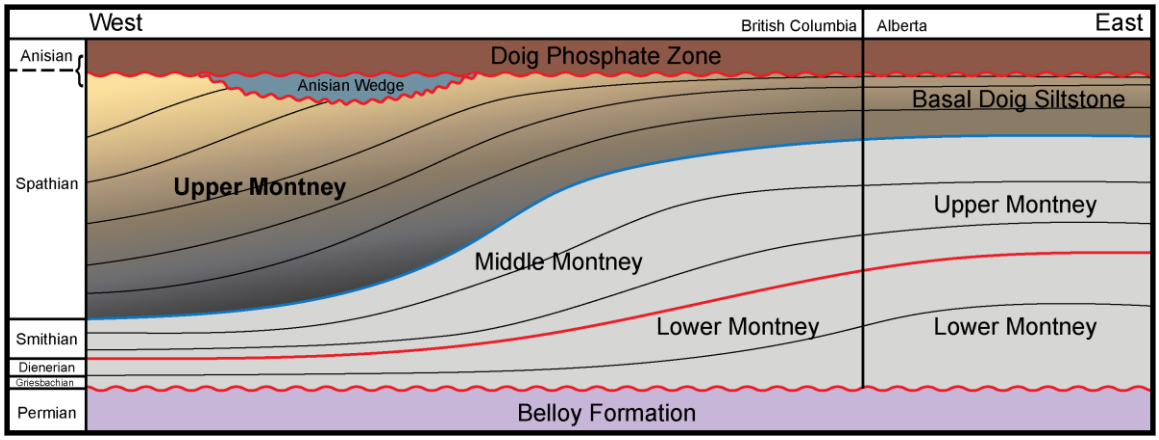

Figure 2.5: Schematic of the Montney subdivisions in Alberta and British Columbia (modified from Zonneveld, 2016).

2.9 Methods

2.9.1 Core Analysis

Fourteen wells with upper Montney core were logged focussing on sedimentological and ichnological characteristic (Table 2.1). Sedimentological analysis concentrated on properties such as lithology, grain size, bedding thickness and contact variations, and primary sedimentary structures. Grain size follows the Wentworth grain size scale (Wentworth, 1922). Ichnological observations included trace fossil identification and intensity of bioturbation (Bioturbation Index – BI, Reineck, 1963; Droser and Bottjer, 1986; Taylor and Goldring, 1993).

Location - UWI	Well Name	Field	Core Interval	Age of the M – D Boundary
200/b-017-I 094-B-01/00	Canbriam Hz Farrell B-017-I/094-B-01	Farrell	2407.0-2425.3m	NP
200/c-085-I 094-B-01/00	Progress et al Altares C-085-I/094-B-01	Altares	2444.6-2466.37m	Likely Anisian
200/c-024-K 094-B-08/00	Progress Hz Graham C-024-K/094-B-08	Graham	2221.0-2248.0m	Anisian (I)
200/c-007-J 094-B-08/00	Progress Hz Altares C-007-J/094-B-08	Altares	2445.0-2466.0m	Anisian (I)
200/c-006-L 094-B-08/00	Progress et al Graham C-006-L/094-B-08	Graham	2610.0-2666.0m	NP
200/d-048-A 094-B-09/00	Suncor Pc Hz Kobes D-048-A/094-B-09	Kobes	1960.2-2069.0m	Sp– An boundary
200/c-033-C 094-B-09/00	CNRL Graham C-033-C/-094-B-09	Graham	2186.0-2232.20m	Anisian (I)
200/d-067-J 094-B-09/00	Progress Kobes D-067-J/094-B-09	Kobes	1891.0-1957.4m	NP
200/d-066-I 094-B-16/00	Shell Hz Beg D-066-I/094-B-16	Beg	1933.0-2037.40m	Anisian (I)
100/16-17-083-25W6/00	Progress et al Altares 16-17-083-25W6	Altares	2233.0-2399.50m	Spathian
100/04-20-084-24W6/00	Arcres Hz Altares 04-20-084-24W6	Altares	2060.0-2087.3m	NP
100/01-31-083-24W6/00	Canbriam Farrell 01-31-083-24W6	Farrell	2080.0-2098.0m	NP
100/05-05-083-24W6/00	Canbriam Farrell 05-05-083-24W6	Farrell	1994.0-2012.05m	NP
100/01-32-083-25W6/00	Progress et al Hz Altares A01-32-083-25W5	Altares	2313.94-2467.10m	NP

Table 2.1: Summary table of wells with upper Montney core logged for the study. Age of the Montney – Doig (M – D) boundary was summarized from Golding et al. (2015). (I) indicates inferred ages and NP (not present) indicates no available core across the boundary.

2.10 Results and Interpretations

Five distinct facies were identified from core, F1 – F5, with F1 subdivided into F1A, F1B, F1C (Figure 2.6-2.8) and F2 into F2A, F2B and F2C (Figure 2.9-2.11). These facies are summarized in Table 2.2. Facies divisions are based on variations in pinstripe laminae and increasing abundance of sedimentary structures that imply higher-energy depositional conditions. Pinstripe laminae refer to thin, millimetre scale planar lamina, which produces a striped pattern that is very common throughout the entire Montney Formation. The white laminae are slightly coarser-grained (coarse silt) and dominated by larger quartz grains and dolomite and calcite cement. Less carbonate cement is observed in slightly finer-grained laminae. The pinstripes are commonly of uniform thickness but are also observed to pinch and swell. Ripples (current or wave) are observed in these coarse laminae. Grain size and lithology variation is limited between facies and it is dominated between fine- to coarse-grained silt and rarely very fine-grained sand. Mineralogy of detrital grains consists primarily of quartz and organics with smaller proportions of potassium feldspar, plagioclase feldspar, and mica. The detrital grains are sub-rounded to sub-angular. The carbonate content varies between facies and is related to the abundance of pinstripes and coarse-grained sediments.

2.10.1 Facies 1 (F1): Pinstripe laminated siltstone

Description

Facies 1 (F1) consists of dark grey, laminated siltstone with varying degrees of white pinstripe laminae and has been divided into three subfacies (Figure 2.6-2.8). Subfacies 1A (F1A) is dark grey, massive to faintly laminated siltstone with rare pinstripe laminae. Subtle changes in colouration reveal horizontal bedding. Curvilinear fractures are common within F1A. Subfacies F1B consists of rare to common pinstripes and subfacies F1C consists of abundant pinstripes. In F1B and F1C, small-scale, starved current ripples, soft sediment deformation structures and water escape features can occur but are rare. Contacts between the subfacies are gradational, making boundaries subjective. Ammonoid impressions (devoid of primary or secondary $CaCO_3$) and bone fragments occur on bedding planes. Phosphatic lenses and the presence of pyrite are common in F1A and F1B. In thin section, F1A is massive and no structures are observed; however, muscovite grains are aligned parallel to bedding. Larger quartz grains and calcite and dolomite cements dominate in the pinstripe laminae (F1B and F1C). Dolomite cement occurs as euhedral to subhedral rhombs in the pinstripe laminae. Well-defined white laminae have sharp boundaries, whereas faint laminae have fuzzy boundaries.

Bioturbation is dominantly absent, however isolated intervals of bioturbation do occur with BI ranging from 0-4 (F1B and F1C). Discontinuous laminae are visible in thin section and presumed to be the result of bioturbation, however trace fossil identification remains difficult as a result of limited grain size and colour variation between the matrix and a presumed burrow.

Cryptic bioturbation is commonly assumed in instances when pinstripe laminae become dashed, discontinuous or blurred. High bioturbation intensities in F1C gives the laminated fabric a mottled appearance. Diminutive trace fossils include *Bergaueria*, *Chondrites*, *Palaeophycus*, *Planolites*, *Phycosiphon*, *Scolicia*, and *Teichichnus*.

Interpretation

The dominance of planar laminated siltstone of F1 suggests deposition in a distal offshore setting where suspension deposition dominated. Deposition occurred below storm wave base, as evidenced by the limited occurrence of wave-generated sedimentary structures observed in F1. Sediment was likely sourced from low-density turbidity currents. The progression from distal to proximal (F1A to F1B to F1C) is evidenced by the increased presence of ripples and soft sediment deformation structures, and the increase in coarser-grained sediment. The rare occurrence of elevated energy structures and water escape features indicates rare episodic events of rapid deposition (Stow, 1979). F1A represents the most distal facies, with deposition dominated by persistent but slow sedimentation from suspended sediment from the plume associated with a low-density turbidity current. The occurrence of small-scale, isolated current ripples and soft sediment deformation features in F1B and F1C represent minor reworking from deep, turbidity-generated currents and proximity to the sediment source. These turbidity currents transported coarser sediment into otherwise quiescent settings, and likely resulted from the common storms that affected the coast of Pangaea during this time resulting in flooding of ephemeral river systems (Davies, 1997; Zonneveld and Moslow, 2014).

Bioturbation in F1 may be underrepresented as a result of the minimal colour and grain size variation and is indicated with BI = 0. Bioturbated intervals cannot be readily assigned to a traditional ichnofacies. It is very common that only one or two ichnotaxa are observed in a bioturbated interval. Diversity is very low and trace fossils are diminutive and range from singular isolated trace fossils that cross cut the pinstripe laminae, up to thicker intervals of trace fossils that may include *Bergaueria*, *Chondrites*, *Palaeophycus*, *Phycosiphon*, *Planolites, Scolicia*, *Teichichnus* and cryptic bioturbation. The bulk of the suite consists of deposit-feeding trace fossils (MacEachern and Bann, 2008; MacEachern et al., 2010) such as *Planolites*, *Teichichnus*, *Scolicia* and *Chondrites*; foraging/grazing trace fossils such as *Phycosiphon*; and dwelling/resting trace fossils (MacEachern and Bann, 2008; MacEachern et al., 2010) such as *Palaeophycus* and *Bergaueria*/*Lockeia*. Although diversity is limited, this trace fossils suite is representative of a stressed *Cruziana* Ichnofacies (sensu MacEachern and Bann, 2008).

Both sedimentation and oxygenation play roles in the sporadic distribution of bioturbated intervals in F1B and F1C. Oxygen deficiency is a limiting factor and leads to a decrease in size, diversity and abundance of the ichnological assemblage (e.g. Bromley and Ekdale, 1984; Ekdale and Mason, 1988; Savrda and Bottjer, 1989; Martin, 2004; Savrda, 2007). However, size is a

difficult criterion to use in the Lower Triassic, an interval characterized by common diminution of infaunal and epifaunal invertebrates (i.e. the 'Lilliput effect', Twitchett, 2007 and references therein).

Geochemical and palaeoenvironmental studies indicate that dysoxic and anoxic oceanic conditions existed during the Early Triassic (Wignall and Hallam, 1992; Wignall and Twitchett, 1996; Schoepfer et al., 2013; Lau et al., 2016). Lau et al. (2016) indicated an expanding oxygen minimum zone rather than deep-ocean anoxia during the Early Triassic. The trace fossil assemblage observed includes forms with a broad range in oxygen tolerance, and therefore it is difficult to evaluate oxygen stress on the assemblage (Bromley and Ekdale, 1984; Bjerstedt, 1988). If oxygen-rich sediment were transported into an anoxic / dysoxic basin via low-density turbidity currents, this would generate sporadic intervals in which colonization was favourable in an overall uninhabitable environment. The oxygen content in fine-grained sediments decreases rapidly below the sediment water interface, substantially reducing the time organisms were capable of surviving (Dashtgard and Gingras, 2012). Basin topography is poorly understood and variances in high and lows may also account for the sporadic nature of bioturbation, both within similar facies of the same core and between different cores. Trace fossil diversity observed in the entire Montney in this setting is reduced and evaluating palaeoenvironmental stresses remains difficult.

2.10.2 Facies 2 (F2): Pinstriped and rippled laminated siltstone

Description

Facies 2 (F2) consists of interlaminated fine and coarse silt with differing degrees of current and/or wave ripples (Figure 2.9-2.11). This increase in current-generated structures progresses from F2A to F2C. The pinstripe laminae of F2 are characterized as planar and horizontal but an increase in the pinch and swell fabric is observed compared to F1. Subfacies F2A is dominated by pinstripe laminae with local occurrences of starved or current ripples. F2A is similar to F1C because abundant pinstripe laminae still dominate this subfacies; only the occurrence of ripples separates these facies and, the contact is subjective. Subfacies 2B consists of common starved and/or current ripples with interbedded pinstripe laminated siltstone. Starved ripples are common in F2A and F2B, and identified as swells in the coarser, white laminae and foresets are not observed. Foresets are observed when the amplitude of a ripples increases. Subfacies 2C consists of wave, currents and combined flow ripples and are punctuated by intervals of planar laminae. Soft-sediment deformation features are very common, with occurrence progressively increasing from F2A to F2C. Ripples in subfacies F2B and F2C have sharp upper and lower contacts and scour surfaces are common within thicker rippled beds. With the progression from F2A through to F2C there is an increase in grain size and carbonate cement (calcite and dolomite) associated with the increase in white laminae. Ferroan dolomite is

abundant and concentrated in the pinstripe laminae and ripples. The dolomite grains are euhedral to subhedral and non-ferroan cores are commonly observed.

Bioturbation is sporadically distributed and each subfacies can range from BI 0-4. Pervasive bioturbation (BI=5) that resulted in the complete destruction of the sedimentary fabric is rare, and was only observed in one instance in decimeter scale intervals, within subfacies F2C (d-48-A/94-B-9, Figure 2.11 D and E). In this instance, the overlap of trace fossils was so significant that trace fossil identification was difficult. A broad generalization is that *Palaeophycus* and *Teichichnus* dominate F2B, whereas *Bergaueria / Lockeia* dominates F2C. Petrographic analysis shows trace fossils generally lack internal structure and cross cut laminae, leaving finer silt or coarse silt-filled depressions in coarse laminae. Ichnogenera present in F2 include *Bergaueria/ Lockeia*, *Chondrites*, *Lingulichnus*, *Palaeophycus*, *Phycosiphon*, *Scolicia*, and *Teichichnus*. *Lingulichnus* was only observed once, in well d-66-I/94-B-I at 1968.15 metres, and is associated with F2B (Figure 2.10 G). This trace fossil suite represents a distal *Cruziana* Ichnofacies (sensu MacEachern and Bann, 2008). Traces fossils are relatively diminutive compared to the archetypal ichnofacies, however are more easily recognizable than F1.

Interpretation

F2 is interpreted to represent deposition in the offshore to offshore transition environment. The progression from F2A to F2C represents increased environmental energy resulting from increased proximity to the sediment source and fair-weather wave-base. F2A represents the most distal occurrence and is closely related to F1C. The contact between these facies is gradational and is signified by a gradual transition zone towards higher energy. Deposition is dominated by suspension fall-out. F2B represents fluctuating energy levels. There is a significant amount of deposition dominated by suspension deposition; however, the increase in current ripples indicates deposition of F2B is more proximal to the sediment source or is approaching fair wave-base. F2C is subject to short-lived periods of high energy and reworking above storm wave base. Common scour surfaces in rippled beds indicate successive event-deposition, and soft sediment deformation features indicated deposition was rapid. This subfacies is the least common within F2, which may indicate few storms were large enough for wave energy to rework deep sediments or low-density turbidity currents were rarely of sufficient magnitude to significantly rework sediments this far into the basin.

Trace fossils are more easily identified in F2 as a result of the increase in coarser grains (white laminae), however the distribution of bioturbation is sporadic. The trace fossil assemblage remains very similar to that described in F1. This trace fossil suite represents a distal *Cruziana* Ichnofacies (sensu MacEachern and Bann, 2008). Trace fossils are relatively diminutive compared to archetypal ichnofacies however more easily recognizable than F1.

The occurrence of *Bergaueria* increases in F2C and is a common element of the *Skolithos* Ichnofacies. The *Skolithos* Ichnofacies is indicative of high levels of energy and this agrees with the abundance of ripples observed in F2C (MacEachern and Bann, 2008). However, the expression of this subfacies is rare within the study area and a single trace fossil renders ichnofacies assignment impossible. Trace fossils associated with suspension feeders are incredibly rare within the study area, and low-density turbidity currents likely resulted in abundant suspended sediment, making feeding very difficult, thus precluding colonization by suspension feeders (Zonneveld et al., 2007). *Lingulichnus* are the *in situ* trace fossil produced by lingulide brachiopods and are commonly found in the Lower and Middle Triassic strata in the WCSB (Zonneveld and Pemberton, 2003; Zonneveld et al., 2007; Zonneveld and Greene, 2010). Studies have shown that lingulides may be tolerant of broad ranges in bathymetry, salinity, temperature and oxygenation (Paine, 1963; Emig, 1982, Robertson, 1989; Zonneveld et al., 2007). Their occurrence is largely controlled by grain size and this relationship has been observed within the Montney in more proximal settings (Zonneveld and Pemberton, 2003; Zonneveld et al., 2007). The trace fossils have been associated with strata interpreted as proximal offshore to marginal marine environments and in sand packages in distal offshore setting interpreted as tempestites (Zonneveld and Pemberton, 2003; Zonneveld et al., 2007; Zonneveld and Greene, 2010). A single occurrence of *Lingulichnus* limits palaeoenvironmental interpretation but the lack of suspension feeding trace fossils overall is indicative of conditions that likely contain high suspended sediment load.

The sporadic nature of bioturbation may be the result of low-density turbidity currents. Bioturbation in the upper Montney was previously interpreted to correspond with rapid deposition (ripples and convolute bedding) (Playter, 2013). This study focussed on microfacies though extensive petrographic analysis, and thus bioturbation is likely underrepresented. Bioturbation is observed in intervals associated with higher energy, and it is also observed in intervals of lower energy and dominated by planar laminae. Playter (2013) referred to Montney trace fossils associated with gravity flows as “doomed pioneers” (Föllmi and Grimm, 1990). “Doomed pioneers” refers to organisms entrained by gravity flows and transported basinward into oxygen-deficient deeper water (Föllmi and Grimm,1990). Turbidity currents in this distal setting generates planar laminae and it is possible that this resulted in bioturbation and trace makers due to ‘doomed pioneers’. The isolated occurrence of *Lingulichnus* in the study area, and it’s frequent occurrence in shallower Montney depositional settings (Zonneveld and Pemberton, 2003; Zonneveld et al., 2007) may indicate basinward transport, during a storm, of an organism that frequented more proximal depositional settings.

2.10.3 Facies 3 (F3): Calcite cemented concretions and beds

Description

Facies 3 consists of a light grey, calcite-cemented siltstone observed as concretions or beds ranging from 5 to 50 centimetres thick (Figure 2.12). Bedforms are variable and range from planar parallel- to wavy parallel-laminae, massive, ripples, and convolute bedding. Facies 3 is easily identifiable in core based on its light grey colour and sharp contacts compared to surrounding dark grey siltstone of F1. Contacts are sharp but the cementation boundaries are curved, planar, or irregular. Vertical hairline, calcite filled fractures are commonly observed in the cemented beds and the fracture boundaries are contained within the horizon. Concretions are spherical or ellipsoidal in shape or, alternatively, may represent the peripherals of larger cemented beds. Laminae in the cemented beds or concretions follow bedding perfectly on the upper and lower surfaces and lamina can be traced from the surrounding siltstone through the concretion itself.

Within these cemented horizons, calcispheres and bioclastic material may be present. Bioclasts observed in thicker cemented beds, are isolated, aligned along bedding and concave-down and bioclasts are visible in the core without magnification. Bioclasts are strongly dominated by the thin-shelled bivalve *Claraia*, however other bivalves, as well as ammonoids, and vertebrate (fish and marine reptile) skeletal elements also occur. In concretions, skeletal material may occupy the center, or be dispersed along laminar bedding planes.

In thin sections, calcispheres can occur as calcite, but may also be preferentially dolomitized compared to other carbonate material observed and preserved calcite cores are occasionally present. Bioclasts are disarticulated and range from fragmented pieces to well preserved single valves and the calcite is assumed to be original shell material. When pyrite is present, it occurred at a later stage than calcite and dolomite cementation.

Interpretation

A concretions is defined as a portion of a sedimentary rock that has a different cementation than its host (Sellés-Martinez, 1996). The relative timing of concretion growth and compaction is dependent on the relationship between lamina inside and outside of the concretion (Sellés-Martinez, 1996). Concretions in the middle and upper Montney have laminae that are deflected on the inside and outside of the concretion and follow its shape. This has been referred to as ‘almond shaped layering’ (Sellés-Martinez, 1996). This morphology suggests the concretion developed in unconsolidated sediment and subsequent compaction caused the external laminae to deflect around the concretion, while the fabric within the concretion was preserved (Criss et al., 1988; Mozley, 1996).

Bioclastic material was deposited through storm transport. The concave-down orientation of the shells indicates reworking by turbidity or bottom water currents by organizing the bioclasts

into a more stable orientation (Middleton, 1967; Kidwell and Holland, 1991). The spacing of bioclasts favours a transportational rather than in-situ origin for these horizons. The presence of calcispheres has been related to pelagic sediments, and are believed to be algal in origin (Hart, 1991; Drzewiecki and Simo, 1997; Moslow et al., 2016).

The alternating intervals of siltstone and carbonate cementation may represent alternation between storm-influenced deposition and suspension-dominated deposition in an offshore environment. The abundance of carbonate material (bioclasts and calcispheres) promoted carbonate cementation within these intervals. Early carbonate cementation during the Early Triassic has been related to oxygen-restricted depositional settings (Woods et al., 1999).

A recent investigation into concretions in the Middle Montney revealed mineralogical characteristics that do not fit the classical definitions of concretions (Wust et al., 2016). Mineralogical data reveals minimal siliciclastic material is present in the concretions, and therefore they likely represent carbonate sediments before compaction and diagenesis (Wust et al., 2016). While beyond the scope of this study, it is worth noting that valid evidence has been discovered suggesting a re-classification of this mixed-carbonate interval may be justified (Wust et al., 2016).

2.10.4 Facies 4 (F4): Bioclastic packstone beds

Description

Bioclastic packstone strata are thin, calcite-cemented shell beds, consisting of bivalves, brachiopods, and ammonoids (Figure 2.13). The shell material is dominantly disarticulated, and includes both whole and fragmentary material. Brachiopods have inflated shells and are identified as terebratulide brachiopods (Sanders, 2016). Bioclastic material is disarticulated but intact. Occasionally, the carbonate structure of the valves is highly fragmented and appears as a series of columns. Bed thicknesses reach a maximum of 10 centimetres. These beds have sharp upper and lower contacts and are associated with dark, laminated siltstone of F1. Some of the upper surfaces are irregular and erosive, and are draped by overlying laminated siltstone. Bioclastic laminated siltstone may occur within the beds or between thicker bioclastic beds, and may display a crinkled appearance. The bioclastic beds pinch out, with these terminae occasionally observed in core. Skeletal debris is relatively uncommon above the Smithian-Spathian boundary; however, for cores that crossed this boundary an additional ten metres was logged to examine facies changes from the middle to the upper Montney.

Interpretation

Previous studies have focussed solely on interpreting these bioclastic intervals in the distal Montney Formation in British Columbia (Sanders, 2016; Moslow et al., 2016). The bioclastic beds observed are part of the informal “Altares Packstone member”, which occurs just below the

Smithian-Spathian boundary (Golding et al., 2015; Sanders, 2016). Sanders (2016) interpreted these deposits as biostromes. Biostromes are low-relief structures built up of biotic material and represent multiple generations of organisms (Kershaw, 1994; Sanders, 2016). Bottom ocean currents initially formed a shell lag that allowed for further colonization of brachiopods and bivalves (Zonneveld, 2001; Sanders, 2016). There is strong evidence indicating early cementation, as some of the beds are cut by erosive surfaces resulting from storm-generated currents (Sanders, 2016). These deposits are thought to represent short-lived intervals in time during which conditions were favourable for colonization (Sanders, 2016). In an alternative interpretation, Moslow et al., (2016) argued that this facies represents the product of tempestite deposition. Evidence provided for this argument includes the presence of sharp contacts, normal grading of beds, and the mixture of skeletal material of different taxa indicating storm transport.

2.10.5 Facies 5 (F5): Bioturbated siltstone

Description

Facies 5 (F5) is characterized by bioturbated siltstone interbedded with pinstripe-laminated siltstone (Figure 2.14). This facies is the most apparently bioturbated interval, in which trace fossils are clearly identifiable and bioturbation is generally pervasive relative to the rest of the upper Montney. The extensive bioturbation has resulted in the pinstripe laminae becoming discontinuous, resulting in the development of a wispy fabric. Phosphate lenses nodules are common and cemented concretions of unknown origin were observed in the d-66-I/94-B-16 core. The pinstripe laminae pinch and swell are likely the result of bioturbation, however, ripples are not observed. This facies is only observed in three cores examined in this study: d-48-A/94-B-09, d-66-I/94-B-16, 4-20-84-24W6. Facies 5 is interbedded with F1, with sharp or gradational boundaries.

Lower bioturbation intensities (BI 2-3) allows for preservation of the primary horizontal fabric. High bioturbation intensities (BI 4-5) develop a mottled fabric and the appearance of continuous pinstripe laminae is rare. Despite varying levels of bioturbation, the overall horizontal fabric characteristic of the Montney is always observable. The trace fossil assemblage consists of low diversity, diminutive trace fossils, shallow tiering, and is *Phycosiphon*-dominated. *Phycosiphon* overprints the entire facies; however, because of the dark nature of the trace fossils and the siltstone, its effect is subtle in photographs. Trace fossils are readily observed when one is able to observe the core directly. In thin section, laminae are completely disrupted and only clusters of coarser grains remain. Disruptions in laminae from trace fossils are massive and the perimeters of individual trace fossils are difficult to identify. *Phycosiphon* is clearly visible in clusters of coarser grains. Other trace fossils include *Chondrites*, *Palaeophycus*, *Planolites*, *Phycosiphon*, *Scolicia* and *Teichichnus*.

Interpretation

The abundance and relatively pervasive bioturbation compared to F1 indicates that F5 was deposited in a well-oxygenated offshore environment. This may have resulted from a shift or decrease in the oxygen minimum zone (OMZ) or may have resulted from intense oxygenation from turbidity currents. Alternatively, F5 could represent isolated event beds in the offshore setting. However, the lack of current-generated structures makes it difficult to identify the mechanism that may have increased the oxygen content (e.g. oxygenation by waves). Interbeds of non-bioturbated, pinstripe laminated siltstone suggest that environmental conditions fluctuated, with short intervals of possible anoxic / dysoxic deposition punctuating an otherwise oxygenated interval. The interbedded nature of F5 with F1 supports depositional interpretations in the offshore environment, and the lack of energy-related structures indicate deposition occurred below storm-wave base.

Phycosiphon are small grazing trails of a worm-like organism, and have been attributed to opportunistic colonizers in storm deposits and muddy sediments (Macquaker et al., 2007). The extensive overprinting of *Phycosiphon* in F5 reveals oxic sediments and high organic matter content in an overall oxygen-stressed offshore environment.

Table 2.2 (next page): Summary of facies used in this study to characterize the Upper Montney

	F1A	F1B	F1C	F2A	F2B	F2C	F3	F4	F5
Core Example								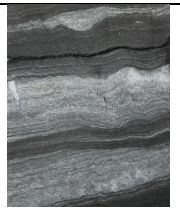	
Sedimentology and Accessories	• Dark grey siltstone • Massive to faintly horizontally laminated • Ungraded • Rare pinstripes • Stylolites • Pyrite	• Dark grey siltstone with rare to common pinstripe laminae • Horizontal • Laminae are continuous but may be discontinuous • Rare, isolated, starved current ripples • Rare, isolated soft sediment deformation feature • Horizontal, calcite filled fractures, slickensides occur	• Dark grey siltstone with common to abundant pinstripe laminae, • Horizontal laminae • Rare, isolated starved current ripples • Rare, isolated soft sediment deformation features • Water escape features	• Pinstripe laminated siltstone with local occurrences of starved current ripples • Horizontal laminae • Rare soft sediment deformation features • Pyrite can occur along ripples forests or as framboids in pinstripe laminae • Water escape features	• Common current ripples with interbedded pinstripe laminated siltstone • Horizontal laminae • Soft sediment deformation features • Pyrite can occur along ripples forests	• Common to continuous current, wave, combined-flow ripples • Thin beds of planar laminae • Scour surfaces are common • Soft sediment deformation features are very common • Pervasive pyritization observed relating to bioturbated beds	• Carbonate cemented beds or concretions • Parallel laminae, convolute bedding, starved ripples, massive • Vertical hairline fractures bound in cemented zone • Stylotlies • Pyrites	• Calcite cemented packstone • Abundant bioclasts	• Bioturbated siltstone with minor interbedded parallel laminated siltstone • Intense bioturbated creates a wispy fabric • Discontinuous laminae • Phosphatic lenses ad nodules • Recrystallized fecal material or burrows
Ichnology/Fossils	• BI = 0 • Possible that bioturbation is underrepresented as a result of minimal grain size and colour variation • Ammonoid impressions on bedding planes	• BI = 0-3 • Bioturbated intervals are sporadic • Diminutive traces of *Bergaueria*, *Chondrites*, *Palaeophycus*, *Phycosiphon*, *Planolites*, *Scolicia* and *Teichichnus* • Ammonoid impressions • Fish bone fragments • Low-diversity, stressed *Cruziana* Ichnofacies	• BI = 0-4 • Bioturbated intervals are sporadic • Higher BI gives the fabric a mottled appearance • Trace fossils consist of *Bergaueria*, *Palaeophycus*, *Phycosiphon*, *Planolites*, *Scolicia* and *Teichichnus* • Low-diversity, stressed *Cruziana* Ichnofacies	• BI = 0-3 • Bioturbation is sporadically distributed • Trace fossil suite: *Bergaueria*, *Palaeophycus*, *Phycosiphon*, *Planolites*, *Teichichnus*, *Scolicia*	• BI = 0-3 • Bioturbation is sporadically distributed • Traces consist of: Bergaueria, *Chondrites*, *Lingulichnus*, *Palaeophycus*, *Phycosiphon*, *Planolites*, *Teichichnus*, *Scolicia*	• BI = 0-5 • Bioturbation is sporadically distributed • Isolated traces to pervasive • Top of beds are bioturbated commonly bioturbated • Traces include: *Bergaueria*, *Lockeia*, *Palaeophycus*, *Planolites*	• Shell fragments aligned along bedding are concave down • Bioclasts in core of concretion • Calcispheres (calcite, dolomite, or calcite cores and dolomite rims)	• Original body fossil preserved of bivalves, brachiopods and ammonoids	• BI = 2-5 • Traces include: *Chondrites*, *Palaeophycus*, *Planolites*, *Phycosiphon*, *Scolicia*, and *Teichichnus*
Occurrence	• Gradational changes with F1B • Typically observed near the lower part of the Upper Montney	• Very common facies • Gradational contacts with F1A and F1C • Sharp contacts above F2 • Associated with F3 and F4	• Gradational contacts with F1B and F2A • Sharp contacts with F1A	• Common facies • Gradational contacts with F1C, F2B and F2C • Rippled beds are sharp based	• Common facies • Gradational contacts with F2A, F2C and F1C • Sharp based ripple beds	• Least common facies • Sharp based ripple beds • Gradational contact with F2B	• Cementation contacts are curved, planar, or irregular • Commonly interbedded in F1 • Rarely associated with F2 (C-33-C)	• Sharp contacts • Erosive contacts • Commonly associated with F1 • Below the Sm-Sp boundary	• Sharp, or gradational boundaries • Associated with F1
Interpretation	• Distal offshore environment • Well below storm wave base • Most distal • Oxygen deficient • Persistent, but slow sedimentation • No evidence of elevated energy events	• Evidence of elevated energy • Oxygen stressed environment • More proximal to source of the sediment gravity flow	• Evidence of elevated energy • Oxygen stresses environment • Most proximal to the source in F1	• Evidence of elevated energy • More proximal to sediment source (most distal of F2) • Occurrence of more ripples than F1C • Offshore	• Evidence of elevated energy • Energy and sedimentation stresses on bioturbation • Upper offshore	• Most proximal to sediment source (coarser-grained) • Above storm wave base • Most proximal • Higher energy and sedimentation • Energy stress on bioturbation • Offshore transition	• Offshore • Alternating storm-influenced deposition and suspension dominated deposition • Aligned shells indicated reworking	• “Altares Packstone Member” • No evidence for elevated energy • Early cementation • Offshore environment • Biostromes • Conditions favourable for colonization	• Increase oxygen • Interbedded parallel laminated siltstone indicates episodic disruption to colonization

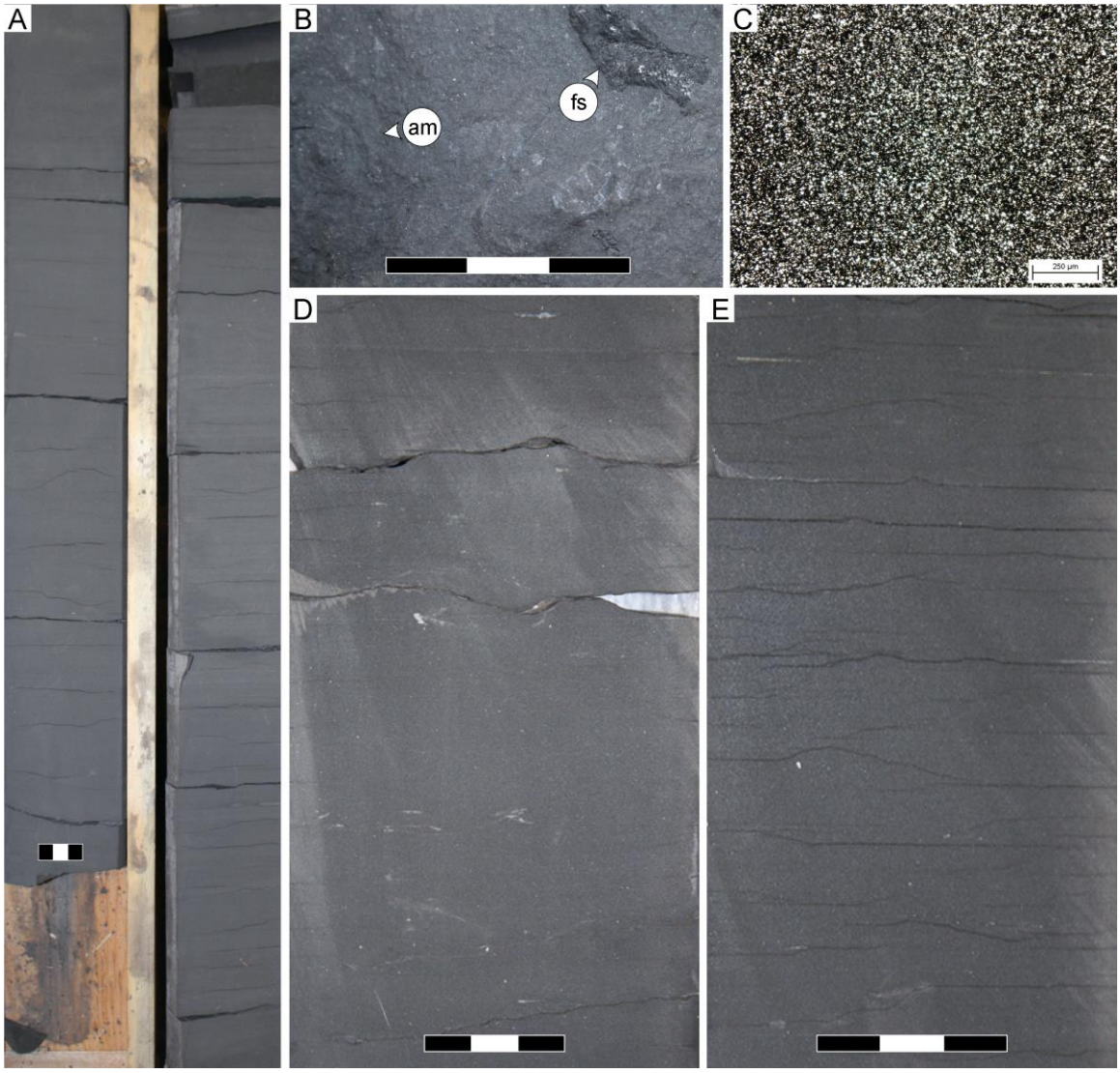

Figure 2.6: Facies 1A **A)** Well c-6-L/94-B-8 from 2655.30 – 2656.60 metres. The upper right is the top of the core interval. **B)** Fish scale and ammonoid impression on bedding surface from well d-48-A/94-B-9 at 2057.30 metres. **C)** Well 1-32-83-25W6 at 2331.6 metres: thin section photo taken in plane polarized light at 20X magnification. Note its fine-grained nature and massive appearance. **D)** Well c-85-I/94-B-1 at 2462.85 metres is massive and no structures are observed. **E)** Well c-85-I/94-B-1 at 2461.85 metres shows abundant curvilinear fractures.

Figure 2.7 (next page): Facies 1B **A)** Well 5-5-83-24W6 at 1999.80 metres: thin planar pinstripe laminae are present. **B)** Well 4-20-84-24W6 at 2075.80 metres: calcite filled horizontal fractures (fr) **C)** Well c-7-J/94-B-8 at 2295.30 metres shows laminae that pinch and swell **D)** Thin section from well d-66-I/94-B-16 at 2009.57 metres taken in plane polarized light at 20X magnification. Discontinuous laminae likely resulted from bioturbation but visible trace fossils are not observed. **E)** Well 5-5-83-24W6 at 1999.30 metres: slickensides are commonly found on bedding surfaces with horizontal fractures. **F)** Well c-7-J/94-B-8 at 2294.64 metres: *Bergaueria* (B) crosscutting pinstripe laminae. **G)** Well d-66-I/94-B-16 (deviated well) at 2012.70 metres: faint laminae with a suite consisting of *Chondrites* (Ch), *Palaeophycus* (Pa) and *Scolicia* (Sc). **H)** d-66-I/94-B-16 (deviated well) at 2008.60 metres: faintly laminated siltstone showing a suite consisting of *Chondrites* (Ch), *Palaeophycus* (Pa) and a fish scale (fs).

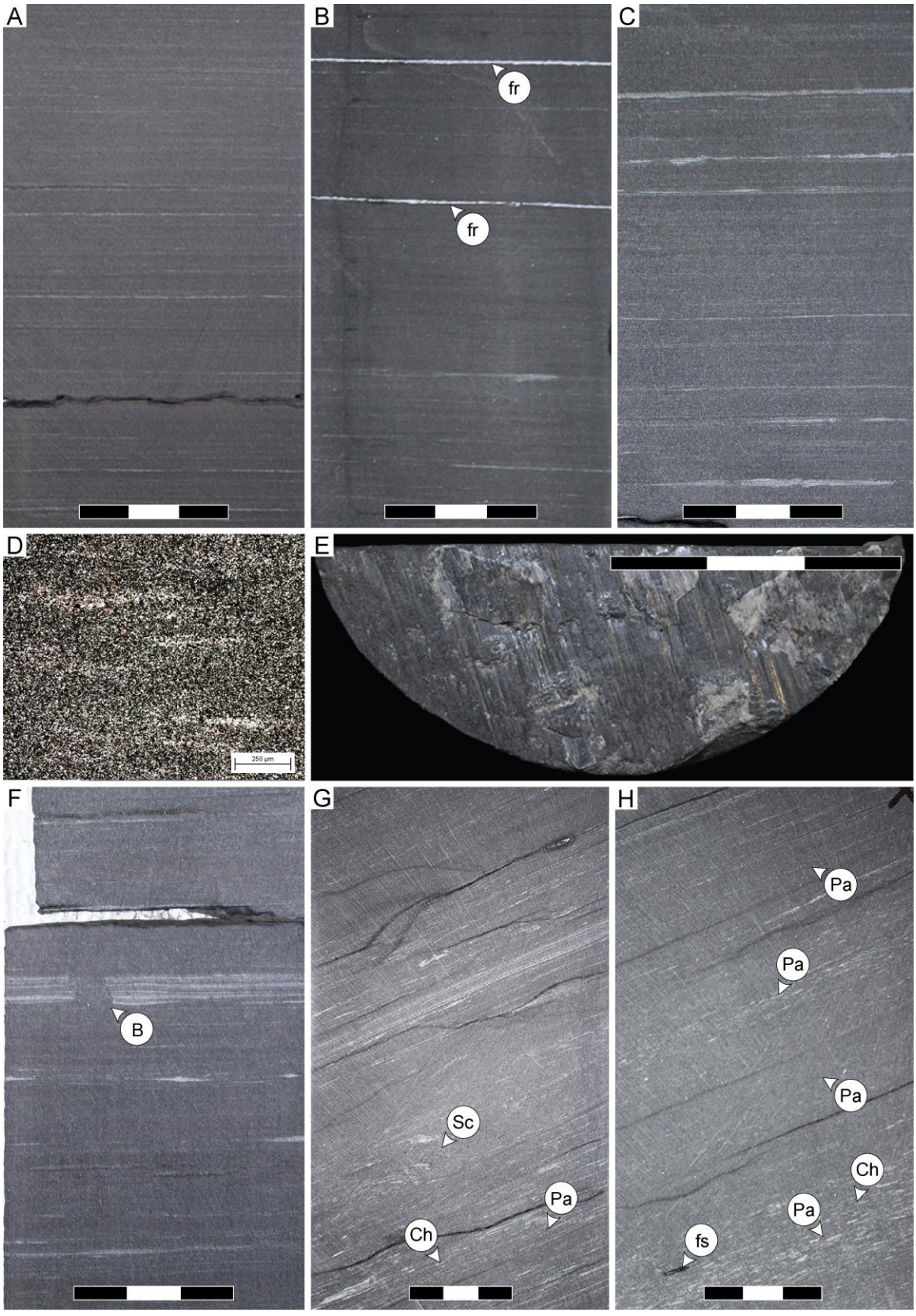
A
B
fr
fr
C
D
250 µm
E
F
B
G
Sc
Pa
Ch
H
Pa
Pa
Pa
Ch
Pa
fs

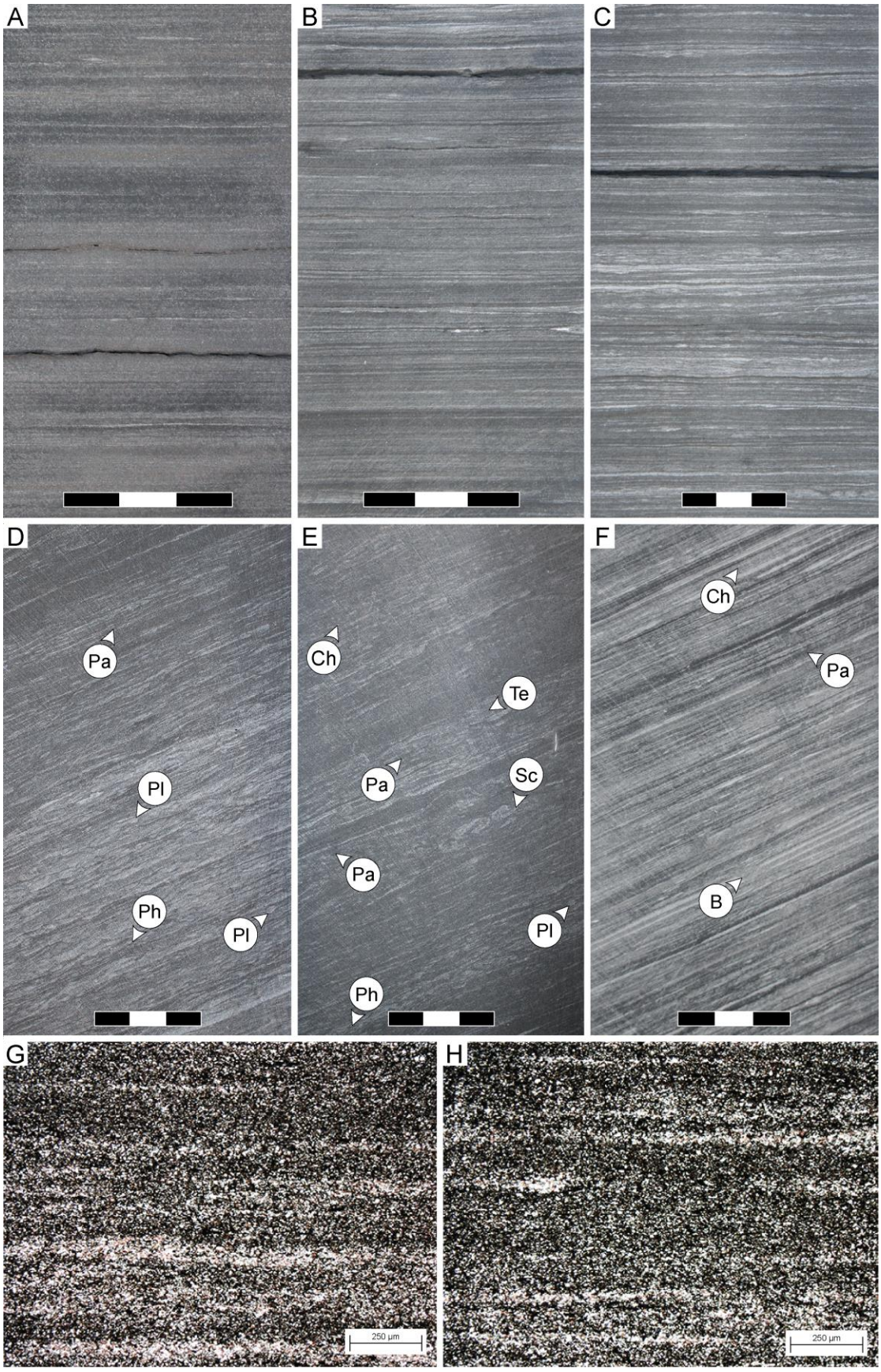
A
B
C
D
Pa
Pl
Ph
Pl
E
Ch
Te
Pa
Sc
Pa
Pl
Ph
F
Ch
Pa
B
G
250 µm
H
250 µm

Figure 2.8 (previous page): Facies 1C **A)** Well c-7-J/94-B-8 at 2307.75 metres: abundant pinstripe laminae **B)** Well d-48-A/94-B-9 at 2009.80 metres: abundant pinstripe laminae **C)** Well c-33-C/94-B-9 at 2203.10 metres: minor bioturbation and laminae pinch and swell **D)** Well d-66-I/94-B-16 (deviated well) at 1997.59 metres: bioturbation develops a mottled appearance and trace fossil suite includes *Palaeophycus* (Pa), *Planolites* (Pl) and *Phycosiphon* (Ph). **E)** Well d-66-I/94-B-16 at 1997.25 metres trace fossils include *Chondrites* (Ch), *Palaeophycus* (Pa), *Planolites* (Pl), *Phycosiphon* (Ph), *Scolicia* (Sc), and *Teichichnus* (Te). **F)** Well d-66-I/94-B-16 (deviated well) at 1959.40 metres: dominated by planar laminae includes *Bergaueria* (B), *Chondrites* (Ch), and *Palaeophycus* (Pa). Note well d-66-I/94-B-16 is a deviated well and bedding is considered horizontal. **G)** Well 1-31-83-24W6 at 2079.95 metres: some discontinuous laminae and laminae pinch and swell **H)** Well 1-31-83-24W6 at 2079.95 metres: laminae towards the bottom have fuzzy boundaries and discontinuous laminae are interpreted to represent bioturbation and the gap in the lamiae appears massive.

Figure 2.9 (next page): Facies 2A **A)** Well c-7-J/94-B-8 at 2303.0 metres: isolated current ripples (cr) are observed **B)** Well c-7-J/94-B-8 at 2309.80 metres bioturbated intervals isolated by planar and low-relief rippled laminae. Overlap of trace fossils is very high and identification is difficult. **C)** Well d-48-A/94-B-9 at 2016.70 metres convolute bedding (cb) **D)** Well c-33-C/94-B-9 at 2217.50 metres isolated current ripples (cr) observed with interbedded parallel laminated siltstone **E)** Well d-66-I/94-B-16 (deviated well) at 1967.20 metres: larger well developed ripples towards the top **F)** Well d-66-I/94-B-16 (deviated well) at 1969.55 metres: diminutive trace fossils of *Bergaueria* (B), *Planolites* (P) and *Teichichnus* (Te). **G)** Well d-48-A/94-B-9 at 2019.00 metres: thin section taken in plane polarized light at 20X magnification. Planar laminae are observed. **H)** Well d-66-I/94-B-16 (deviated well) at 1963.75 metres taken in plane polarized light at 50X magnification. This close up of a pinstripe laminae shows the sharp boundaries of a laminae and the abundant coarser quartz grains and calcite cement that dominate the laminae.

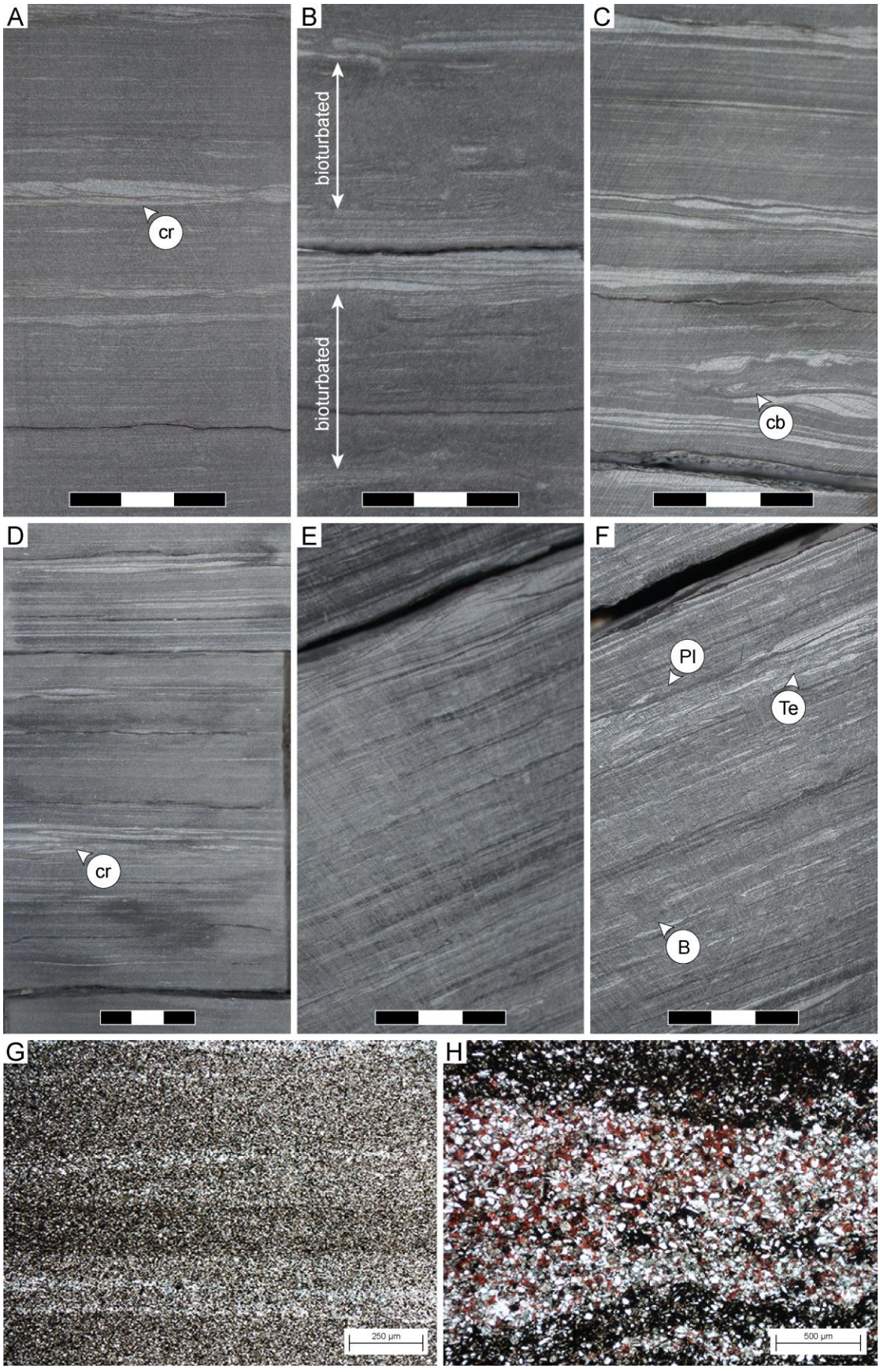
A
cr
B
bioturbated
bioturbated
C
cb
D
cr
E
F
Pl
Te
B
G
250 µm
H
500 µm

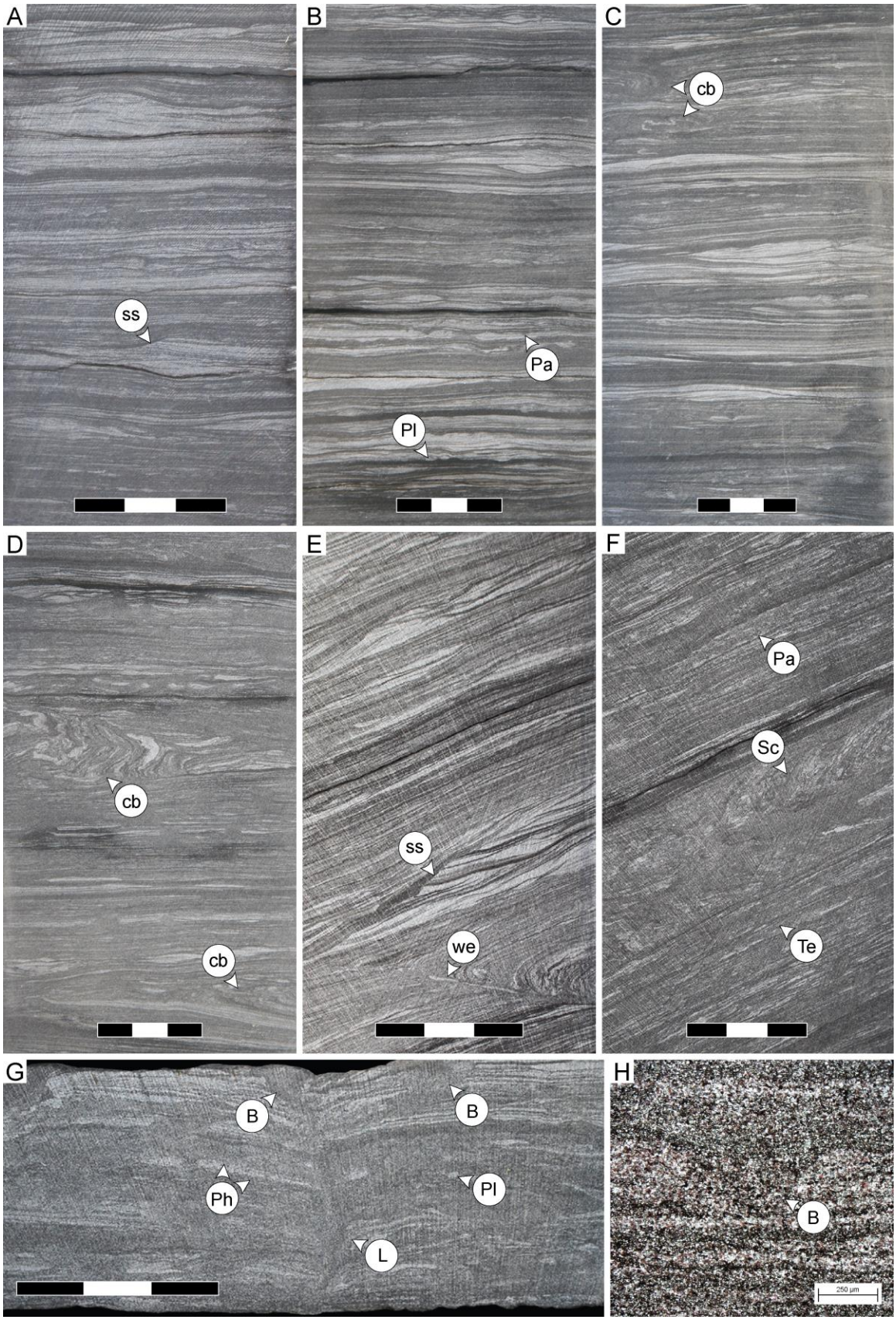
A
ss
B
Pa
Pl
C
cb
D
cb
cb
E
ss
we
F
Pa
Sc
Te
G
B
B
Ph
Pl
L
H
B
250 µm

Figure 2.10 (previous page): Facies 2B **A)** Well d-48-A/94-B-9 at 2007.85 metres: scour surface observed (ss) **B)** Well c-33-C/94-B-9 at 2208.10 metres: diminutive trace fossils of *Palaeophycus* (Pa) and *Planolites* (Pl) **C)** Well c-33-C/94-B-9 at 2210.40 metres: convolute bedding observed (cb) **D)** Well c-33-C/93-B-9 at 2232.60 metres convolute bedding observed (cb) **E)** Well d-66-I/94-B-16 (deviated well) at 1948.60 metres: scour surface (ss) and water escape structure (we) **F)** Well d-66-I/94-B-16 (deviated well) at 1970.70 metres: trace fossils include *Palaeophycus* (Pa), *Scolicia* (Sc) and *Teichichnus* (Te). **G)** Well d-66-I/94-B-16 (deviated well) at 1968.15 metres trace fossils observed include *Bergaueria* (B), *Lingulichnus* (L), *Planolites* (Pl) and *Phycosiphon* (Ph). **H)** Well d-66-I/94-B-16 (deviated well) at 1949.85 metres: thin section photo of *Bergaueria* observed forming a pit into coarse laminae taken at 20X magnification.

Figure 2.11 (next page): Facies 2C **A)** Well d-48-A/94-B-9 at 1980.60 metres: scour surface (ss) and convolute bedding (cb) observed **B)** Well d-48-A/94-B-9 at 1982.65m: isolated horizons with *Bergaueria* (B) **C)** Well d-48-A/94-B-9 at 1984.75 metres: pervasive pyritization in rippled beds **D)** Well d-48-A/94-B-9 at 1992.90 metres: bioturbated intervals with high overlap but *Bergaueria* (B) is observed extending from the basal surface isolated by non-bioturbated intervals and convolute bedding (cb) **E)** Well d-48-A/94-B-9 at 1995.75 metres: pervasive bioturbation completely destroying sedimentary structures, this is rarely observed. **F)** Well d-67-J/94-B-9 at 1901.20 metres: high overlap and *Bergaueria* (B) observed **G)** Well d-67-J/94-B-9 at 1913.0 metres: water escape (we) observed **H)** Well c-33-C/94-B-9 at 2214.15 metres: diminutive trace fossils of Planolites (Pl) **I)** Well d-48-A/94-B-9 at 1985.50 metres: abundant ferroan dolomite is observed in the laminae. **J)** Well d-48-A/94-B-9 at 1996.30 metres: the laminae is terminated by *Bergaueria*. The lower surface is curved and the internal structure of the trace is massive fine-grained siltstone.

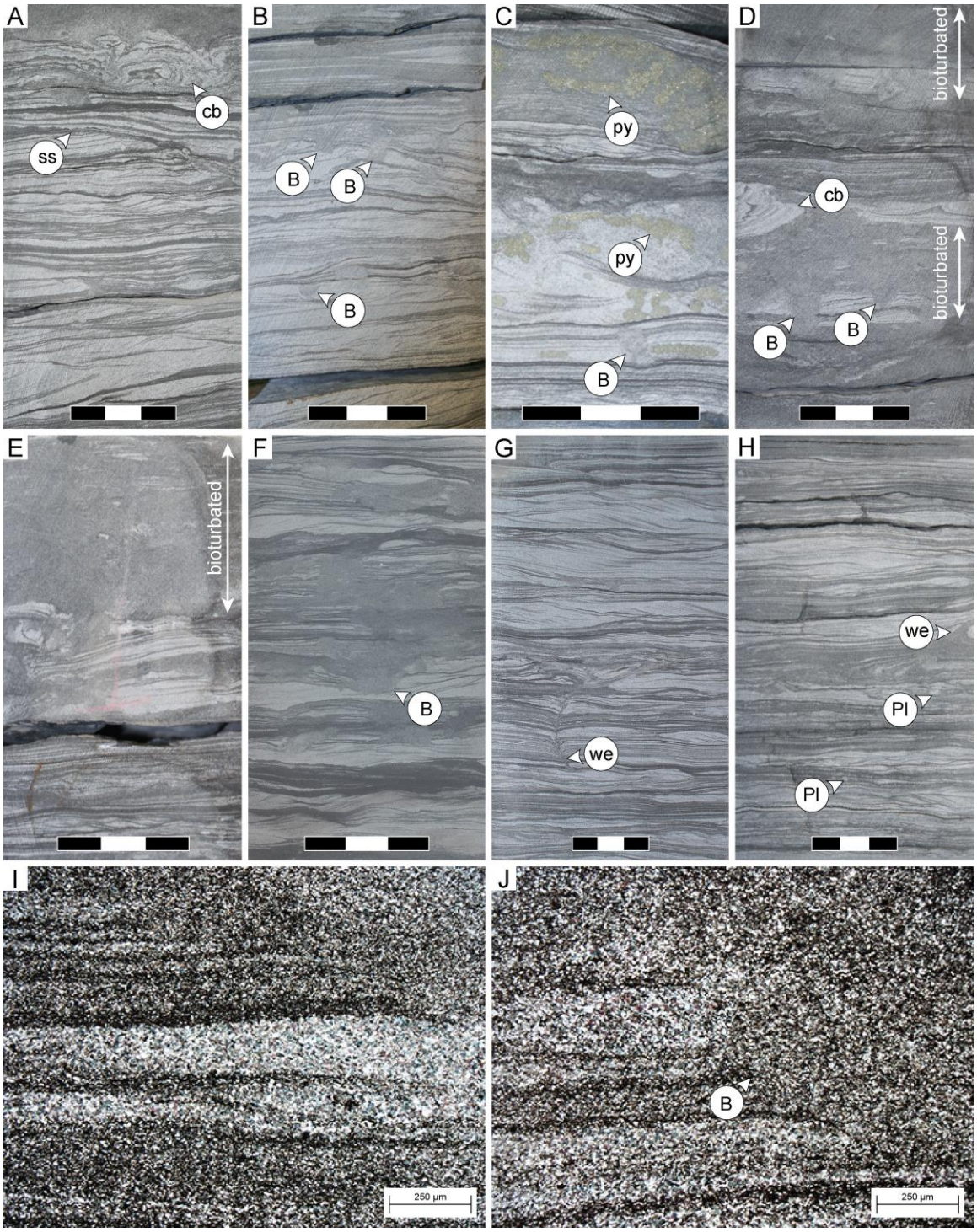
A
cb
ss
B
B
B
B
C
py
py
B
D
bioturbated
cb
bioturbated
B
B
E
bioturbated
F
B
G
we
we
H
we
Pl
Pl
I
250 µm
J
B
250 µm

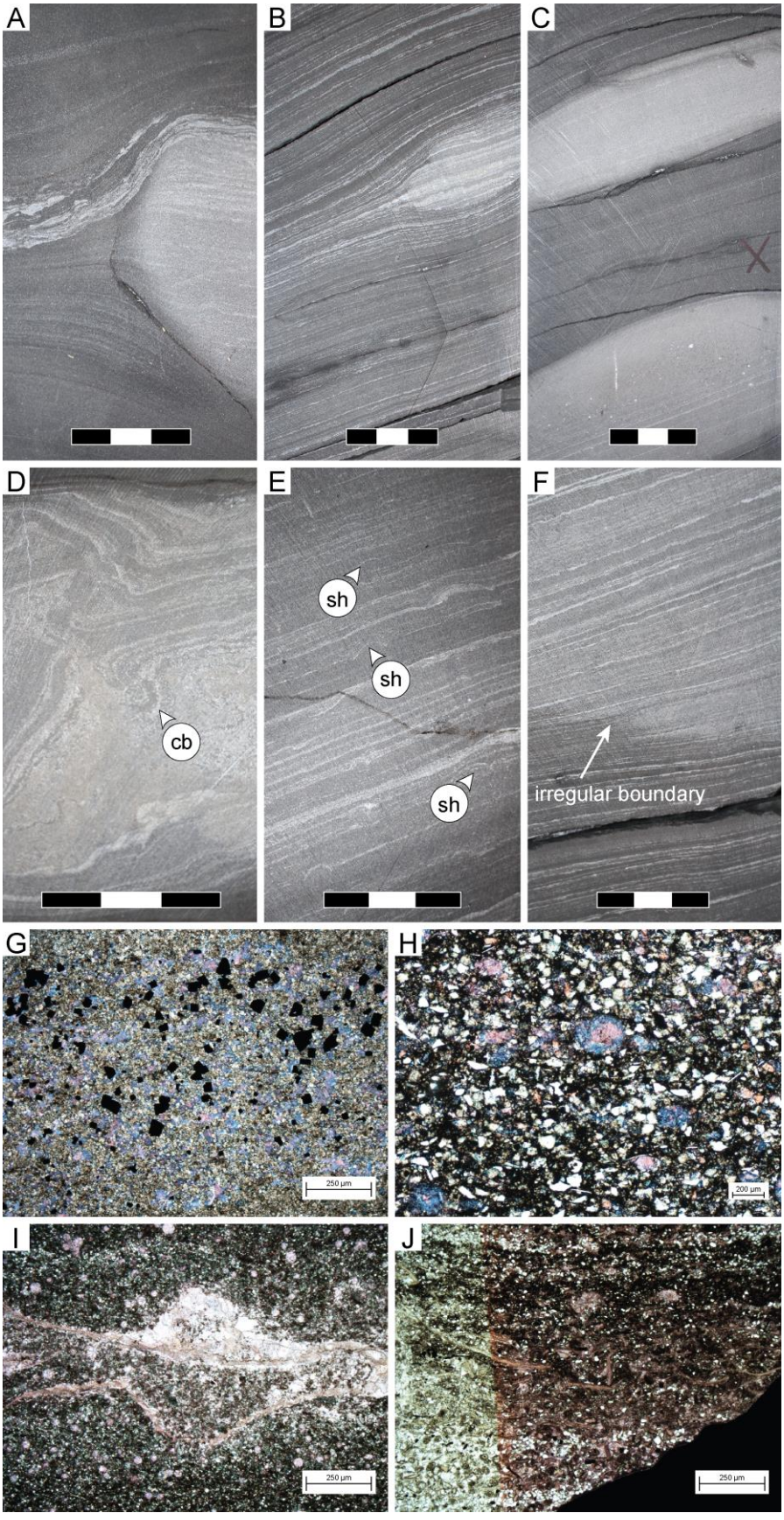
A
B
C
D
E
F
cb
sh
sh
sh
irregular boundary
G
H
I
J
250 µm
200 µm
250 µm
250 µm

Figure 2.12 (previous page): Facies 3 **A)** Well c-6-L/94-B-8 at 2664.60 metres: large spherical concretion with a shell bed draping over the top. The laminae can be traced from the outside on the concretion through the inside. **B)** Well d-66-I/94-B-16 (deviated well) at 2028.20 metres: Small concretion and the laminae can be traced from the outside on the concretion through the inside. **C)** Well d-66-I/94-B-16 (deviated well) at 2016.80 metres: curved cemented beds with a few laminae observed but relatively massive in structure. **D)** Well d-48-A/94-B-9 at 2063.45 metres: calcite cemented bed dominated by convolute bedding. White speckles are interpreted as calcispheres. **E)** Well d-66-I/94-B-16 (deviated well) at 2018.20 metres: bioclasts observed along bedding oriented concave down **F)** Well d-66-I/94-B-16 (deviated well) at 2027.0 metres: bioclastic material present and irregular cementation boundary. **G)** Well c-6-L/94-B-8 at 2635.70 metres plane polarized light at 20X magnification calcispheres and later stage pyritization **H)** Well 1-32-83-25W6 at 2333.20 metres: taken at 50X magnification in plane polarized light. Calcispheres have calcite cores and ferroan dolomite rims **I)** Well 16-17-83-25W6 at 2299.58 metres: thin section photo taken at 20X magnification in plane polarized light. Bioclasts observed and sparry calcite filling in void space **J)** Well d-48-A/94-B-9 at 2059.80 metres: thin section photo taken at 20X magnification in plane polarized light. Abundant bioclastic material and calcispheres

Figure 2.13 (next page): Facies 4 **A)** Well 16-17-83-25W6 at 2390.93 metres: packstone beds of variable thickness and irregular boundaries. **B)** Well 16-17-83-25W6 at 2397.95 metres: erosive surface cutting into packstone bed and overlying siltstone drapes over the bioclastic packstone **C)** Well d-66-I/94-B-16 (deviated well) at 2025.80 metres: peripheral of a packstone bed is observed. **D)** Well d-66-I/94-B-16 (deviated well) at 2026.35 metres: ammonoid (am) preserved in bioclastic packstone **E)** c-6-L/94-B-8 at 2665.90 metres: thin packstone bed and bioclastic material is less dense. **F)** Well 16-17-83-25W6 at 2392.0 metres: thin section photo taken in plane polarized light at 20X magnification. Shows the dense packing of the bioclastic beds and dolomite cement is observed in the small interstitial space. **G)** Well 16-17-83-25W6 at 2392.0 metres: thin section photos taken in plane polarized light at 50X magnification. This photo is a close up of the photo to the left. Packstone beds can be interbedded with thin layers of siltstone and coarser grains of quartz also occur within these beds. **H)** Well 16-17-83-25W6 at 2394.30 metres: thin section photo taken in plane polarized light at 20X magnification. This photo displays the occurrence of laminated siltstone within these beds and the irregular boundaries likely result from random orientation of the bioclasts.

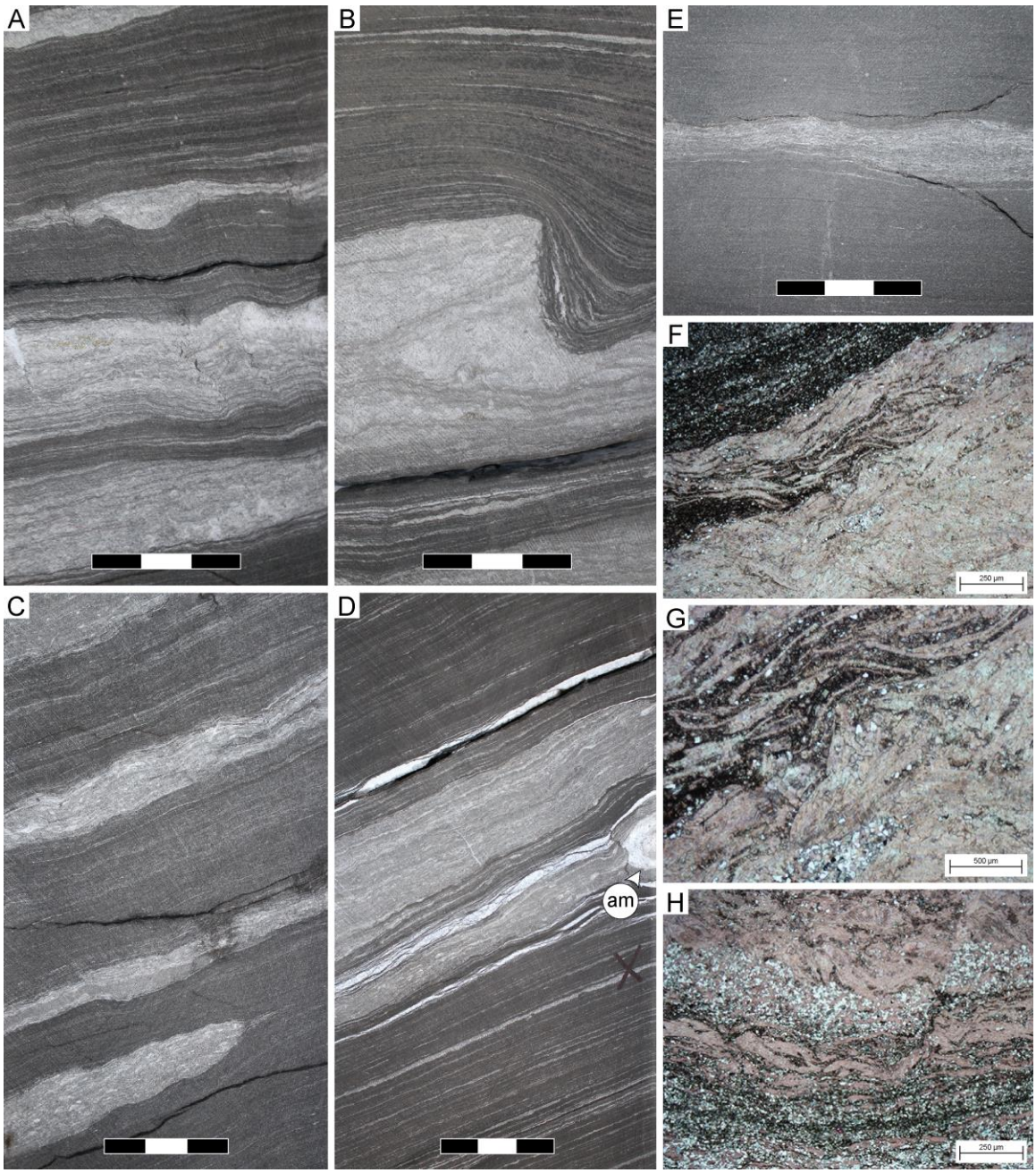
A
B
E
F
250 µm
C
D
am
G
500 µm
H
250 µm

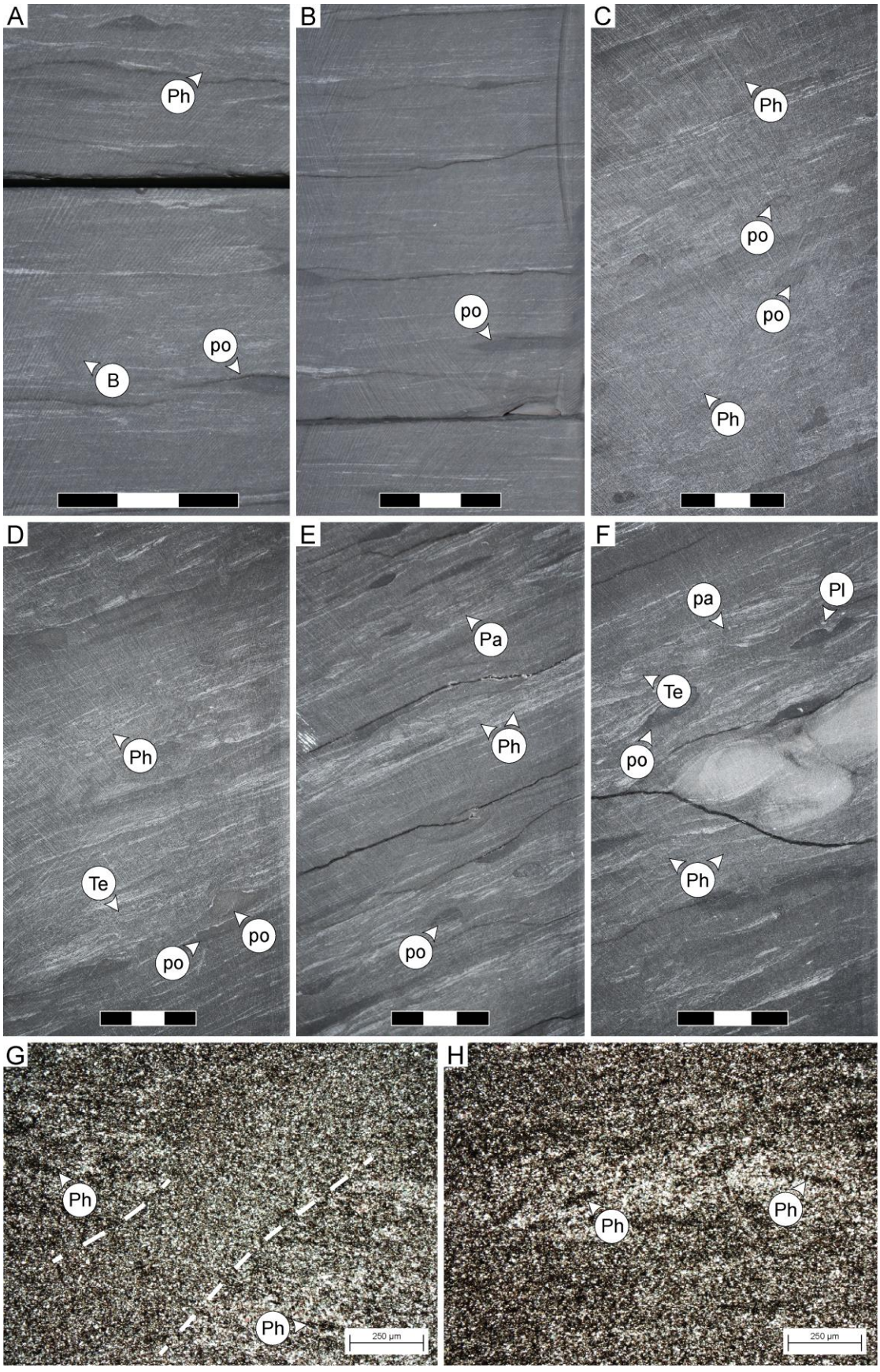
A
Ph
po
B
B
po
C
Ph
po
po
Ph
D
Ph
Te
po
po
E
Pa
Ph
po
F
pa
Pl
Te
po
Ph
G
Ph
Ph
250 µm
H
Ph
Ph
250 µm

Figure 2.14 (previous page): Facies 5 **A)** d-48-A/94-B-9 at 2055.30 metres: wispy fabric is dominant and phosphate lenses (po) occur. Diminutive trace fossils of *Bergaueria* (B) and *Phycosiphon* (Ph) **B)** Well d-48-A/94-B-9 at 2055.40 metres: discontinuous laminae and phosphatic lenses are present. **C)** Well d-66-I/94-B-16 (deviated well) at 2007.71 metres: intense overprinting of *Phycosiphon* (Ph). This example has abundant discontinuous laminae. **D)** Well d-66-I/94-B-16 (deviated well) at 2008.20 metres: trace fossils include *Phycosiphon* (Ph) and *Teichichnus* (Te) **E)** Well d-66-I/94-B-16 (deviated well) at 2013.65 metres: bioturbated intervals interbedded with non-bioturbated, planar laminated siltstone. Trace fossils include *Palaeophycus* (Pa) and *Phycosiphon* (Ph). **F)** Well d-66-I/94-B-16 (deviated well) at 2014.20 metres: phosphate nodule and lenses are present and the only occurrence observed within the study of these large cemented concretions of unknown origin. Trace fossils include *Palaeophycus* (Pa), *Planolites* (Pl), *Phycosiphon* (Ph), and *Teichichnus* (Te). **G)** Well d-66-I/94-B-16 (deviated well) at 2008.84 metres: a vertical structure/trace fossil is observed separating coarser laminae to the left and right. *Phycosiphon* (Ph) are observed at the dark arches. H) Well d-66-I/94-B-16 (deviated well) at 2008.84 metres: shows a lens of coarser laminae that produce the wispy fabric of this facies and *Phycosiphon* (Ph) are more readily identified in the coarser lenses.

2.11 Discussion

2.11.1 Deposition of the Upper Montney and Significance of the Pinstripe Laminae

Fine-grained sediment is transported from the continents by fluvial discharge, coastal erosion and aeolian transport (Stow, 1985). Palaeoenvironmental conditions during the Triassic, and the mineralogy of the Montney Formation (quartz, feldspar, minor mica and minor clay) are consistent with sediment delivery in an arid coastal depositional system. Although aeolian transport was likely a significant contributor to delivering fine- to very fine-grained silt (3-15 microns) to the system, medium to coarse silt and very fine-grained sand would have been transported dominantly by fluvial processes. Although perennial river systems were likely rare on the coastline of Triassic northwestern Pangaea, and like all modern desert systems, ephemeral river systems were likely common. A modern analogue, the coast of Namibia, is influenced by strong, arid winds that transport sand from the coast, producing massive dunes (20-50 metres high, 165 kilometres long, and 6-20 kilometres wide) in the coastal interior (Skeleton Coast erg; Krapf et al., 2003). Sand is delivered to the coastline primarily through fluvial discharge in a series of ephemeral river systems that flow sporadically for short periods that may be separated by years, decades or longer (Jacobson, 1995; Krapf et al., 2003; Stollhofen et al., 2014). To date, only two perennial river delta systems have been identified: the Dixonville delta in Alberta, and the Ring-Pedigree Delta on the Alberta-British Columbia border (Zonneveld and Moslow, 2014). Although aeolian dunes are impressive features, fluvial systems are the primary transport vector in deserts / arid zone settings. Dryland rivers routinely have suspended load concentrations that greatly exceed those of tropical / temperate systems (Powell, 2009).

Perennial river delta deposits differ from ephemeral river deltas in part by their anomalously high clay content (Zonneveld and Moslow, 2014), an unusual feature in the Montney Formation. The abundance of clays in perennial river deltas is attributed to chemical weathering during long periods of aqueous submersion (Zonneveld and Moslow, 2014). In ephemeral rivers, periods of submersion were short and episodic, and thus chemical degradation of feldspars and micas was minimal and mechanical weathering (abrasion through grain-grain interactions) was

dominant. Thus, little clay was transported down the Montney ephemeral river systems (Zonneveld and Moslow, 2014).

Sediment provenance studies have determined that sediment was sourced into the WCSB from allochthonous terranes, as well as from rivers feeding westward into the basin from the autochthon (Golding, 2016). The accretion of the Yukon-Tanana terrane against the North America margin occurred during the late Permian (named the Klondike orogeny) (Beranek and Mortensen, 2011; Golding et al., 2016). Olenekian-aged zircons derived from the Yukon-Tanana terrane suggest the initiation of a foreland basin occurred in the Early Triassic. As such, Montney deposition occurred in a more complex basin than the previously believed passive margin setting (Gibson and Barclay, 1989; Davies 1997; Beranek and Mortensen, 2011; Golding et al., 2016). Zircons from samples collected along the Alaska Highway west of Fort Nelson and subsurface wells (including c-85-I/94-B-1, d-48-A/94-B-9, and 16-17-83-25W6) west of Fort St. John, British Columbia have similar signatures and are Anisian in age (Golding et al., 2016). During deposition of the upper Montney, changing basin morphology resulted in more continuous and widespread sedimentation by the Anisian (Golding et al., 2016). This also suggests that structural features associated with the Peace River Embayment have little effect on the distribution of sediments within the basin by the Anisian (Golding et al., 2016). These data supply critical information in the attempt to understand depositional processes and circulation patterns within the basin.

Processes that affect the transportation and deposition of fine-grained sediments in the deep ocean can be categorized into three main groups: turbidites, contourites, and pelagites / hemipelagites (Stow, 1985). The first two processes will be discussed as affecting deposition of the upper Montney. The latter was not observed and therefore will not be considered. There is a continuum between these deep processes and their identification is especially difficult in fine-grained sediments (Hill, 1984). The Montney Formation was likely deposited in a low-relief clastic ramp setting with water depths not likely exceeding approximately 150 metres (Zonneveld, pers. comm. 2017). The upper Montney is interpreted to be the result of unconfined low-density turbidity currents. Classical sand turbidites have been recognized in the Montney Formation but they are, at present, restricted to a few locations. The turbidites related to the Upper Montney are silt turbidites and extensive studies relating to fine-grained deposits have been conducted as a result of the onset of the Deep Sea Drilling Project (DSDP) in 1968 (e.g. Piper, 1973; Jipa and Kidd, 1974; Piper and Brisco, 1975; Stow, 1979; Hill, 1984; Stow and Tabrez, 1998; Stow et al., 2002).

Fine-grained turbidites of the upper Montney compare favourably with the silt turbidite model of Stow and Piper (1984). Silt turbidites display the same vertical sequence as classic sand turbidites (Bouma, 1962), but lack significant grain size variations and, in the case of the upper Montney, are dominated by silt alone (Stow and Piper, 1984). In a distal setting, the sediment is finely laminated, graded, homogenous or a combination of these structures (Stow,

1979; Hesse and Chow, 1980; Gorsline, 1984). This corresponds to Bouma D and E subdivisions and comprise Facies 1. This facies corresponds to the most distal expression of the turbidites and reflects deposition well below storm wave base. Cores through the lower upper Montney commonly alternate F1A and F1B, representing planar laminated silt followed by suspension deposition. The overall pattern of the Upper Montney is a progradational system as represented by the progression from F1 to F2 upwards. Bouma B-C and B-C-D sequences are common when F2 is present. The increase in pinstripes (i.e. grain size) corresponds to settings more proximal to the sediment source and where wave-reworking is present. The limited occurrence of F2C indicated deposition occurred below fair-weather wave base. The best expression of F2C occurred in d-49-A/94-B-9 and may be attributed to rapid progradation and geographic isolation, however, the distribution of cores limits understanding facies distribution.

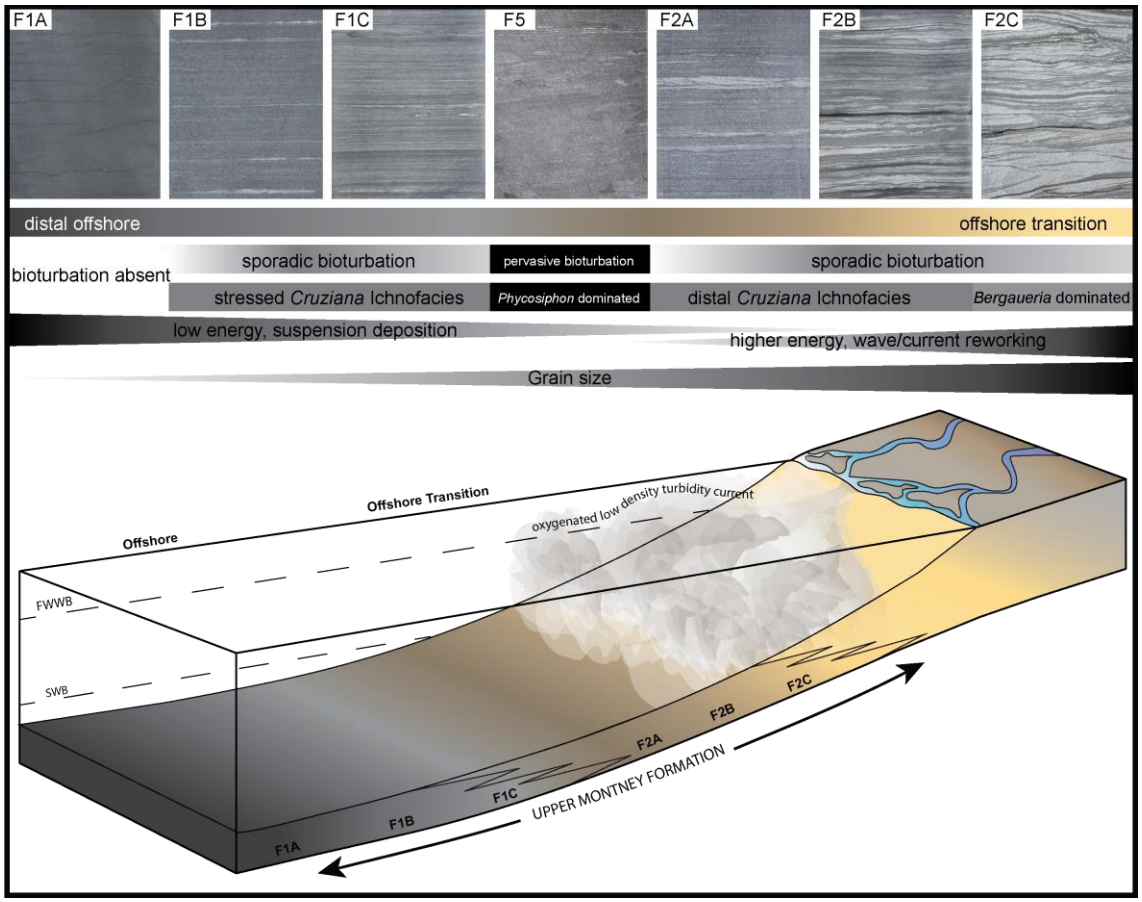

Figure 2.15: Depositional model of the upper Montney Formation. One facies association was identified representing the distal offshore to offshore transition zone. F3, F4 and F5 are not included on this model. F4 occurs below the Smithian – Spathian boundary, F3 represents isolated intervals of possibly storm deposited material. F5 represents an oxygenated interval in the offshore environment.

Low-density turbidity currents are the best mechanism to explain the generation of pinstripe laminae. It has been suggested that the alternation of fine and coarse laminae is the product of velocity fluctuations resulting in the interchange of bed load and suspended load

(Piper, 1978; Hesse and Chough, 1980). Fine-grained turbidites off the coast of Nova Scotia have documented the occurrence of fine silt laminae in mud turbidites that relate to division D of the Bouma sequence (Bouma, 1962; Hesse and Chough, 1980). Fluid mechanics show that the lowest layers (viscous sublayer and buffer/transitional layer respectively) of the boundary layer in turbulent flow experience high- and low-velocity streaks that result in “bursts-and-sweeps” (Kline et al., 1967; Bridge, 1978; Hesse and Chough, 1980). As a result of density decreasing, the viscous sublayer cannot remain in turbulence and laminar flow occurs periodically producing clay laminae (Hesse and Chough, 1980). Individual silt laminae form due to shear sorting during multiple burst-and-sweep cycles (Hesse and Chough, 1980). Stow (1977), proposed that silt and clay laminae form as a result of clay flocculation. In this model, during the waning stages of a current when shear stress drops enough, silt deposition occurs, resulting in clay concentration increase, which leads to re-flocculation. Both mechanisms explain the formation of fine scale silt laminae, but the proportion of clay in the upper Montney is less than in these studies and flocculation processes were minimal (Stow, 1977; Hesse and Chough, 1980). Despite the lithology variation, the “bursts-and-sweeps” model seems more likely as a mechanism for the upper Montney and also explains the occurrence of small-scale ripples of flat beds (Hesse and Chough, 1980). This model considers bed-scale interactions of fine-grained sediment within turbidity currents, as a result of the separation of coarser silt grains from finer silt grains. As a result of diagenesis, coarser laminae were preferentially subject to carbonate cementation. This fine-scale grain size variation resulted in the pinstripe laminae fabric.

Silt turbidites have been documented on the continental margin of Antarctica, the Gulf of Alaska, the Arabian Sea, and the Angola Basin (Piper, 1973; Jipa and Kidd, 1974; Piper and Brisco, 1975; Stow, 1984; van Weering and van Iperen, 1984). Strong evidence for distinguishing turbidity currents is the occurrence of soft-sediment deformation features, water escape features and climbing ripples with no erosion (Piper and Brisco, 1975). The first two are readily observed in F1 and F2 in the upper Montney. However, the occurrence of starved ripples has been interpreted to represent contourites in many silt turbidites (Piper and Brisco, 1975). There is a continuum between fine-grained turbidites and contourites, and the distinction becomes particularly difficult for distal expressions of fine-grained deposits.

The occurrence of thin silt laminae is a feature observed in both contourites and turbidites and distinguishing criteria is difficult (Piper and Brisco, 1975). Despite establishing various criteria, it is possible that contourites may be distal turbidites (Piper and Brisco, 1975). General characteristics from the literature are dependent on the location of study and how they compare with local fine-grained turbidite deposits (e.g. Piper and Brisco, 1975; Shor and Flood, 1984, Stow and Piper, 1984). Fine-scale laminae in contourites are irregular or wispy and discontinuous (Piper and Brisco, 1975 Stow and Piper 1984) Laminae associated with turbidites are more regular and continuous (Piper and Brisco, 1975). Figure 2.16-D represents a sample from the

margin of Antarctica (site 268) in which the silt laminae are interpreted to have formed from bottom currents. Figure 2.16 A-C are examples that are interpreted as turbidites from the Angola Basin, the North Sea, and Nova Scotia, respectively. This visual comparison closely resembles characteristics found in the upper Montney; however, the distinction between contourites and turbidites remains ambiguous. A consideration to keep in mind when comparing different formations to the Montney Formation is that similar sedimentary structures that may be produced by similar processes (i.e. contour currents or low-density turbidity currents), and this can be considered independent of composition (i.e. mud or silt). The upper Montney likely experienced both turbidity current and contour current processes. Low-density turbidity currents are responsible for supplying sediment into the deep basin and pinstripe-laminated fabric can form under these low-energy conditions. The rare occurrences of starved ripples in F1 may have resulted from deep contour currents or indicate proximity to the turbidity current.

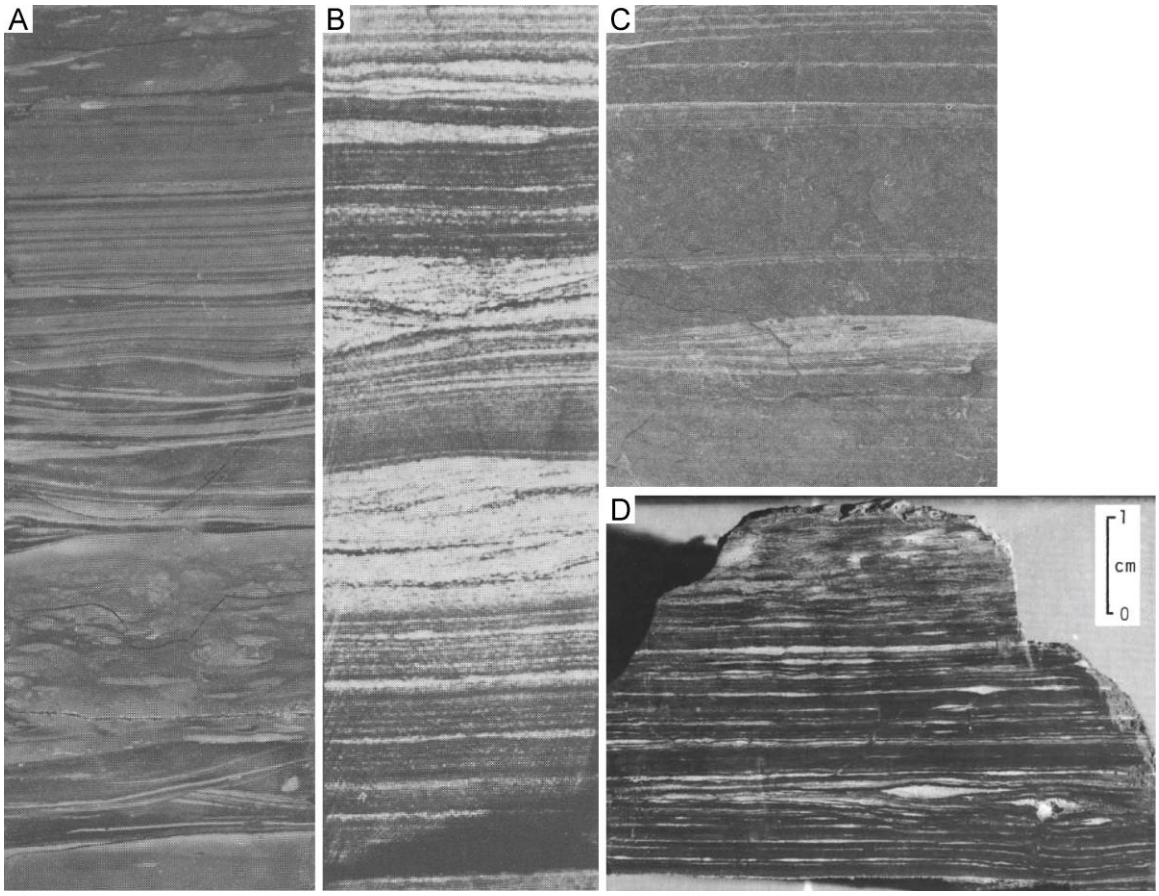

Figure 2.16: A) Silt turbidite from the Upper Cretaceous, site 530A, Angola Basin. Modified from Stow and Piper (1984). **B)** Silt and mud turbidites from the upper Jurassic, North Sea. Modified from Stow and Piper (1984). **C)** Mud turbidite with silt laminae from the Halifax Formation, Nova Scotia. Modified from Stow and Piper (1984). **D)** Silt laminae are interpreted to have formed from contour currents. Laminae are lenticular and minor bioturbation is observed. Modified from Piper and Brisco (1975).

Contour currents have been interpreted to be responsible for deposition of the "*Claraia* Zone" in the lower Montney Formation (Sanders, 2016). However, there is a limited understanding of circulation patterns on the margin of Pangaea during the Early Triassic. Kutzbach (1990) modelled circulation, temperature, and salinity in an attempt to explore possible conditions of the ocean's climate during the early Mesozoic. The models indicate that a strong thermohaline circulation can occur when north-south temperature gradients are small (Kutzbach, 1990). This resulted in strong overturning and has been linked with anoxia (Kutzbach, 1990). A drawback of Kutzbach's model is that he considered only large-scale circulation patterns (Kutzbach, 1990). Processes within the Montney basin occur at a much smaller scale, and with the possibility of a partial western restriction, circulation could have been much different. Certainly, a western sediment source was in close proximity to the study area during deposition of the upper Montney as zircons derived from allochthonous terranes have been identified in the WCSB by the early Anisian (Golding et al., 2016). True geostrophic contourites have been associated with currents on shallow platforms of depth 500-700 metres and abyssal plain of depths greater than 5000 metres (Faugères and Stow, 1993). The currents at play were likely due to strong winds rather than thermohaline processes and reworked material deposited by turbidity currents (Faugères and Stow, 1993).

Bioturbation in the upper Montney is distributed sporadically and understanding of the distribution proves to be difficult. Geochemical analyses have revealed that Early Triassic oceans experienced anoxic waters on continental margins globally (Lau et al., 2016). Modelling by Lau et al. (2016) provide evidence for an expanded oxygen minimum zone rather than deep-ocean anoxia. Anoxia decreased for 5-million years after the end-Permian extinction and pre-extinction conditions returned in the Middle Triassic with biological communities increasing in abundance, diversity and size (Lau et al., 2016). The sporadic nature of bioturbation may be attributed to turbidity currents delivering appreciable quantities of oxygen to low oxygen settings (Emery et al., 1962). The most prolific assemblage of marine fauna from the Early Triassic (Spathian) was from the Virgin Formation in southwest Utah (Hofmann et al., 2012). To provide a sense of the diversity, 30 benthic species and 14 ichnogenera were observed in this siltstone formation (Hofmann et al., 2012). Additional studies from this area also conclude that environmental conditions such as alkaline and anoxic water affected shallow marine environments (Boyer et al., 2004; Hofman et al., 2012). The assemblage observed is interpreted to indicate normal marine, well-oxygenated conditions resulting from current agitated waters and low siliciclastic input (Hofmann et al., 2012). Within the Spathian, the occurrence of bioturbation is dependent on local parameters within the sub-basin and is intensely controlled by the delivery of oxygen-rich water via turbidity currents. However, turbidity currents may have negatively affected bioturbation due to high sedimentation and/or high frequency.

2.11.2 Sequence Stratigraphy

The upper Montney Formation represents a prograding depositional sequence and forms steeply dipping clinoforms. The overall coarsening upward sequence is characterized by the progression from F1A through to F2C representing deposition within the distal offshore to offshore transition zone. The overall prograding sequence consists of numerous partial sequences (e.g. F1A-F1B-F2A; F1B-F1C-F2A; F2A-F2B). Rapid prograding sequences resulted in facies to switch very readily and are difficult to correlate to wire-line logs. The sequence stratigraphic framework follows the regional paradigm, and building upon that framework is beyond the scope of this study.

The base of the upper Montney is marked by the Sm-Sp boundary and is easily identifiable on well logs by an increase on the gamma log. This surface is interpreted to mark a major transgression and its identification is difficult in this distal setting, whereas in more proximal settings a lag deposit is observed. The lower portion of the sequence is dominated by F1 and a flooding surface marks the change to the occurrence of F2. Overall, there are three significant surfaces (including the Sm-Sp boundary) that are interpreted as flooding surfaces and correspond to facies changes in core. These surfaces are marked in blue in Figure 2.18. However, additional surfaces are marked in black are also indicated in Figure 2.18, but their significance in unclear. Based off the log signature, they appear as gamma kicks which are commonly identified as flooding surfaces, however the core does not reflect this interpretation. Small prograding sequences within F2 are difficult to relate to the well log.

Figure 2.17 (next page): Representative lithology log of the well d-48-A/94-B-9. This log represents the entire upper Montney from the Smithian-Spathian boundary to the base of the Doig Phosphate Zone.

d-48-A/94-B-9

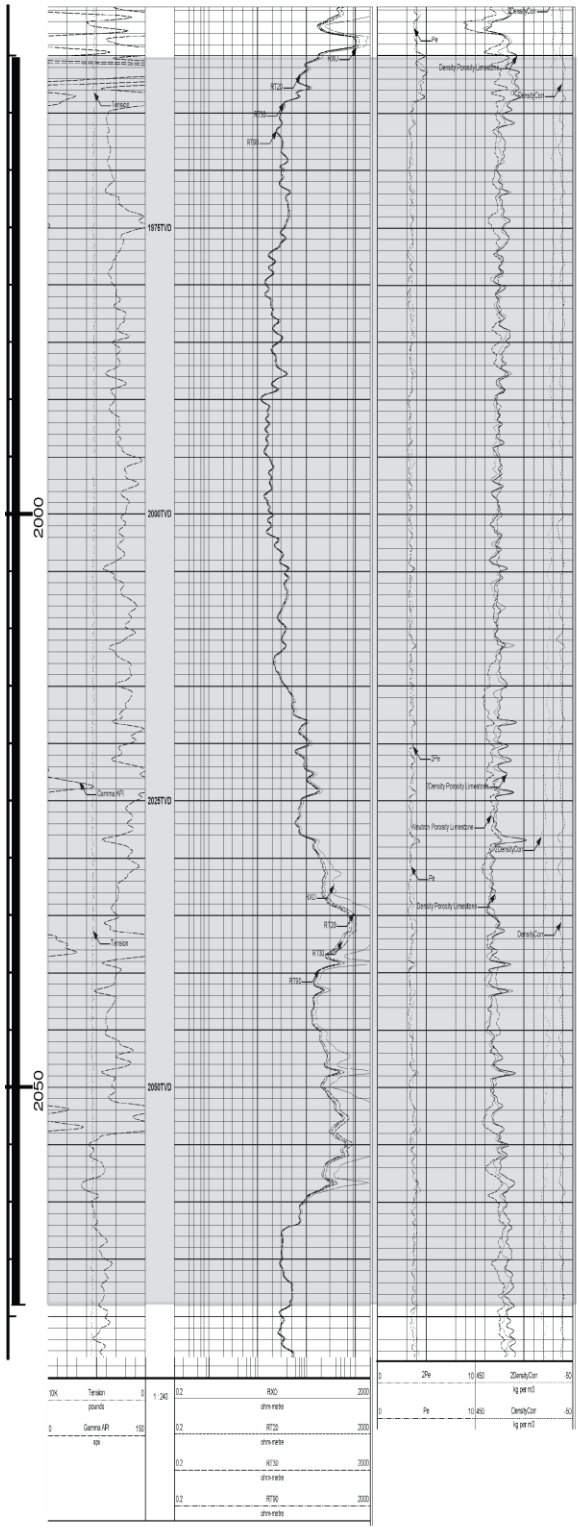
2000
2050
1978TVD
2008TVD
2028TVD
2058TVD
Tension
Gamma API
RXO
RT20
RT30
RT90
Pe
Density Porosity Limestone
Neutron Porosity Limestone
DensityCorr

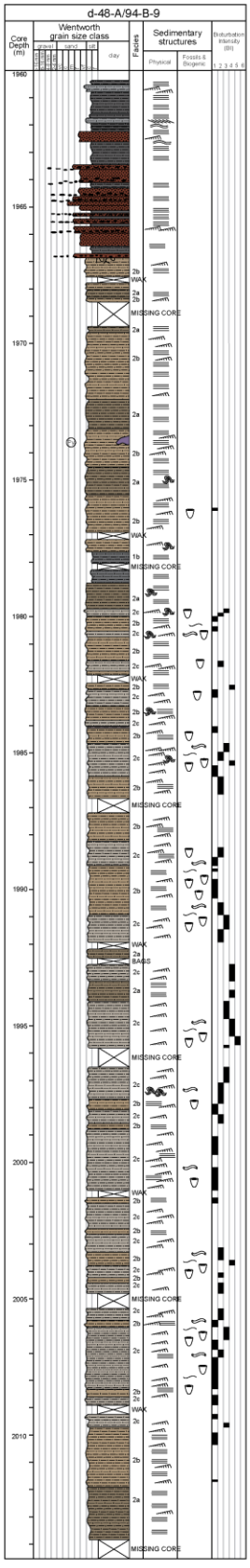
d-48-A/94-B-9
Core Depth (m)
Wentworth grain size class
gravel
sand
silt
clay
Facies
Sedimentary structures
Physical
Fossils & Biogenic
Bioturbation Intensity (BI)
MISSING CORE
WAK
BAGS
SAMPLING BAGS

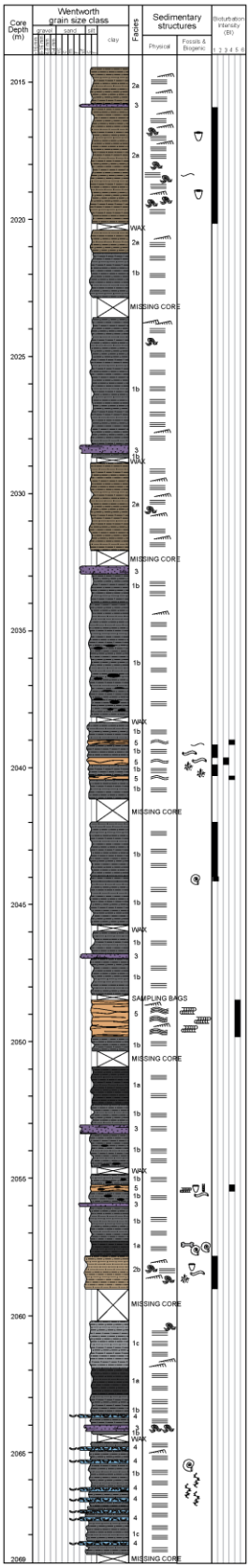
Core Depth (m)
Wentworth grain size class
gravel
sand
silt
clay
Facies
Sedimentary structures
Physical
Fossils & Biogenic
Bioturbation Intensity (BI)
MISSING CORE
WAK
SAMPLING BAGS

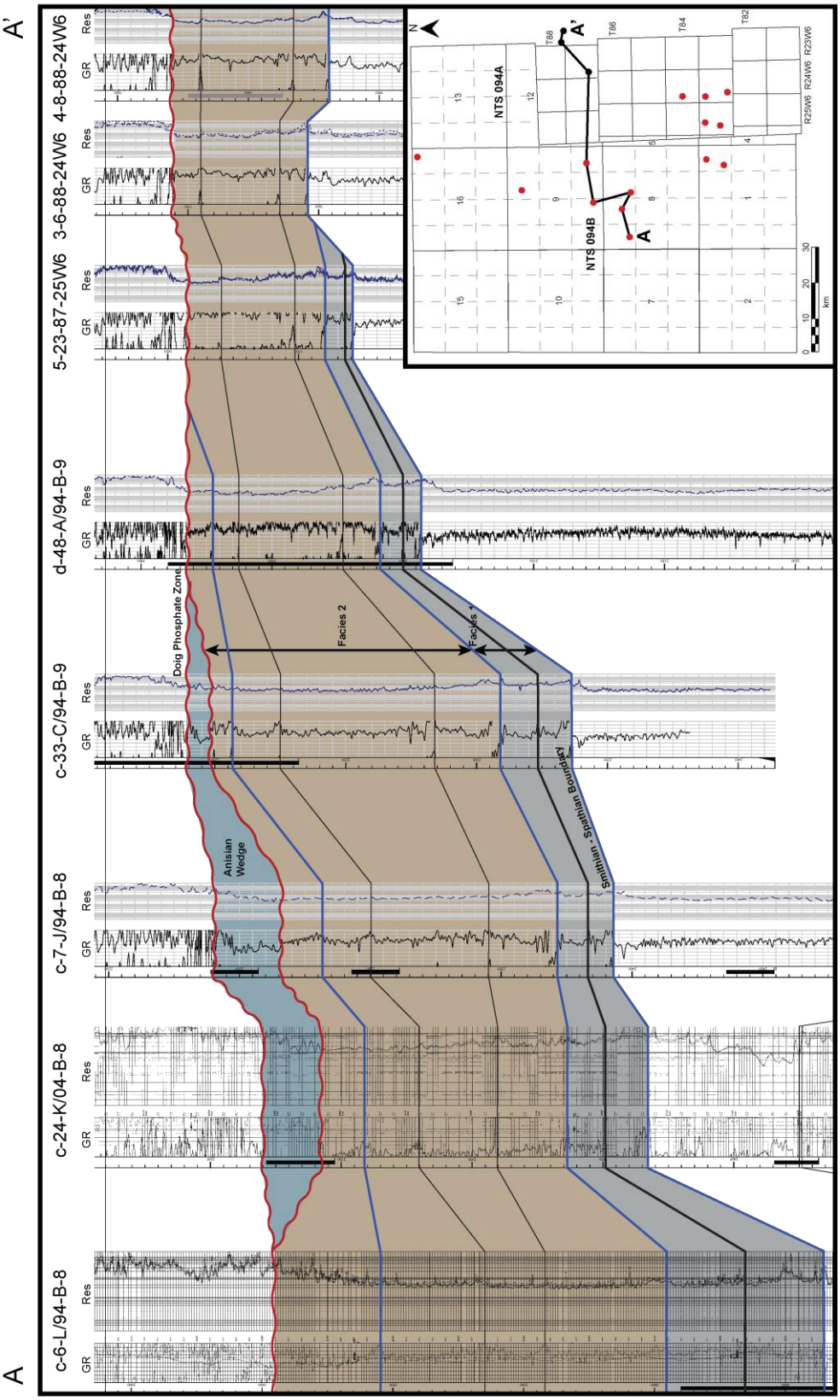
A
A'
c-6-L/94-B-8
c-24-K/04-B-8
c-7-J/94-B-8
c-33-C/94-B-9
d-48-A/94-B-9
5-23-87-25W6
3-6-88-24W6
4-8-88-24W6
Res
GR
Doig Phosphate Zone
Facies 2
Facies 1
Anisian Wedge
Smithian - Spathian Boundary
N
NTS 094A
NTS 094B
A
A'
T88
T86
T84
T82
R25W6
R24W6
R23W6
km

Figure 2.18 (previous page): Cross section of the upper Montney Formation. This is a dip-section across the study area. The surfaces in blue correlate to the core and represent true flooding surface and reflect facies changes. The black surfaces are interpreted flooding surfaces based on the gamma log however their significance is unclear. The black rectangles along the depth track correspond to available core used in this study. Top of the Doig-Phosphate Zone was used as the datum.

2.12 Conclusions

The upper Montney Formation of northeastern British Columbia is a fine-grained deposit that is interpreted as a progradational succession with deposition occurring within a narrow interval in the offshore setting. Detailed sedimentological, ichnological and lithological data suggest that deposition occurred from the distal offshore environment to the offshore transition zone, where low-density turbidity currents were the dominant mode of sediment transport. Five facies were identified, however one facies association representing an overall prograding sequence is characterized by the progression from F1A through to F2C. F1 is observed in the lower portion of the upper Montney and it is overlain by F2. Numerous small-scale parasequences are observed and the readily changing facies do not always correspond to surfaces identified on the gamma log. Bioturbation is characterized as a stressed *Cruziana* Ichnofacies, however, the distribution of bioturbated intervals is very sporadic. Multiple factors are at play that affects the distribution: turbidity current flow, suspended sediment load, anoxic / dysoxic conditions, and oxygenation by turbidity currents.

The formation is dominated by fine- to coarse-grained silt in which fine scale silt laminae form due to shear sorting from “burst-and-sweep” cycles affecting grains in the low layers of a turbulent flow (Hesse and Chough, 1980). This small-scale sorting of grains formed the pinstripe-laminated fabric that dominates this interval. As the overall sequence progrades and approaches fair-weather wave base wave reworking becomes more prominent.

Deposition during this time was sourced from two locations, eastern Laurentia and a western accreting Yukon-Tanana terrane. Paleozoic zircons found within Olenekian-aged deposits reveal strong evidence that the onset of the foreland basin began in the early Triassic (Beranek and Mortensen, 2011; Golding et al., 2016). The implications of changing basin morphology from the previously believed passive margin are not yet understood (Gibson and Barclay, 1989; Davies 1997). This western high would have restricted the basin, which has implications for basin circulation and understanding the affects of currents and distribution of anoxia. As well, structure through this region is poorly documented.

The challenge with the Montney is its fine-grained nature and the consequence that changes are subtle. There are major challenges that still arise when understanding the Montney and the success of a well over another. Issues with correlating the core to well logs occur because major cycles interpreted from a gamma log don’t match observations in core. The correlation to core logs identifies meaningful surfaces based on core observations.

CHAPTER 3: THE RELATIONSHIP BETWEEN BIOTURBATION AND PERMEABILITY IN FINE-GRAINED DEPOSITS, AN EXAMPLE FROM THE UPPER MONTNEY FORMATION, NORTHEAST BRITISH COLUMBIA

3.1 Introduction

Profile permeametry analysis (spot-permeability) has been the method of choice for various studies investigating the relationship between permeability and bioturbation (e.g. Pemberton and Gingras, 2005; Tonkin et al., 2010; Lemiski et al., 2011; La Croix et al. 2013; Baniak et al., 2015; Zhang et al., 2015; Furlong et al., 2016). Spot-permeability analysis provides a small-scale measurement where burrow and matrix permeability can be assessed. Spot-permeametry discussed in this chapter was conducted using a Core Laboratories Pressure Decay Profile Permeameter (PDPK-400). Major benefits of this machine include: high-resolution data relative to routine core data, point precision for measurements, ability to measure small-scale heterogeneities, rapid data collection, and overall low operating cost (Clarkson et al., 2012). However, its utility in tight reservoirs has not been evaluated and uncertainty remains as to its reliability. The data suite was collected from a core (d-66-I/94-B-16) from the upper Montney Formation in northeast British Columbia.

Spot permeametry analysis was undertaken on eleven samples, representing a range of pinstripe laminated, rippled and bioturbated fabrics that were deposited on the distal margin of a shallow ramp between the distal offshore and offshore transition zone. The results of spot-permeametry testing indicate that the occurrence of bioturbation enhances permeability; however, it is dependent on relatively high bioturbation intensities that destroy or significantly disrupt primary sedimentary structures and limit carbonate cementation. Cryptic bioturbation that disrupts the laminae, forming a dashed fabric, do not significantly change the distribution of pore aperture sizes. The occurrence of bioturbation has recently proven to be significant for reservoir properties such as permeability and water saturation within the Montney Formation (e.g. Clarkson et al., 2012; Wood, 2013; Zhang, 2015; Furlong et al, 2016), but may be easily overlooked as a result of its sporadic distribution and discrete nature.

The purpose of this chapter is to investigate the function of spot-permeametry on a fine-grained unconventional reservoir to characterize biogenic permeability and permeability anisotropy. This study provides insight into small-scale heterogeneities observed within different fabrics from fine-scale measurements from a spot-permeameter. The heterogeneities (fine laminae and micro-burrows) are much smaller than the size of the probe tip, however, this is the most discrete measurement that can be obtained. For this study, a new technique was designed to evaluate anisotropy within a given fabric. As a result of the analysis performed on a deviated well, true vertical and horizontal permeability was not analyzed. However, the bulk permeability of a representative fabric was determined. This study provides insight into permeability trends

related to bioturbation and evaluates the effectiveness of a spot-permeameter for a fine-grained reservoir.

3.2 Background

Many studies have demonstrated the importance of the relationship between reservoir properties (i.e. porosity and permeability) and bioturbation (e.g. Gingras et al., 1999; Pemberton and Gingras, 2005; Tonkin et al., 2010; Lemiski et al., 2011; La Croix et al., 2013; Baniak et al., 2015). Biogenic permeability affects the storability and deliverability of resources in reservoirs and is an important aspect in the construction of robust, predictive reservoir models (Gingras et al., 2012). Bioturbation alters the primary sedimentary fabric by destroying physical sedimentary structures, changing grain distributions and altering geochemical characteristics of the host sediments (Gingras et al., 2012). As a result, trace fossils have significant implications for the distribution of permeability and porosity in petroleum reservoirs. These modifications can result in the reduction or enhancement of bulk permeabilities in biogenic fabrics (Gingras et al., 2012).

Pemberton and Gingras (2005) proposed five categories for biogenic flow networks: (1) surface-constrained discrete heterogeneities, (2) non-constrained discrete heterogeneities, (3) weakly defined heterogeneities, (4) cryptic heterogeneities, and (5) diagenetic heterogeneities. These categories were developed to provide a framework for burrow-related heterogeneities. Within these five categories, biogenically enhanced permeability can be classified into two types of flow media: dual-porosity or dual-permeability networks (Gingras et al., 2009; Gingras et al., 2012). Dual-porosity networks occur when the matrix permeability and the burrow permeability are within two orders of magnitude (Gingras et al., 2009; Gingras et al., 2012). Dual-permeability networks occur when matrix permeability and burrow permeability highly contrast (differs by greater than two magnitudes of order) (Gingras et al., 2009; Gingras et al., 2012). In dual-porosity systems, both the burrows, and the matrix, contribute to fluid flow, whereas in dual-permeability systems only high permeability zones contribute to fluid flow (Gingras et al., 2009; Gingras et al., 2012).

Imaging techniques provide the ability to model the three-dimensional burrow networks. Computed tomography (micro-CT) scans have proven useful for providing three-dimensional images of biogenic networks in small volumes of rock (e.g. La Croix et al., 2013; Baniak et al., 2015). This method can characterize pore geometries and visualize burrow networks; however, it requires a density difference between the burrows and the matrix (La Croix et al., 2013). For this reason, micro-CT scans have limited success for the Montney Formation. Magnetic resonance imaging (MRI) provides a three dimensional image of fluids within a rock sample and can be used to map the distribution of pore space (e.g. Gingras et al., 2002a,b).

Biogenic fabrics can be incredibly involved and complex. Core analysis and outcrop studies provide two-dimensional spatial information, but observations are dependent on the size

and quality of the outcrop or rock sample (Gingras et al., 2012). Outcrops may provide insight into the spatial distribution of the burrow network, however, samples for biogenic permeability analysis techniques usually consist of small core pieces or core plugs (Gingras et al., 2012). Upscaling small-scale observations to the core, well bore or reservoir level is limited. Upscaling issues relate to the nature of the biogenic fabric and the representative elemental volume (REV) of the sample. The REV represents the sample volume that is large enough to capture a representative amount of heterogeneity (Bear, 1972). Issues arise when re-scaling data of different volumes in heterogeneous media because permeability varies with sample volume, therefore the determination of the REV is required (Nordahl and Ringros, 2008). Variations in bioturbated fabrics may increase or decrease the continuity and heterogeneity of permeability distribution. Cryptic bioturbated or complete biogenic reworked fabrics remove internal heterogeneities and result in more uniform distribution of permeability (Pemberton et al., 2008). Biogenic fabrics consisting of discrete burrows are extremely heterogeneous and their continuity may be less predictable (Gingras et al., 2012).

3.3 Previous Research

Minimal information is currently available regarding the relationship between permeability and bioturbation in unconventional reservoir plays. Only within the last few years have studies investigated this relationship in the Montney Formation in Alberta and British Columbia (e.g. Clarkson et al., 2012; Wood, 2013; Zhang, 2015; Furlong, 2016). Bioturbation is easily misidentified within the distal Montney, as a result of the diminutive size of trace fossils, a lack of colour variation and subtle grain size variation (i.e. grain size variation within very restricted limits). Discrete changes in sedimentary structures and bioturbation will go unnoticed unless the core under examination is properly cleaned. Cores are commonly covered in drilling mud that coats these discrete heterogeneities and cause the core to appear more homogenous. Even when cleaned, the rough outer surface of an unslabbed core may preclude detailed examination on fine scales. The understanding of the distribution of bioturbation remains somewhat uncertain within the basin, which is undoubtedly a factor contributing to confusion regarding the causes of compartmentalization of resources.

Zhang (2015) tested biogenic permeability of the Montney Formation in the Puskwa Field in Alberta. Permeability measurements were obtained using the PDPK-400 spot-permeameter. Zhang (2015) interpreted the Montney Formation to represent deposition within proximal offshore to lower shoreface environments, with permeability values within this region ranging from 0.02-0.9 and 2-20 millidarcies. This is a significant range in permeability measurements and is related to the proximity of the study area and coarser-grained sediment (coarse silt to very fine-grained sandstone). Bioturbated sandstone units were regarded as fluid flow conduits as a result of their

higher bioturbation intensity and corresponding higher permeability measurements (Zhang, 2015).

Preliminary studies of intensely bioturbated zones within the Anisian Wedge (see Chapter 2) showed significantly higher permeabilities ranging from 0.2 to 1.0 millidarcies compared to non-bioturbated zones of very similar nature to the upper Montney, ranging from 0.01-0.08 millidarcies (Furlong et al., 2016). This study characterizes a unique bioturbated interval that is significantly different from the upper Montney within the study area. However, it represents another instance in which permeability was enhanced by the occurrence of bioturbation.

Clarkson et al. (2012) investigated non-routine core analytical methods to characterize permeability heterogeneities and pore structure of the basal part of the upper Montney in the Pouce Coupe area. This study demonstrated that routine core analyses are inadequate to evaluate reservoir characteristics because the tests are not performed *in situ* reservoir conditions. The same spot-permeameter (PDPK-400) was used and the permeability data was corrected to *in situ* conditions by using pulse decay permeability (PDK-200) measured at reservoir overburden conditions (Clarkson et al., 2012). A new technique, N_2 absorption isotherms were used to estimate pore size distribution and pore shape to aid in identifying a flow-unit. A flow-unit is defined as a unit characterised by a similar pore type (Clarkson et al., 2012). This study concluded that within the observed core only one flow unit existed (Clarkson et al., 2012).

Wood (2013) reported that water distribution was related to stratigraphic architecture and the degree of bioturbation. Within the lower Montney, low gradient clinoforms and a relatively homogenous fabric resulted in efficient water displacement and water content close to irreducible water saturation. In contrast, greater facies variation in the upper Montney results in less efficient water displacement and as such more water is retained (i.e. higher percent of BVW – bulk water volume) (Wood, 2013). The BVW correlates positively to porosity and higher degrees of bioturbation. The bioturbation within this study was qualitatively characterized by the extent to which sedimentary structures and laminae were disrupted (Wood, 2013).

3.4 Methods

3.4.1 Facies Selection

One well within the previously described study area (d-66-I/94-B-16) was chosen for spot-permeability analysis. This core was chosen because it is a complete upper Montney core on the northern extent of the study area. The facies chosen for analysis in this paper are described and are interpreted in Chapter 2 (Figure 3.1). Eleven samples were chosen for spot-permeametry analysis representing a range of pinstripe laminae, rippled and bioturbated fabrics. A sample ranges from 6 to 20 centimetres in length and are slabbed pieces of core. Overall, the samples are part of a prograding sequence and interpreted to represent deposition within the distal offshore and offshore transition environment. However, this sequence consists of numerous

small-scale, prograding or shoaling upward successions. Grain size is limited to fine- and coarse-grained silt. The occurrence of pinstripe laminae is almost continuously observed with varying frequency and containing coarser grains and more carbonate (calcite and dolomite) cement.

Figure 3.1 (next page): Litholog of the core d-66-I/94-B-16 illustrating facies (Chapter 2) and depth of samples collected for spot-permeability analysis.

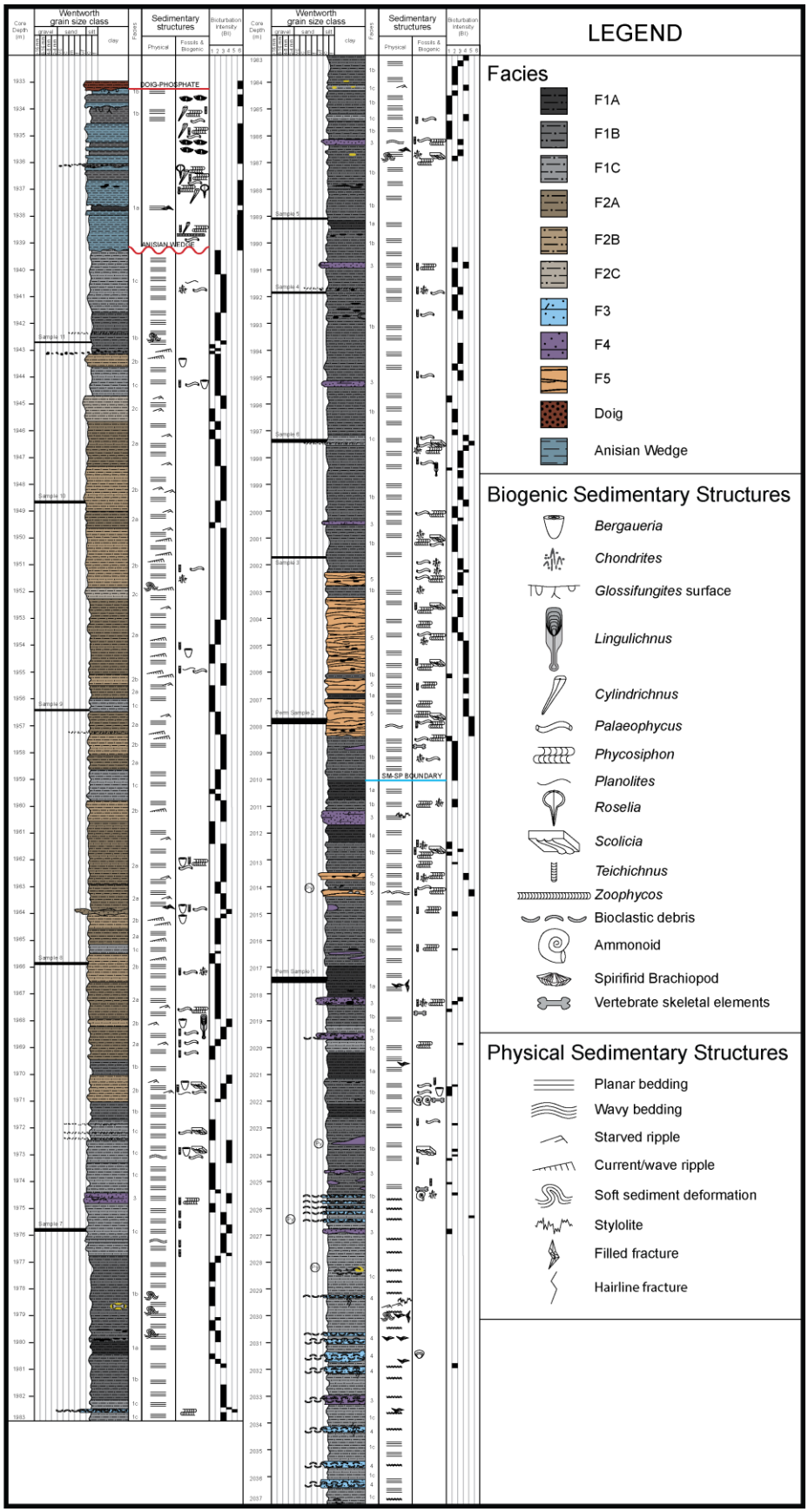
Wentworth grain size class
Sedimentary structures
Physical
Fossils & Biogenic
Bioturbation Intensity (BI)
Facies
Core Depth (m)
clay
DOIG-PHOSPHATE
ANISIAN WEDGE
SM-SP BOUNDARY
LEGEND
Facies
F1A
F1B
F1C
F2A
F2B
F2C
F3
F4
F5
Doig
Anisian Wedge
Biogenic Sedimentary Structures
Bergaueria
Chondrites
Glossifungites surface
Lingulichnus
Cylindrichnus
Palaeophycus
Phycosiphon
Planolites
Roselia
Scolicia
Teichichnus
Zoophycos
Bioclastic debris
Ammonoid
Spirifirid Brachiopod
Vertebrate skeletal elements
Physical Sedimentary Structures
Planar bedding
Wavy bedding
Starved ripple
Current/wave ripple
Soft sediment deformation
Stylolite
Filled fracture
Hairline fracture

3.4.2 Spot-Permeametry

Spot-permeametry was conducted on selected facies from the d-66-I/94-B-16 well using a Core Laboratories PDPK-400 Pressure-Decay Profile Permeameter (PDPK-400) (Figure 3.2). The PDPK-400 measures the permeability of a sample from 0.001 millidarcy (mD) to greater than 30 Darcy (D) (Core Laboratories Instruments, 1996). The small probe tip (inner diameter 0.46 centimetres) is used for samples with permeabilities less than 0.01 millidarcy. The probe tip was sealed against the flat core surface using a pneumatic cylinder. Nitrogen gas injected through the probe was recorded as a function of time. The study utilized a 1 x 1 centimetre grid pattern drawn onto the surface of slabbed core samples. The grid was drawn perpendicular to the edges of the core sample. Care was taken when drawing the grids to optimize the entire surface and to avoid edge effects. For each point, five measurements were taken, then the maximum and minimum values for each point were discarded and the remaining three values were averaged (e.g. Lemiski et al., 2011; La Croix et al., 2013). In some cases, anomalously high measurements were recorded. This was likely due to surface or internal fractures and these values were removed from the data set. Fracture points resulted in a distinct drop observed on a pressure vs. time graph viewed on the monitor. The anomalously high measurements were removed and adjacent values were averaged to represent the missing point. Horizontal points were prioritized, then vertical, and then diagonal, in that order respectively, to calculate an average value for the omitted fracture value. Averaged fracture values were not used to average adjacent fracture points.

The averaged permeability value for each point was plotted on core photographs. The dot marks the exact point at which a measurement was taken and corresponds to the center of each square. The square represents the small volume for the measured permeability. Twenty-two bins were formed for the range in permeability values and each bin was assigned a colour and a number (0-21). Heat maps were developed where cooler colours represent lower permeabilities, and warmer colours represent higher permeabilities. Eleven samples from the well d-66-I/94-B-16 from the Upper Montney Formation were analysed.

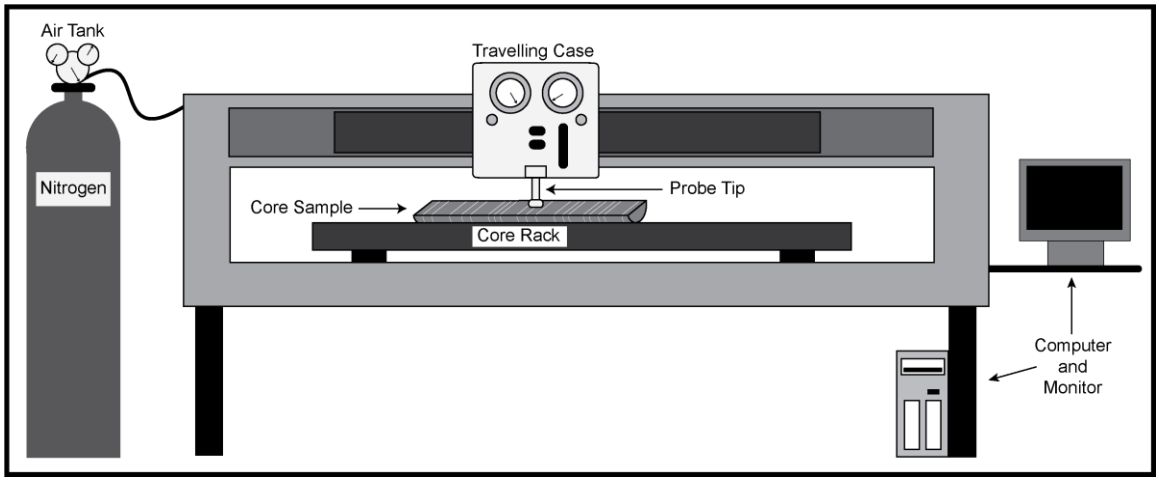

Figure 3.2: Core Laboratories PDPK – 400 Pressure Decay Profile Permeameter and the main components of the system. Modified from Core Laboratories Instruments (1996), Lemiski (2010), LaCroix (2010) and Camacho (2013).

3.4.3 Scoring Permeability Matrices – Vertical and Horizontal

A new technique was designed to investigate permeability anisotropy (vertical and horizontal). Note that the samples analyzed were from a deviated well and therefore vertical and horizontal directions are relative to the edge of the core sample and do not follow bedding. This technique simply compares a single point to two other points directly above and below, or to the left and right. An arbitrary score is assigned representing how similar or different the values are.

For each permeability measurement, bin numbers (0-21) were assigned to each point. The perimeter values were excluded and not assigned a score. Each point was assigned two score values, one for the vertical direction and one for the horizontal direction (Figure 3.3). The score is the sum of the differences for a given point for the corresponding direction (vertical or horizontal). The greater the number the more different the adjacent values are, and the smaller the score the more similar adjacent values are. A grey-scale was used to visualize the scores, lighter shades represent low scores (more similar) and darker shades represent high scores (more different).

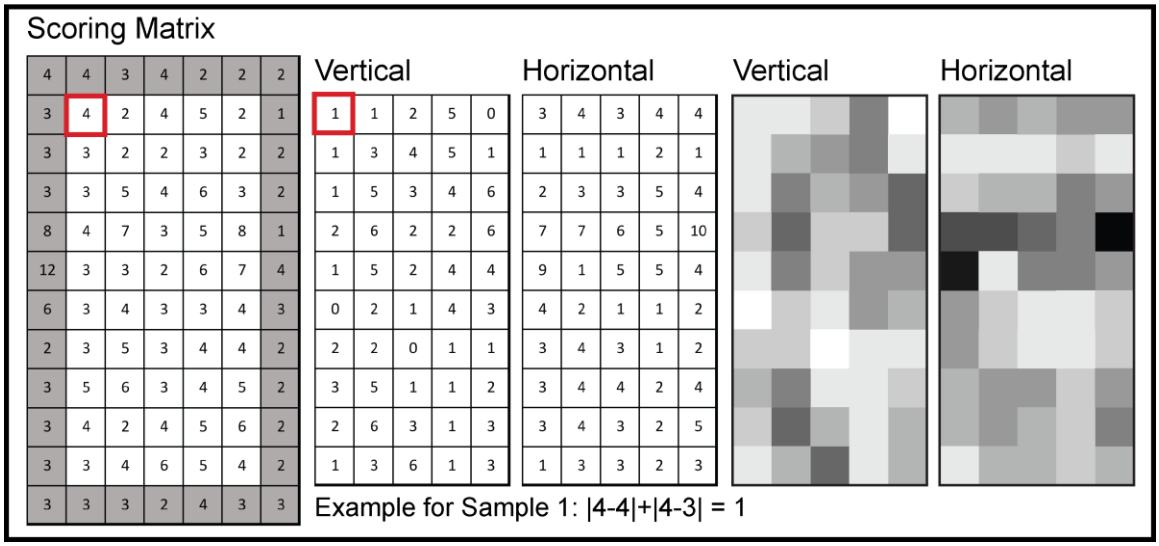

Figure 3.3: Sample 1 used as an example to show how the scores for each sample were derived. Each number in the scoring matrix is the bin number assigned for a given permeability value. The vertical and horizontal matrices represent the scores for that given direction.

3.4.4 Bulk Permeability – Double Integral Technique

Each sample was reduced to a single value to provide a representative bulk permeability value. The average was determined using a double integral method. The double integral method is a technique used to solve for the average value of a function of two variables f(x,y) over a rectangular area. It is commonly used to find average values of a temperature field and such a method can be extended and used over a set of permeability data. Permeability data collected for each sample is represented as a matrix, with specific rows and columns. This matrix can be treated as a rectangular area, similar to the area upon which two-dimensional integration takes place. Using the definition shown below, any set of permeability data in the form of a two-dimensional matrix can be averaged more precisely than conducting an arithmetic mean. See Appendix II for sample calculation.

$$\bar{f} = \frac{\int_c^d \left(\int_a^b f(x,y)dx \right) dy}{(d-c)(b-a)}$$

3.4.5 Global Matrix

A global matrix was designed in an attempt to upscale the permeability results for each sample as a crude representation of the length of the entire core (Figure 3.4). For each sample, every column of the permeability matrix (measured values from spot-permeametry) was averaged. The midpoint of every sample is represented by single row of numbers and seven columns. This reduction of the original matrix limits the small-scale heterogeneities measured on the surface of the core to a representative row of permeability values. The row of averaged

permeability values represents the width of the core and is only seven centimetres across. When all eleven samples are combined together, they form a new matrix of seven columns by eleven rows, herein termed the global matrix.

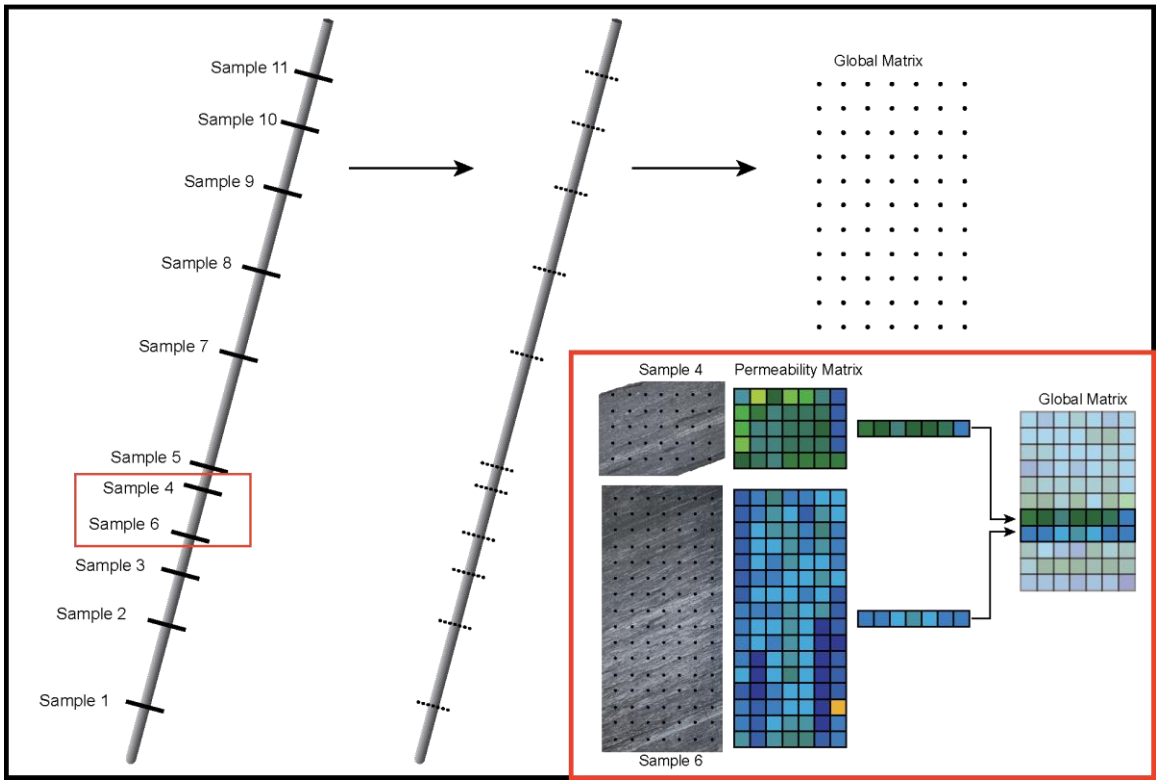

Figure 3.4: Schematic diagram representing the construction of the global matrix. Each sample is reduced to one row and seven columns. The combination of all the rows makes a new makes (i.e. the global matrix) of eleven rows and seven columns.

3.4.6 High-Pressure Mercury Injection Porosimetry

High-pressure mercury injection porosimetry was performed on four samples to characterize pore-throat distribution. This does not provide a representation of porosity distribution within the well, but rather a general comparison of pore-throat size distribution of discrete bioturbated and non-bioturbated fabrics to characterize these subtle heterogeneities. These samples represent the common bioturbated fabrics observed in the upper Montney and the changes correspond to subtle changes in porosity and permeability.

Samples were obtained from both non-bioturbated and bioturbated fabrics of Facies 1B, 2A and 5. Two samples (Figure 3.5 A and B) represent F1B, however, one sample has continuous planar pinstripe laminae whereas the other sample, the pinstripe laminae appear dashed. In the latter sample, bioturbation is commonly misidentified as cryptic bioturbation, however, diminutive trace fossils of *Chondrites* and *Palaeophycus* are present within this facies.

Each sample was cut into a cube approximately 2.5 centimetres a side. Samples were analyzed by Core Laboratories in Calgary, Alberta using a Micomeritics Autopore IV 9520

automated mercury injection system. Table 3.1 summarizes the permeability samples and their corresponding permeability sample, BI and trace fossil observed.

Sample for Hg-Injection	Corresponding Permeability Sample	Facies	BI	Trace Fossils
A	Sample 5	F1B	0	N/A
B	Sample 3	F1B	1	*Chondrites, Palaeophycus, Phycosiphon*
C	N/A	F2A	3	*Bergaueria, Planolites, Phycosiphon*
D	Sample 2	F5	5	*Phycosiphon*-dominated, *Chondrites*, *Palaeophycus*, *Planolites*, and *Teichichnus*.

Table 3.1: Summary table of the samples for high-pressure mercury injection analysis and their corresponding permeability samples, BI and observed trace fossils.

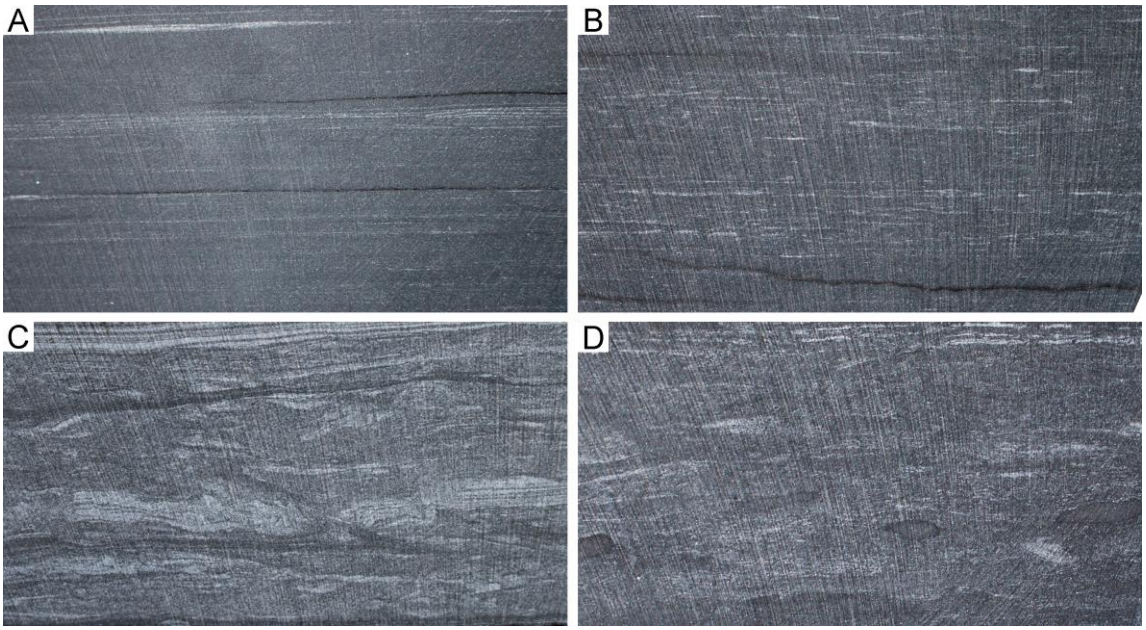

Figure 3.5: Core photographs of the samples selected for high-pressure mercury injection porosimetry. These samples represent common bioturbated fabrics observed in the upper Montney and they increase in bioturbation intensities A through D.

3.5 Results and Discussion

3.5.1 Spot permeability

Core photographs, with corresponding spot-permeability test locations are presented in Figure 3.6 A-K. These figures include a heat map representing the permeability measurements, vertical and horizontal score matrices, and a histogram showing the distribution of permeability values. Spot-permeametry results (by depth) are summarized in Table 3.2.

Figure 3.6 (next 4 pages; A-K): Spot permeability results for 11 samples from the well d-66-I/94-B-16. This is a deviated well and therefore the bedding is dipping however bedding is truly horizontal. Each sample has a core photograph with spot-permeameter test locations, a heat map representing the permeability measurements, and a histogram showing the distribution of permeability values.

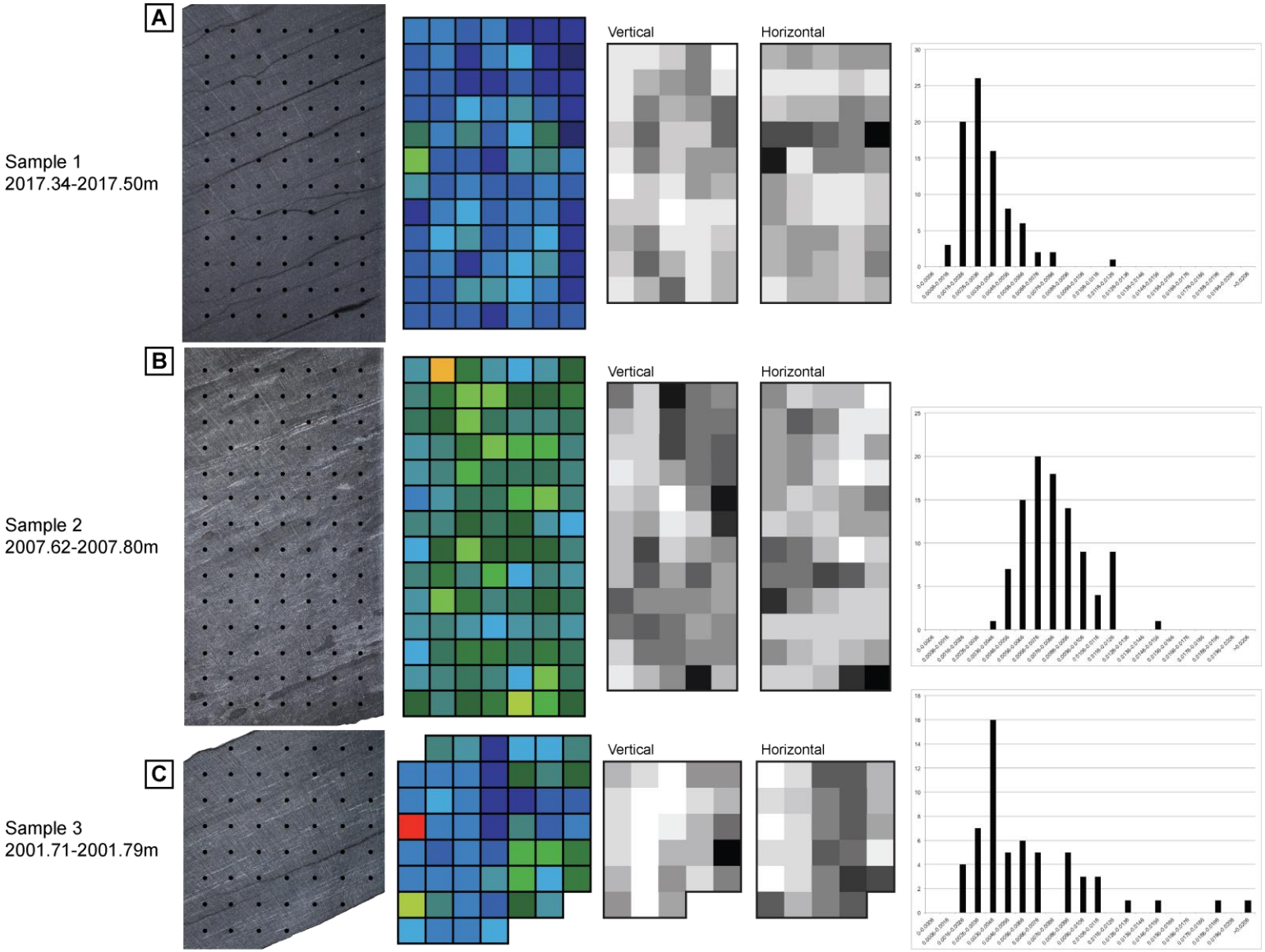
A
Sample 1
2017.34-2017.50m
Vertical
Horizontal
B
Sample 2
2007.62-2007.80m
Vertical
Horizontal
C
Sample 3
2001.71-2001.79m
Vertical
Horizontal

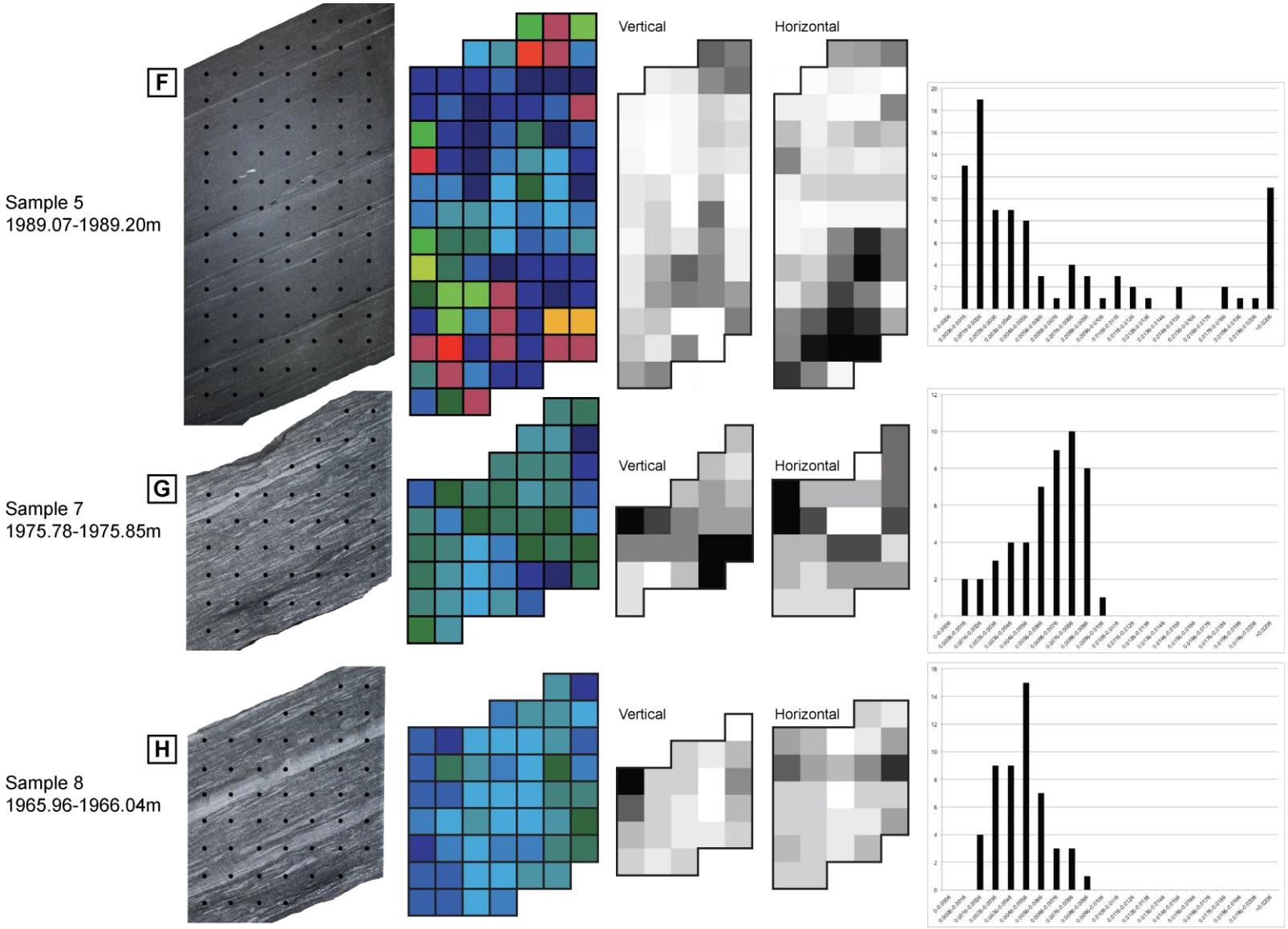
F
Sample 5
1989.07-1989.20m
Vertical
Horizontal
G
Sample 7
1975.78-1975.85m
Vertical
Horizontal
H
Sample 8
1965.96-1966.04m
Vertical
Horizontal

D

Sample 6
1997.14-1997.34m

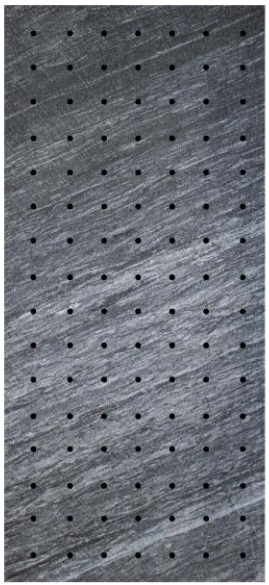

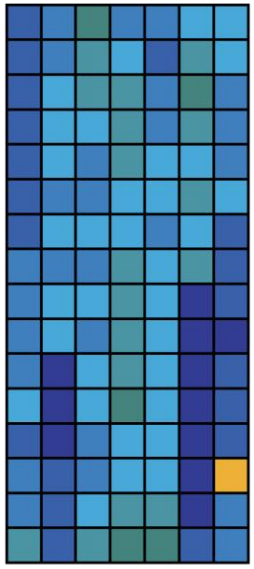

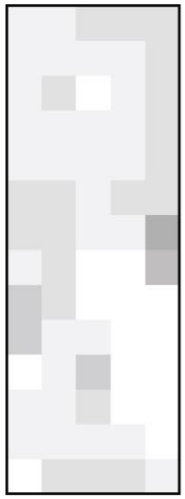

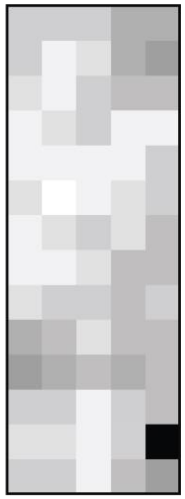

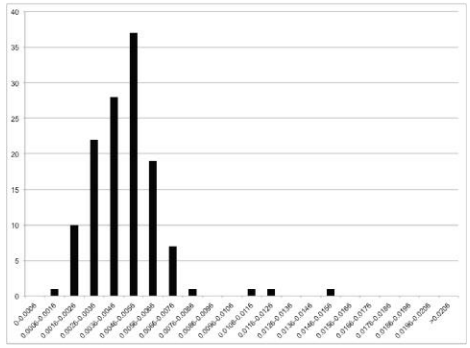

E

Sample 4
1991.76-1991.82m

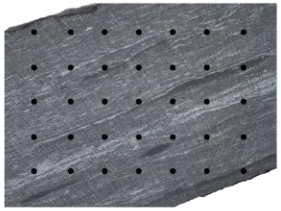

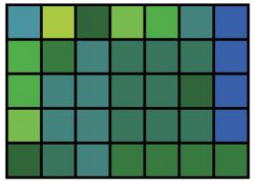

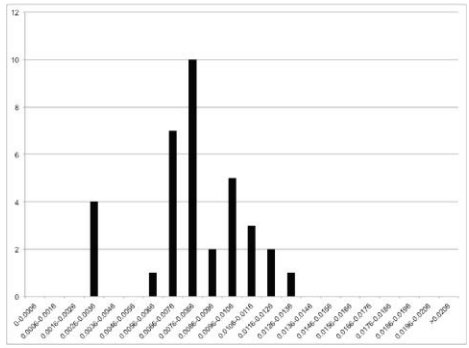

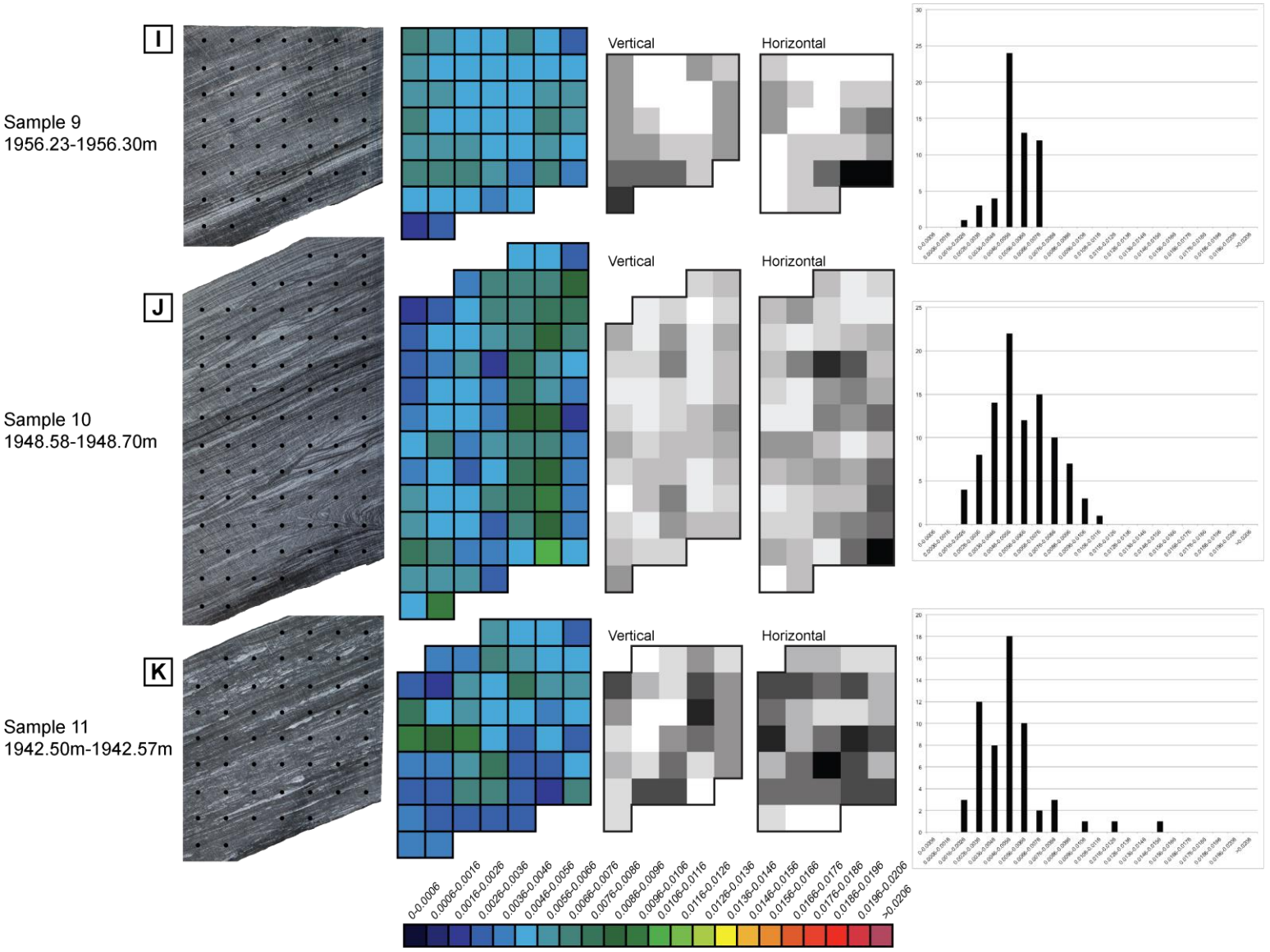
I
Sample 9
1956.23-1956.30m
Vertical
Horizontal
J
Sample 10
1948.58-1948.70m
Vertical
Horizontal
K
Sample 11
1942.50m-1942.57m
Vertical
Horizontal
0-0.0006
0.0006-0.0016
0.0016-0.0026
0.0026-0.0036
0.0036-0.0046
0.0046-0.0056
0.0056-0.0066
0.0066-0.0076
0.0076-0.0086
0.0086-0.0096
0.0096-0.0106
0.0106-0.0116
0.0116-0.0126
0.0126-0.0136
0.0136-0.0146
0.0146-0.0156
0.0156-0.0166
0.0166-0.0176
0.0176-0.0186
0.0186-0.0196
0.0196-0.0206
>0.0206

Sample	Depth Interval	Facies	Local BI (%)	Max (mD)	Min (mD)	Bulk-K (mD)
1	2017.34-2017.50	F1A	0	0.0122	0.0007	0.0037
2	2007.62-2007.80	F5	95	0.0148	0.0043	0.0060
3	2001.71-2001.79	F1B	30	0.0193	0.0017	0.0059
6	1997.14-1997.34	F1C	70	0.0150	0.0016	0.0045
4	1991.76-1991.82	F1B	50	0.0135	0.0027	0.0083
5	1989.07-1989.20	F1B	0	0.0559	0.0009	0.0086
7	1975.78-1975.85	F1C	60	0.0103	0.0012	0.0063
8	1965.96-1966.04	F2B	20	0.0090	0.0018	0.0048
9	1956.23-1956.30	F1C	5	0.0074	0.0020	0.0054
10	1948.58-1948.70	F2B	2	0.0112	0.0019	0.0057
11	1942.50-1942.57	F1C	45	0.0100	0.0017	0.0049

Table 3.2: Summary of spot-permeability samples arranged by depth.

Spot-permeability results suggest that there is an overall increase in permeability with the increase in bioturbation (Figure 3.7). There is an overall increase in the median value, maximum and minimum permeability values. The maximum and minimum permeability values present represent a range within two orders of magnitude from 10^{-4} to 10^{-2} however, there is significant overlap in permeability values between all the samples.

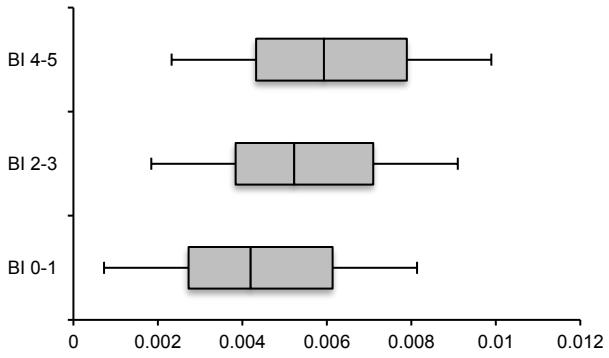

Figure 3.7: Box and whisker graph showing the distribution and increase in permeability values with increasing bioturbation intensities. The BI 0-1 includes: Sample 1, Sample 5, Sample 9 and Sample 10; BI 2-3 includes: Sample 4, Sample 8 and Sample 11; BI 4-5 includes: Sample 2 and Sample 6.

The size of the trace fossils observed does not permit the assessment of individual burrow permeability. Due to the spot-permeameter probe tip having a relatively larger diameter (0.46 centimetres), it does not have the ability to exactly measure the permeability of micro-scale burrows. The assumption that the permeability of the matrix is equivalent to a non-bioturbated sample and the permeability of a burrow is relatable to a pervasively bioturbated fabric is made. Sample 1 and Sample 2 represent matrix and burrow permeabilities, respectively. Sample 1 has a bulk-permeability of 3.7×10^{-3}; Sample 2 is pervasively bioturbated and has a bulk-permeability of 6.0×10^{-3}. These end-member examples demonstrate that pervasive bioturbation slightly enhances permeability characteristics relative to an otherwise extremely low permeability matrix

and are within two orders of magnitude. This biogenic network can be classified as weakly defined textual heterogeneities (WDH) from the classification of Pemberton and Gingras (2005). The biogenic fabrics within the upper Montney best fit within this classification, in which the bioturbated media differs slightly from the matrix. However, permeabilities are significantly lower for this unconventional play then reservoirs examined during development of this classification scheme (Gingras, pers. comm., 2017). The data between burrow- and matrix-permeability allows us to infer a dual-porosity system (Pemberton and Gingras, 2005; Gingras et al., 2012). The majority of the rock volume contributes to flow and the interactions between burrows and the matrix are high (Gingras et al., 2012).

Understanding the cause of higher permeability readings has proven to be difficult. Sample 7 (F1C) (Figure 3.6 G) and Sample 8 (F2B) (Figure 3.6 H) represent different facies; however, Sample 7 has a higher degree of bioturbation, and this is arguably the reason for its higher permeability. This difference in permeability values is subtle and within the same order of magnitude and the difference may be insignificant at the reservoir scale. In contrast, comparing Sample 6 (F1C) and Sample 4 (F1B), Sample 6 is more pervasively bioturbated, but Sample 4 has a higher permeability within the same order of magnitude. The increase in permeability is generalized by the increase in bioturbation, however there is a strong relationship between cementation and bioturbation.

Petrographic analysis is unable to characterize cementation within the micropores within these fine-grained rocks, which is a factor that needs to be assessed. The relationship between bioturbation and cementation within the micropores is beyond the scope of this study, but is nonetheless important for characterizing permeability trends. Scanning electron microscope (SEM) analyses would be required to characterize cementation within micropores. A study by Playter (2013) conducted SEM analysis on samples from the upper Montney within the study area. This study confirms calcite cementation has occluded micropores and that additional porosity formed during dedolomitization. However, the relationship between post-depositional diagenesis and bioturbation was not investigated in this study. Although a sample may be highly bioturbated, the occurrence of abundant cement within the pore space results in reduced permeability. Future research should attempt to develop a predictive model for the distribution of bioturbation. It is clear, from this study and others (e.g. Pemberton and Gingras, 2005; Tonkin et al., 2010; Lemiski et al., 2011; La Croix et al. 2013; Baniak et al., 2015; Zhang et al., 2015; Furlong et al., 2016) that bioturbation affects permeability and understanding its distribution will be of great value for reservoir modelling in the Montney Formation.

3.5.2 Scoring Matrices

The scoring matrices were designed to compare permeability anisotropy. Adjacent permeability values in the vertical and horizontal directions were compared to each other and

assigned an arbitrary score based on how similar or different the values are. As a result of the analysis performed on a deviated well, the bedding is dipping relative the edges of the core. Permeability along bedding was not characterized by this analysis. Although it was predicted that permeability trends would follow bedding, trends were not apparent except in the horizontal scoring matrix for Sample 5 (Figure 3.6 F).

The results of the scoring matrix are summarized in Table 3.3. A qualitative assessment describes general observations and which direction matrix had the overall lower (more homogenous) and higher (more heterogeneous) score. The overall lower score was evaluated based on the matrix that was represented with lighter shades, and darker shades for the overall higher score. The scoring technique evaluates the anisotropy of the samples, however in a given score matrix three or more connected squares of the same score (same shade) are described as small, isolated isotropic zones.

Sample	Facies	Vertical Score Matrix	Horizontal Score Matrix
1	F1A	• Small, isolated isotropic zones • Lower overall score	• Small, isolated isotropic zones • 2 locations of high scores • Higher overall score
2	F5	• Small, isolated isotropic zones • More high score locations • Higher overall score	• Small, isolated isotropic zones • Lower overall score
3	F1B	• Small, isolated isotropic zones • Lower overall score	• Small, isolated isotropic zones • Higher overall score
4	F1C	• Larger isotropic zones • Most homogenous • Lower overall score	• Small isotropic zones • Low scores but higher than vertical • Higher overall score
5	F1B	• Small, isolated isotropic zones • Lower overall score • Very close to horizontal score matrix	• Small, isolated isotropic zones • Higher overall score
6	F1B	• Lower overall score	• Higher overall zone • Higher scores on lower half follow bedding
7	F1C	• Small, isolated isotropic zones • Higher overall score	• Small, isolated isotropic zones • Lower overall score
8	F2B	• Small, isolated isotropic zones • Lower overall score	• Small, isolated isotropic zones • Higher overall score
9	F1C	• Small, isolated isotropic zones • Higher overall score	• Small, isolated isotropic zones • Lower overall score
10	F2B	• Small, isolated isotropic zones • Lower overall score	• Small, isolated isotropic zones • Higher overall score
11	F1C	• Small, isolated isotropic zones • Lower overall score	• Small, isolated isotropic zones • Higher overall score

Table 3.3: Summary table of the score matrices for the vertical and horizontal direction. This assessment is qualitative and based on visual observations. The grey shading indicates which direction matrix (vertical or horizontal) has the lower overall score. The vertical matrices dominantly have lower overall scores.

Based on the results in Table 3.3, the majority of the samples have overall lower scores in the vertical direction. In other words, the vertical direction is more homogenous. This was not an expected result since horizontal permeabilities tend to be higher in laminated media (Gingras et al., 2012). Permeability data from well d-67-J/94-B-9 show that horizontal permeability (K-90) is higher than vertical permeability (Kv) (Figure 3.8). Although a different method of analysis was used to measure permeability it is consistent with predictions and verifies predictions.

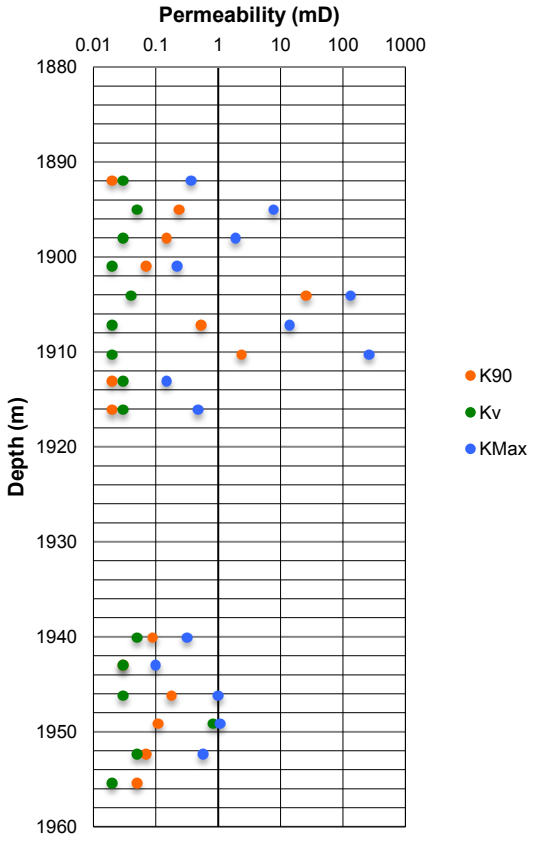

Figure 3.8 Graph of available core data for the well d-67-J/94-B-9. Vertical (Kv) and horizontal (K90) permeability were obtained from core plugs.

The result of vertical score matrices having an overall lower score may be influenced by the direction in which spot measurements are obtained. Consecutive measurements were taken down a column in the vertical direction during the data collection process. Internal calibrations within the spot-permeameter may occur between sequential measurements and influence the results.

This theory was tested on a Montney Formation core sample from a non-deviated well in which the measurements along the grid followed bedding. Spot-permeametry data were collected using the same method as described above. Two runs of data collection were conducted: 1st, consecutive down the columns and 2nd, consecutive along the rows until the grid was completed. The scoring technique struggles to characterize permeability anisotropy because different results occur depending on the order in which the data was obtained. This is a limitation of the spot-permeameter (PDPK-400) and should be kept in mind when single spot-permeability measurements are taken along the length of an entire core.

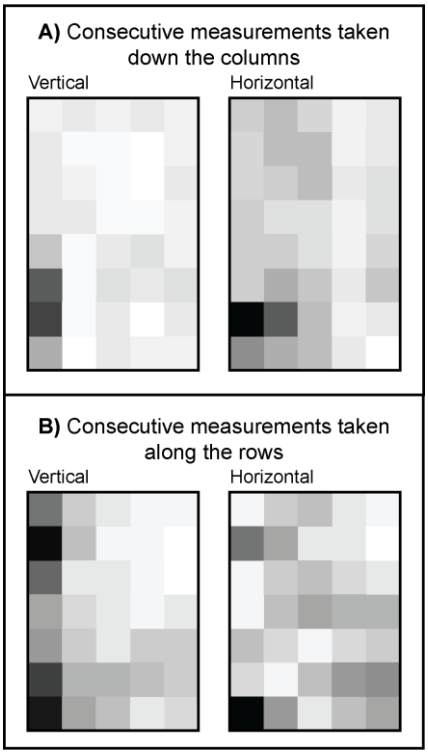

Figure 3.9: Results of the scoring matrices from two runs of data collection occurring down the columns (A) and across the rows (B).

3.5.3 Bulk Permeability and Relationship to Core Data

The bulk permeability of each sample (double integral method) was plotted with routine core data for the given core interval (Figure 3.9). Spot-permeability measurements are higher than permeability from routine core data.

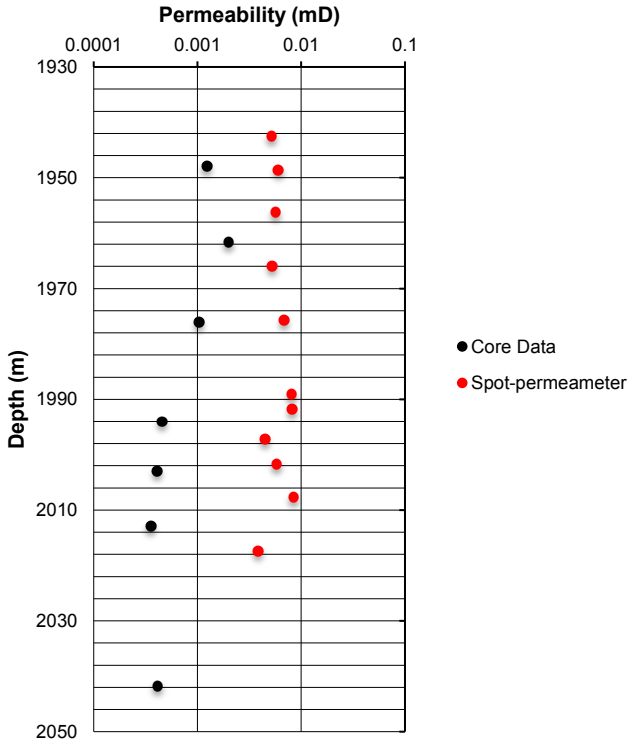

Figure 3.10: Graph of porosity data from routine core methods and bulk-permeability from spot-permeametry.

The difference in permeability values result from the different methods used to obtain the permeability. There is a variety of permeability measuring techniques and each comes with a detection limit. Figure 3.11 shows the range in permeability values from various forms of analysis performed on samples from the Montney Formation. The “PDPK klink” represents data obtained using the same method that was used in this chapter and has a relatively low detection limit. The difference in methods accounts for the discrepancy in permeability values. However, the two data sets do not appear to follow similar trends. Spot-permeametry is the most discrete measurement that can be obtained and provides a better representation of heterogeneities. However, the size of the grid (1 x 1 centimetre) used for spot-permeametry is much greater than the scale of heterogeneity (millimetre scale laminae). Core plugs capture a lower degree of reservoir heterogeneity relative to the spot-permeameter, and higher variability relative to full-diameter core. Future work should establish the representative elementary volume (REV) that best represents heterogeneities observed in the Montney Formation.

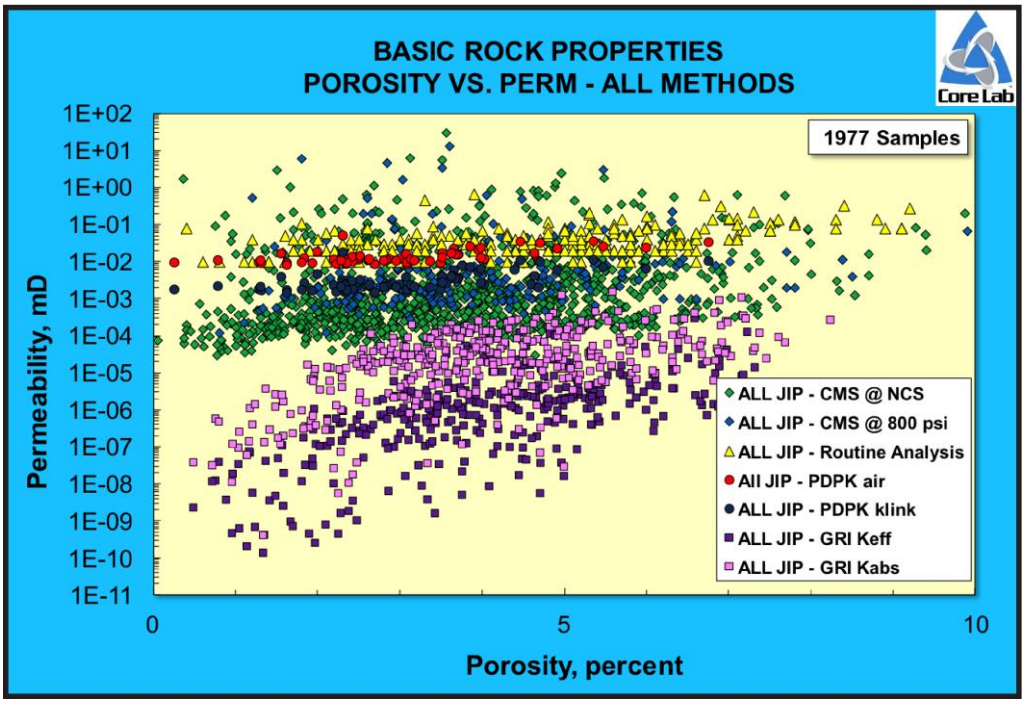

Figure 3.11: CoreLabs provided this graph. It shows the range in permeabilities obtained by different methods on Montney samples.

3.5.4 Global Matrix

The global matrix is a crude representation of the permeability distribution relative to the entire core (Figure 3.4). The global matrix represents permeability across seven centimetres of core and the sampling distribution was reduced to equal distances (1 x 1 centimetre). The global matrix removes small scale heterogeneities observed within each sample and compares coarse permeability trends of all samples. The heat map reveals zones of continuity and higher permeabilities that correspond to higher permeability fabrics (Figure 3.12). The scoring technique was applied to the global matrix and the horizontal scoring matrix has an overall lower score. Further research is required to understand the distribution of high permeability zones.

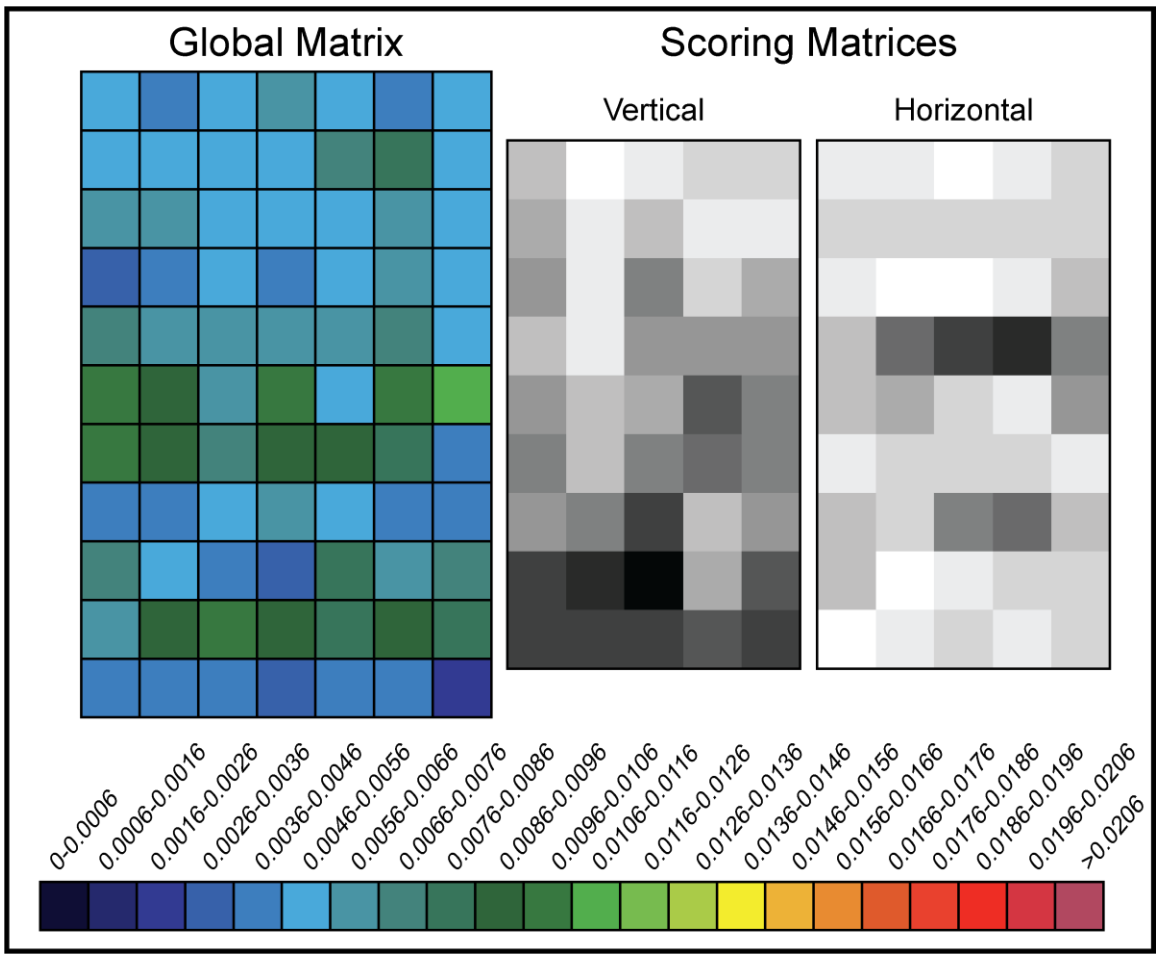

Figure 3.12: Global matrix results including the heat map representing measured permeability values, and the vertical and horizontal scoring matrices. The global matrix shows zones of continuity and higher permeability.

3.5.5 High Pressure Mercury Injection Porosimetry

High-pressure mercury injection porosimetry tests results show a unimodal or bimodal distribution, depending on the sample, with the larger peak corresponding to the dominant pore throat size (Figure 3.13). All samples contain pores within the micropore range (<0.0025 μm – 0.5 μm). As a result of increased bioturbation, pore size increases and developed a bimodal distribution, however the occurrence of bioturbation needs to be prominent. The occurrence of dashed laminae (discontinuous on a core scale; Figure 3.13 B) is commonly misidentified as cryptic bioturbation. However diminutive trace fossils of *Chondrites* and *Palaeophycus* are present within this sample. The trace fossils are cryptic in the sense that the trace fossils are small in scale and subtle in expression (Pemberton et al., 2006). The identification is also difficult due to minimal grain size and colour variation. Minor bioturbation is not sufficient to change pore throat distribution and remains comparable to the non-bioturbated sample (Figure 3.13 A). The relationship to pore-throat size distribution is also related to the occurrence of cement and this

relationship requires further investigation. Pervasive bioturbation (Figure 3.13 D, also spot-permeability Sample 2) disrupts the laminated fabric and increases both pore throat aperture and permeability. The analysis of these samples reveals the pervasiveness of bioturbation required to effect reservoir characteristics. This provides a generalization of bioturbated fabrics that are expected to have greater potential to affecting storability within the reservoir.

Figure 3.13 (next page): High-pressure mercury injection porosimetry was performed on four samples to characterize pore-throat distribution. A – D are arranged in order of increasing bioturbation intensity. The fabric between A and B is very similar, however minor bioturbation forms dashed pinstripe laminae. The distribution of pore sizes is very similar and overall there is a unimodal distribution. C and D represent an increase in the bioturbation and the fabric is noticeably disrupted and forms a bimodal pore size distribution.

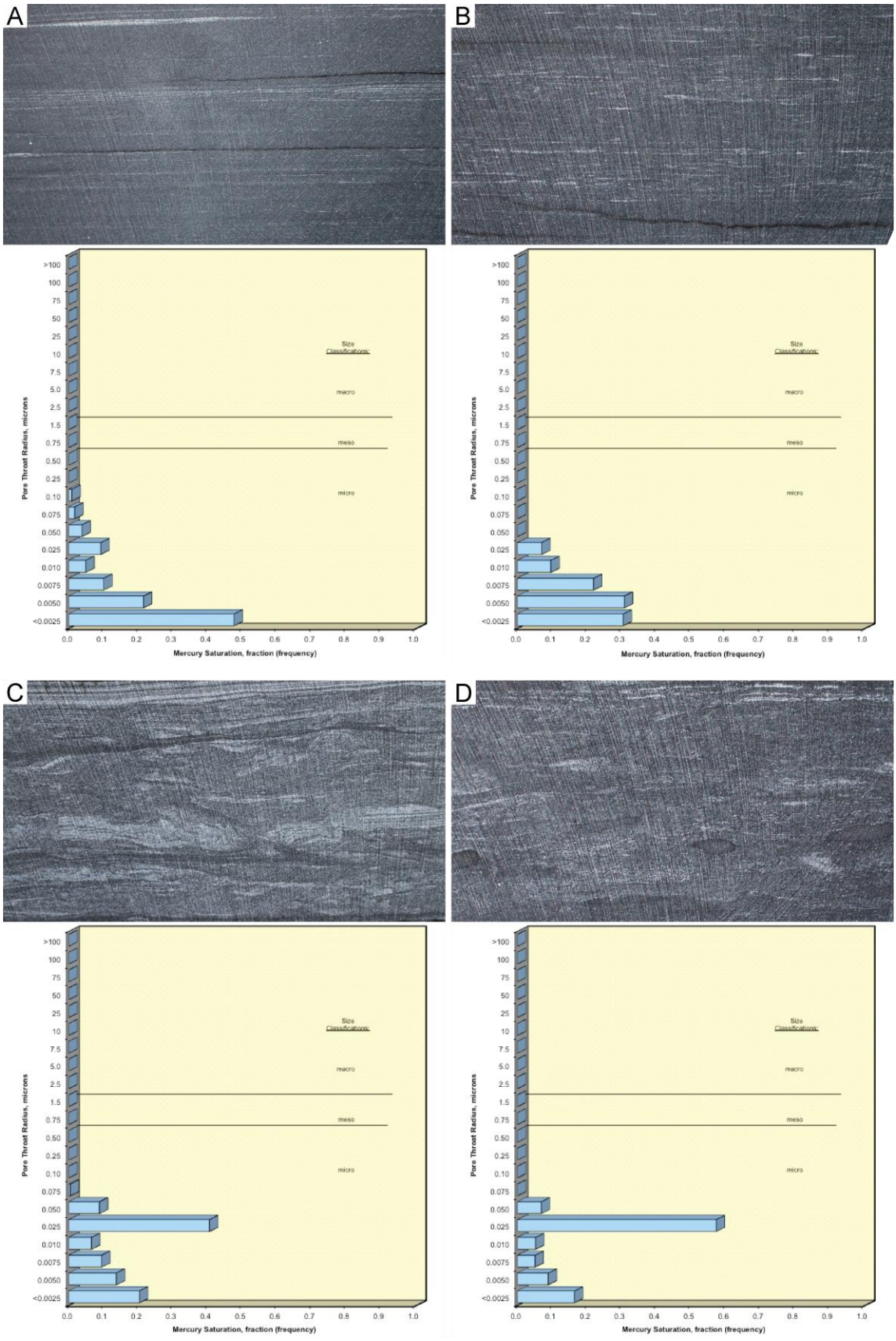
A
B
C
D
Pore Throat Radius, microns
>100
100
75
50
25
10
7.5
5.0
2.5
1.5
0.75
0.50
0.25
0.10
0.075
0.050
0.025
0.010
0.0075
0.0050
<0.0025
Size Classifications:
macro
meso
micro
0.0
0.1
0.2
0.3
0.4
0.5
0.6
0.7
0.8
0.9
1.0
Mercury Saturation, fraction (frequency)

3.6 Conclusions

The utility of spot-permeametry within low-permeability, fine-grained reservoirs was poorly understood and this paper presents a comprehensive examination of this method. Spot-permeametry was used to analyze small-scale heterogeneities and anisotropy of the upper Montney Formation. Eleven samples with varying degrees of pinstripe laminae, rippled and bioturbated fabrics where measured with a spot-permeameter using a grid method. The scale of the grid (1 x 1 centimetre) was significantly larger than the scale of the heterogeneity, however the permeability results characterize a given fabric. Permeability increased as a result of bioturbation, however, the bioturbation observed needs to be apparent in order to change permeability and porosity characteristics (i.e. grain scale; or cryptic bioturbation appears not to affect overall permeability).

The global matrix represents the length of the core coarsely upscaled wherein small-scale heterogeneities observed within each sample are reduced. When all the permeability samples are compared together, horizontal isotropy was higher. As well, zones of continuity and higher permeability were observed. The global matrix provides a representation how the relative permeability of a sample (i.e. fabric) performs relative to other samples in the core.

Although analyses were performed on a deviated well, true vertical and horizontal permeability was not analyzed. A new technique was designed to characterize anisotropy and arbitrary scores were assigned for the vertical and horizontal directions. The scores evaluate how similar or different adjacent permeability values are for a given point. This technique concluded that the samples are dominantly more homogenous in a vertical direction. The spot-permeameter is unable to characterize anisotropy and the data is influenced by the order in which the permeability measurements were obtained. However, spot-permeability using a grid technique likely captures the heterogeneity of a fabric and the bulk-permeability is valid representative of a given bioturbated or sedimentologic fabric.

Future research should focus on developing a predictive model for the distribution of bioturbation. Bioturbation is characterized as sporadic and its distribution, both vertically and laterally, remains uncertain. The occurrence of bioturbation has important implications for reservoir properties because there is a strong relationship with pore filling cements. As well, permeability data should be compared with whole-diameter core permeability data to establish a representative volume that meaningfully captures heterogeneities.

CHAPTER 4: SUMMARY AND CONCLUSIONS

This thesis investigates the sedimentology, ichnology and biogenic permeability of the upper Montney Formation in northeast British Columbia. Fourteen cores provided the data set for this study. Chapter 2 evaluates the palaeoenvironmental and stratigraphic interpretations of the upper Montney based on previous publications and detailed core analysis. Chapter 3 deals with the assessment of reservoir characterization. The data and interpretations provide valuable tools for understanding heterogeneity and advancing reservoir models.

Chapter 2 develops a facies classification scheme based on ichnological and sedimentological criteria. The study interval is dominated by silt and, to a lesser extent, very fine-grained sandstone. Five major facies were established representing one facies association: pinstripe laminated siltstone (F1), pinstripe and rippled laminated siltstone (F2), calcite cemented concretions and beds (F3), bioclastic packstone beds (F4), and bioturbated siltstone (F5). Facies were developed based on variations in pinstripe frequency, sedimentary structures representing increasing energy and the nature of biogenic sedimentary structures. Overall, deposition occurred within the distal offshore to offshore transition zone.

The Upper Montney Formation was deposited during the Olenekian (Smithian and Spathian), an interval that suffered under the prolonged effects of delayed post-extinction biotic recovery. Bioturbation is sporadic both vertically and laterally and represents a stressed *Cruziana* Ichnofacies. The distribution of bioturbation reveals highly variable physico-chemical stresses. Trace fossils are diminutive and although classically related to environmental stresses (e.g. salinity, sedimentation, oxygen), it is difficult criterion to use in this intervals as diminution of infaunal and epifaunal invertebrates is a common affect association with extinctions (i.e. the Lilliput effect', Twitchett, 2007; MacEachern et al., 2009; Gingras et al., 2011).

Chapter 3 explores the relationship between biogenic rock fabrics and permeability and porosity modifications. A spot-permeameter (PDPK-400) was used to understand the relationship between bioturbated textures and heterogeneities. The utility of the spot-permeameter was assessed to recognize its ability to measure permeability in fine-grained reservoirs. Bulk permeability provides a representative value for a given fabric and relative permeability trends differ from core data. Horizontal permeabilities were expected to be more similar in a laminated media, however, scoring matrices unsuccessfully characterized permeability anisotropy and vertical permeabilities were more homogenous. Spot-permeametry is the most discrete permeability measurement that can be obtained and permeability increases with increased bioturbation.

Issues arise with the upper Montney Formation and characterizing biogenic permeability. Bioturbation is sporadic within the same facies as well as its distribution vertically and laterally remains uncertain. This has implications when attempting to relate the effects of bioturbation into a reservoir model. Due to the spot-permeameter probe tip having a relatively larger diameter

(0.46 centimetres) relative to the trace fossils, it does not have the ability to exactly measure the permeability of micro-scale burrows. Comparing non-bioturbated and pervasively bioturbated samples are considered equivalent to matrix and burrow permeability. This biogenic networks is classified as weakly defined textural heterogeneities (Pemberton and Gingras, 2005). This infers a dual-porosity system in which the burrow and matrix permeabilities are within two orders of magnitude (Pemberton and Gingras, 2005; Gingras et al., 2012). This classification best fits with this established classification system, however future work should evaluate the variability of biogenic textures in unconventional reservoirs to establish a new classification scheme.

The spot-permeameter is considered an effective tool for evaluating small-scale heterogeneities. This assessment requires multiple measurements taken across the surface of the sample to essentially capture many small variations to provide a representation permeability of a given fabric. The biogenic and sedimentary fabrics relate directly to sedimentary facies and corresponding depositional environments. Detailed study into the fabrics can be related to the facies and are more easily built into reservoir models.

High-pressure mercury porosimetry was also conducted on four samples to provide a comparison of common fabrics observed within the upper Montney. These results concluded that bioturbation has to be prolific in order to alter pore-throat size distribution. Bioturbation has the ability to increase pore throat sizes and directly affecting the permeability.

REFERENCES

Armitage, J.H. 1962. Triassic oil and gas occurrences in northeastern British Columbia, Canada. Journal of the Alberta Society of Petroleum Geologists, v. 10, p. 35–56.

Barclay, J., F. Krause, R. Campbell, and J. Utting, 1990. Dynamic casting and growth faulting: Dawson Creek graben complex, Carboniferous-Permian Peace River embayment, western Canada: Bulletin of Canadian Petroleum Geology, v. 38, no. 1, p. 115–145.

Baniak, G. M., Gingras, M. K., Burns, B. A., and Pemberton, S. G. 2015. Petrophysical Characterization of Bioturbated Sandstone Reservoir Facies In the Upper Jurassic Ula Formation, Norwegian North Sea, Europe. Journal of Sedimentary Research, 85(1), 62-81.

Bear, J. 1972. Dynamics of fluids in porous media. New York: American Elsevier Pub. Co.

Beatty, T. W., Zonneveld, J. P., and Henderson, C. M. 2008. Anomalously diverse Early Triassic ichnofossil assemblages in northwest Pangea: A case for a shallow-marine habitable zone. Geology, 36(10), 771-774.

Benton, M. J., and Twitchett, R. J. 2003. How to kill (almost) all life: the end-Permian extinction event. Trends in Ecology and Evolution, 18(7), 358-365.

Beranek, L. P., Mortensen, J. K., Orchard, M. J., and Ullrich, T. 2010. Provenance of North American Triassic strata from west-central and southeastern Yukon: correlations with coeval strata in the Western Canada Sedimentary Basin and Canadian Arctic Islands. Canadian Journal of Earth Sciences, 47(1), 53-73.

Beranek, L. P., and Mortensen, J. K. 2011. The timing and provenance record of the Lake Permian Klondike orogeny in northwestern Canada and arc-continent collision along western North America. Tecotonics. 30(5)

Bird, T.D. Barclay, J.E. Campbell, R.I. and Lee, P.J. 1994. Triassic gas resources of the Western Canada Sedimentary Basin, Geological Survey of Canada Bulletin 483, 96 p.

Bjerstedt, T. W. 1988. Multivariate analyses of trace fossil distribution from an Early Mississippian oxygen-deficient basin, Central Appalachians. Palaios, 53-68.

Blakey, R. C. 2013. Using paleogeographic maps to portray Phanerozoic geologic and paleotectonic history of western North America. AAPG Bulletin, 97, 146.

Bridge, J. S. 1978. Origin of horizontal lamination under turbulent boundary layers. Sedimentary Geology, 20, 1-16.

Bromley, R. G., and Ekdale, A. A. 1984. Chondrites: a trace fossil indicator of anoxia in sediments. Science, 224, 872-875.

Bouma, A.H. 1962. Sedimentology of some flysch deposits. Amsterdam. Elsevier, 162 p.

Boyer, D. L., Bottjer, D. J., and Droser, M. L. 2004. Ecological signature of Lower Triassic shell beds of the western United States. Palaios, 19(4), 372-380.

Camacho, C. A. P. 2013. Bioturbation and resource quality: A case study from the Upper Cretaceous Lysing and Nise formations, Ellida and Midnatsoll fields, Norwegian Sea. University of Alberta (Canada). Unpublished M.Sc. Thesis. University of Alberta

Cant, D.J. 1988. Regional structure and development of the Peace River Arch, Alberta: a Paleozoic failed-rift system? Bulletin of Canadian Petroleum Geology, v. 36, p. 284–295.

Clarkson, C. R., Jensen, J. L., Pedersen, P. K., and Freeman, M. 2012. Innovative methods for flow-unit and pore-structure analyses in a tight siltstone and shale gas reservoir. AAPG bulletin, 96(2), 355-374.

Core Laboratories Instruments. 1996, Profile Permeameter PDPK-400 Operations Manual, 40 p.

Criss, R. E., Cooke, G. A., and Day, S. D. 1988. An organic origin for the carbonate concretions of the Ohio Shale (No. 1836). USGPO.

Dashtgard, S. E., and Gingras, M. K. 2012. Marine invertebrate neoichnology. Trace Fossils as Indicators of Sedimentary Environments: Elsevier Developments in Sedimentology, 64, 273-298.

Davies, G.R. 1997. The Triassic of the Western Canada Sedimentary Basin: tectonic and stratigraphic framework, Palaeogeography, Paleoclimate and biota. In: Triassic of the Western Canada Sedimentary Basin. T.F. Moslow and J. Wittenberg (eds.). Bulletin of Canadian Petroleum Geology, v. 45, p. 434–460.

Davies, G.R. Moslow, T.F. and Sherwin, M.D. 1997. The lower Triassic Montney Formation, west-central Alberta. In: Triassic of the Western Canada Sedimentary Basin. T.F. Moslow and J. Wittenberg (eds.). Bulletin of Canadian Petroleum Geology, v. 45, p. 474–505.

Davies, G.R. and Hume, D. 2016. Lowstand/Slope-onlap Wedge in the Montney: Stratigraphic and Sequence Framework, Reservoir Significance. GeoConvention 2016, Abstract, 4 p.

Dixon, J. 2000. Regional lithostratigraphic units in the Triassic Montney Formation of Western Canada. Bulletin of Canadian Petroleum Geology, v. 48, p. 80–83.

Droser, M. L., and Bottjer, D. J. 1986. A semiquantitative field classification of ichnofabric: research method paper. Journal of Sedimentary Research, 56(4).

Drzewiecki, P. A., and Simo, J. T.1997. Carbonate platform drowning and oceanic anoxic events on a mid-Cretaceous carbonate platform, south-central Pyrenees, Spain. Journal of Sedimentary Research, 67(4).

Edwards, D.E., Barclay, J.E., Gibson, D.W., Kvill, G.E. and Halton, E. 1994. Triassic strata of the Western Canada Sedimentary Basin: In: Geological Atlas of the Western Canada Sedimentary Basin. G.D. Mossop and I. Shetsen (comps.). Canadian Society of Petroleum Geologists and Alberta Research Council, p. 259-275.

Embry, A. F. 1997. Global sequence boundaries of the Triassic and their identification in the Western Canada Sedimentary Basin. Bulletin of Canadian Petroleum Geology, 45(4), 415-433.

Emig, C. C. 1982. Terrier et position des Lingules (brachiopode, inarticulés). Bulletin de la Société zoologique de France, 107, 185-194.

Emery, K. O., and Hülsemann, J. 1961. The relationships of sediments, life and water in a marine basin. Deep Sea Research (1953), 8(3-4)

Ekdale, A. A., and Mason, T. R. 1988. Characteristic trace-fossil associations in oxygen-poor sedimentary environments. Geology, 16(8), 720-723.

Faugères, J. C., and Stow, D. A. 1993. Bottom-current-controlled sedimentation: a synthesis of the contourite problem. Sedimentary Geology, 82(1-4), 287-297.

Ferri, F. and Zonneveld, J-P. 2008. Were Triassic rocks of the Western Canada Sedimentary Basin deposited in a foreland? Canadian Society of Petroleum Geologists Reservoir, v. 35, p. 12–14.

Föllmi, K. B., and Grimm, K. A. 1990. Doomed pioneers: Gravity-flow deposition and bioturbation in marine oxygen-deficient environments. Geology, 18(11), 1069-1072.

Furlong, C. M., Alexander, F., Gegolick, A., Gingras, M., Prenoslo, D., Sanders, S. C., and Zonneveld, J. P. 2016. Bioturbation Influence on Permeability Distribution within the Lower Triassic Montney Formation of the Western Canadian Sedimentary Basin. In AAPG Annual Convention and Exhibition.

Furlong, C.M., Gingras, M.K., and Zonneveld, J-P. 2017. The 'Anisian Wedge': Insight on the complexity of the Montney-Doig Boundary. GeoConvention 2017.

Gibson, D. W., and Gibson, D. W. 1974. Triassic rocks of the southern Canadian Rocky Mountains. Geological Survey of Canada. Department of Energy, Mines and Resources. no. 230.

Gibson, D., and J. Barclay, 1989, Middle Absaroka sequence the Triassic stable craton, in Ricketts, B.D., ed., Western Canada Sedimentary Basin - A case history: Calgary, p. 219–231.

Gibson, D.W. and Edwards, D.E. 1990. An overview of Triassic stratigraphy and depositional environments in the Rocky Mountain Foothills and western Interior Plains, Peace River Arch area, northeastern British Columbia. In: Geology of the Peace River Arch. S.C. O'Connell and J.S. Bell (eds.). Bulletin of Canadian Petroleum Geology, v. 38A, p. 146-158.

Gingras, M. K., Pemberton, S. G., Saunders, T., and Clifton, H. E. 1999. The ichnology of modern and Pleistocene brackish-water deposits at Willapa Bay, Washington; variability in estuarine settings. Palaios, 14(4), 352-374.

Gingras, M.K., MacMillan, B., Balcom, B.J., 2002a. Visualizing the internal physical characteristics of carbonate sediments with magnetic resonance imaging and petrography. Bull. Can. Petrol. Geol. 50, 363–369.

Gingras, M.K., MacMillan, B., Balcom, B.J., Saunders, T., Pemberton, S.G., 2002b. Using magnetic resonance imaging and petrographic techniques to understand the textural attributes and porosity distribution in Macaronichnus-burrowed sandstone. J. Sediment. Res. 72, 552–558.

Gingras, M. K., Pemberton, S. G., Henk, F. B., Maceachern, J. A., Mendoza, C., Rostron, B., ... and Konhauser, K. 2009. Applications of ichnology to fluid and gas production in hydrocarbon reservoirs.

Gingras, M. K., MacEachern, J. A., and Dashtgard, S. E. 2011. Process ichnology and the elucidation of physico-chemical stress. Sedimentary Geology, 237(3), 115-134.

Gingras, M. K., Baniak, G., Gordon, J., Hovikoski, J., Konhauser, K. O., La Croix, A., and Zonneveld, J. P. 2012. Porosity and permeability in bioturbated sediments. Trace Fossils as Indicators of Sedimentary Environments. Developments in Sedimentology, 64, 837-868.

Golding, M., M. Orchard, J.-P. Zonneveld, C. Henderson, and L. Dunn, 2014, An exceptional record of the sedimentology and biostratigraphy of the Montney and Doig formations in British Columbia: Bulletin of Canadian Petroleum Geology, v. 62, no. 3, p. 157–176.

Golding, M., M. Orchard, J.-P. Zonneveld, and N. Wilson, 2015, Determining the age and depositional model of the Doig Phosphate Zone in northeastern British Columbia using conodont biostratigraphy: Bulletin of Canadian Petroleum Geology, v. 63, no. 2, p. 143–170.

Golding, M. L., Mortensen, J. K., Ferri, F., Zonneveld, J. P., and Orchard, M. J. 2016. Determining the provenance of Triassic sedimentary rocks in northeastern British Columbia and western Alberta using detrital zircon geochronology, with implications for regional tectonics. Canadian Journal of Earth Sciences, 53(2), 140-155.

Gorsline, D. S. 1984. A review of fine-grained sediment origins, characteristics, transport and deposition. Geological Society, London, Special Publications, 15(1), 17-34.

Hart, M. B. 1991. The Late Cenomanian calcisphere global bioevent. Proceedings of the Ussher Society, 7(4), 413-417.

Hayes, L.E., Beatty, T.W., Henderson, C.M., Love, G.D., and Summons, R.E., 2007. Evidence for photic zone euxinia through the end-Permian mass extinction in the Panthalassic Ocean (Peace River Basin, Western Canada). Palaeoworld, v. 16, p. 39-50.

Hayes, M. 2012. Montney Formation Play Atlas NEBC. BC Oil and Gas Commission. 28 p.

Henderson, C. M., Richards, B. C., and Barclay, J. E. 1994. Permian strata of the Western Canada sedimentary basin. Geological atlas of the Western Canada Sedimentary Basin. Compiled by GD Mossop and I. Shetsen. Canadian Society of Petroleum Geologists and Alberta Research Council, Special Report, 4, 251-258.

Hesse, R., and Chough, S. K. 1980. The Northwest Atlantic Mid-Ocean Channel of the Labrador Sea: II Deposition of parallel laminated levee-muds from the viscous sublayer of low-density turbidity currents. Sedimentology, 27(6), 697-711.

Hill, P. R. 1984. Facies and sequence analysis of Nova Scotian Slope muds: turbidite vs 'hemipelagic'deposition. Geological Society, London, Special Publications, 15(1), 311-318.

Hofmann, R., Hautmann, M., Wasmer, M., and Bucher, H. (2013). Palaeoecology of the Spathian Virgin Formation (Utah, USA) and its implications for the Early Triassic recovery. Acta Palaeontologica Polonica, 58(1), 149-173.

Jacobson, P. J., Jacobson, K. N., and Seely, M. K. 1995. Ephemeral rivers and their catchments: sustaining people and development in western Namibia. Desert Research Foundation of Namibia.

Jipa, D., and Kidd, R. B. 1974. Sedimentation of coarser grained interbeds in the Arabian Sea and sedimentation processes of the Indus Cone. Initial Reports of the Deep Sea Drilling Project, 23, 471-495.

Kendall, D. R. 1999. Sedimentology and Stratigraphy of the Lower Triassic Montney Formation, Peace River Basin, subsurface of northwestern Alberta. Unpublished M.Sc. University of Calgary, 368 p.

Kidwell, S. M., and Holland, S. M. 1991. Field description of coarse bioclastic fabrics. Palaios, 426-434.

Kline, S. J., Reynolds, W. C., Schraub, F. A., and Runstadler, P. W. 1967. The structure of turbulent boundary layers. Journal of Fluid Mechanics, 30(04), 741-773.

Knoll, A. H., Bambach, R. K., Payne, J. L., Pruss, S., and Fischer, W. W. 2007. Paleophysiology and end-Permian mass extinction. Earth and Planetary Science Letters, 256(3), 295-313.

Krapf, C. B., Stollhofen, H., and Stanistreet, I. G. 2003. Contrasting styles of ephemeral river systems and their interaction with dunes of the Skeleton Coast erg (Namibia). Quaternary International, 104(1), 41-52.

Kutzbach, J. E., Guetter, P. J., and Washington, W. M. 1990. Simulated circulation of an idealized ocean for Pangaean time. Paleoceanography, 5(3), 299-317.

La Croix, A. D. 2010. Ichnology, sedimentology, stratigraphy, and trace fossil-permeability relationships in the Upper Cretaceous Medicine Hat Member, Medicine Hat gas field, southeast Alberta, Canada. Unpublished M.Sc. Thesis. University of Alberta

La Croix, A. D., Gingras, M. K., Pemberton, S. G., Mendoza, C. A., MacEachern, J. A., and Lemiski, R. T. 2013. Biogenically enhanced reservoir properties in the Medicine Hat gas field, Alberta, Canada. Marine and Petroleum Geology, 43, 464-477.

Lau, K. V., Maher, K., Altiner, D., Kelley, B. M., Kump, L. R., Lehrmann, D. J., and Payne, J. L. 2016. Marine anoxia and delayed Earth system recovery after the end-Permian extinction. Proceedings of the National Academy of Sciences, 113(9), 2360-2365.

Lemiski, R. T. 2010. Sedimentology, ichnology, and resource characteristics of the low-permeability Alderson Member, Hatton Gas Pool, southwest Saskatchewan, Canada. Unpublished M.Sc. Thesis. University of Alberta

Lemiski, R. T., Hovikoski, J., Pemberton, S. G., and Gingras, M. 2011. Sedimentological, ichnological and reservoir characteristics of the low-permeability, gas-charged Alderson Member (Hatton gas field, southwest Saskatchewan): Implications for resource development. Bulletin of Canadian Petroleum Geology, 59(1), 27-53.

MacEachern, J. A., and Bann, K. L. 2008. The role of ichnology in refining shallow marine facies models. Recent Advances in Models of siliciclastic shallow-marine stratigraphy: SEPM, Special Publication, 90, 73-116.

MacEachern, J. A., Pemberton, S. G., Bann, K. L., and Gingras, M. K. 2009. Departures from the archetypal ichnofacies: effective recognition of physico-chemical stresses in the rock record.

MacEachern, J. A., Pemberton, S. G., Gingras, M. K., and Bann, K. L. 2010. Ichnology and facies models. In: Facies Models, edition 4. James, N. P. and Dalrymple, R. W. (eds) Geological Assciation of Canada, St. Johns, Newfoundland, p. 19-58

Macquaker, J. H., Taylor, K. G., and Gawthorpe, R. L. 2007. High-resolution facies analyses of mudstones: implications for paleoenvironmental and sequence stratigraphic interpretations of offshore ancient mud-dominated successions. Journal of Sedimentary Research, 77(4), 324-339.

Markhasin, B. 1997. Sedimentology and stratigraphy of the Lower Triassic Montney Formation, subsurface of northwestern Alberta. Unpublished M.Sc. Thesis, University of Calgary, 153 p.

Martin, K. D. 2004. A re-evaluation of the relationship between trace fossils and dysoxia. Geological Society, London, Special Publication, 228(1), 141-156

Mederos, S. 1995. Sedimentology and sequence stratigraphy of the Montney Formation in the Sturgeon Lake A and B pool. Unpublished M.Sc. Thesis, University of Alberta, Edmonton, 229 p.

Middleton, G. V. 1967. The Orientation of Concavo-Convex Particles Deposited from Experimental Turbidity Currents: NOTES. Journal of Sedimentary Research, 37(1).

Mozley, P. S. 1996. The internal structure of carbonate concretions in mudrocks: a critical evaluation of the conventional concentric model of concretion growth. Sedimentary Geology, 103(1-2), 85-91.

Moslow, T.F. and Davies, G.R. 1997. Turbidite reservoir facies in the Lower Montney Formation, west-central Alberta. In: Triassic of the Western Canada Sedimentary Basin. T.F. Moslow and J. Wittenberg (eds.). Bulletin of Canadian Petroleum Geology, v. 45, p. 507–536.

Moslow, T.F. 2000. Reservoir architecture of a fine-grained turbidite system: Lower Triassic Montney Formation, Western Canada Sedimentary Basin. In: Deep-water Reservoirs of the World, Conference Proceedings, Gulf Coast SEPM. P. Weimer, R.M. Slatt, J. Coleman, N.C. Rosen, H. Nelson, A.H. Bouma, M.J. Styzen, and D.T. Lawrence (eds.). p. 686–713.

Moslow, T. F., Haverslew, B., Henderson, C. M. 2016. Sedimentary Facies, Petrology, Condont Biotstratigraphy and Reservoir Quality of a Continuous (295,) Full Diameter Core of the Lower Triassic Montney Fm., Northeaster British Columbia, Western Canada Sedimentary Basin. Canadian Society of Petroleum Geologists: International Core Conference.

National Energy Board, BC Oil and Gas Commission, Alberta Energy Regulator and BC Ministry of Natural Gas Development. 2013. Energy briefing note: the ultimate potential for unconventional petroleum from the Montney Formation of British Columbia and Alberta; National Energy Board, BC Oil and Gas Commission, Alberta Energy Regulator and BC Ministry of Natural Gas Development, 17 p.

Nordahl, K., and Ringrose, P. S. 2008. Identifying the representative elementary volume for permeability in heterolithic deposits using numerical rock models. Mathematical geosciences, 40(7), 753-771.

O'connell, S. C. 1994. Geological history of the Peace River arch. Geological Atlas of the Western Canada Sedimentary Basin, GD Mossop and I. Shetsen (comp.), Canadian Society of Petroleum Geologists and Alberta Research Council, Special Report, 4, 431-438.

Orchard, M. J., and Zonneveld, J. P. 2009. The Lower Triassic Sulphur Mountain Formation in the Wapiti Lake area: lithostratigraphy, conodont biostratigraphy, and a new biozonation for the lower Olenekian (Smithian) Earth Science Sector (ESS) Contribution 20080714. Canadian Journal of Earth Sciences, 46(10), 757-790.

Paine, R. T. 1963. Ecology of the brachiopod Glottidia pyramidata. Ecological Monographs, 33(3), 187-213.

Panek, R. 2000. The Sedimentology and Stratigraphy of the Lower Triassic Montney Formation in the Subsurface of the Peace River Arch, Northwestern Alberta. Unpublished M.Sc. Thesis, University of Calgary, 226 p.

Paull, R. K., Paull, R. A., and Laudon, T. S. 1997. Conodont biostratigraphy of the Lower Triassic Mackenzie Dolomite Lentil, Sulphur Mountain Formation in the Cadomin area, Alberta. Bulletin of Canadian Petroleum Geology, 45(4), 708-714.

Pemberton, S. G., and Gingras, M. K. 2005. Classification and characterizations of biogenically enhanced permeability. AAPG bulletin, 89(11), 1493-1517.

Piper, D. J. W. 1973. The sedimentology of silt turbidites from the Gulf of Alaska. Initial Reports of the Deep Sea Drilling Project, 18, 847-867.

Piper, D. J. W., and Brisco, C. D. 1975. Deep-water continental-margin sedimentation, DSDP Leg 28, Antarctica. Initial Reports of the Deep Sea Drilling Project, 28, 727-755.

Piper, D. W. 1978. Turbidite muds and silts on deepsea fans and abyssal plains. Sedimentation in submarine canyons, fans, and trenches.

Playter, T. L. 2013. Petrographic and X-ray Microtomographic Analysis of the Upper Montney Formation, Northeastern British Columbia, Canada. Unpublished M.Sc. Thesis. University of Alberta.

Powell, D. M. 2009. Dryland rivers: processes and forms. In Geomorphology of Desert Environments (pp. 333-373). Springer Netherlands.

Reineck, H. E., 1963. Sedimentgefüge im Bereich der südlichen Nordsee. Abhandlungen der senckenbergische naturforschende Gesellschaft, v. 505, p. 1 – 138.

Richards, B. C., Barclay, J. E., Bryan, D., Hartling, A., Henderson, C. M., and Hinds, R. C. 1994. Carboniferous strata of the Western Canada sedimentary basin. Geological Atlas of the Western Canada Sedimentary Basin, 221-250.

Robertson, J. D. 1989. Physiological constraints upon marine organisms. Earth and Environmental Science Transactions of The Royal Society of Edinburgh, 80(3-4), 225-234.

Sanders, S. 2016. Bioclastic Accumulations along the Western Margin of the Early Triassic Montney Formation. Unpublished M.Sc. Thesis, University of Alberta, 292 p.

Savrda, C. E., and Bottjer, D. J. 1989. Trace-fossil model for reconstructing oxygenation histories of ancient marine bottom waters: application to Upper Cretaceous Niobrara Formation, Colorado. Palaeogeography, Palaeoclimatology, Palaeoecology, 74(1-2), 49-74.

Savrda, C.E. 2007. Trace fossils and benthic oxygenation. In: Trace Fossils: Concepts, Problems, Prospects. Miller III, W. (ed.). Elsevier, p. 149–158.

Schoepfer, S. D., Henderson, C. M., Garrison, G. H., Foriel, J., Ward, P. D., Selby, D., and Shen, Y. 2013. Termination of a continent-margin upwelling system at the Permian–Triassic boundary (Opal Creek, Alberta, Canada). Global and Planetary Change, 105, 21-35.

Sellés-Martinez, J. 1996. Concretion morphology, classification and genesis. Earth-Science Reviews, 41(3), 177-210.

Sepkoski Jr, J. J. 1992. A compendium of fossil marine animal families. Contributions in biology and geology/Milwaukee Public Museum, 83, 1-156.

Shor, A. N., Kent, D. V., and Flood, R. D. 1984. Contourite or turbidite?: Magnetic fabric of fine-grained Quaternary sediments, Nova Scotia continental rise. Geological Society, London, Special Publications, 15(1), 257-273.

Stollhofen, H., Stanistreet, I. G., von Hagke, C., and Nguno, A. 2014. Pliocene–Pleistocene climate change, sea level and uplift history recorded by the Horingbaai fan-delta, NW Namibia. Sedimentary Geology, 309, 15-32.

Stow, D. A. V. 1977. Late Quaternary stratigraphy and sedimentation on the Nova Scotian outer continental margin. Unpublished PhD. Dalhousie University.

Stow, D. A. 1979. Distinguishing between fine- grained turbidites and contourites on the Nova Scotian deep water margin. Sedimentology, 26(3), 371-387.

Stow, D. A., and Piper, D. J. W. 1984. Deep-water fine-grained sediments: facies models. Geological Society, London, Special Publications, 15(1), 611-646.

Stow, D. A. 1985. Fine-grained sediments in deep water: an overview of processes and facies models. Geo-Marine Letters, 5(1), 17-23.

Stow, D. A., and Tabrez, A. R. 1998. Hemipelagites: processes, facies and model. Geological Society, London, Special Publications, 129(1), 317-337.

Stow, D. A., Faugères, J. C., Howe, J. A., Pudsey, C. J., and Viana, A. R. 2002. Bottom currents, contourites and deep-sea sediment drifts: current state-of-the-art. Geological Society, London, Memoirs, 22(1), 7-20.

Taylor, A. M., and Goldring, R. 1993. Description and analysis of bioturbation and ichnofabric. Journal of the Geological Society, 150(1), 141-148.

Tonkin, N.S., McIlroy, D., Meyer, R., Moore-Turpin, A., 2010. Bioturbation influence on reservoir quality: a case study from the Cretaceous Ben Nevis Formation, Jeanne d'Arc Basin, offshore Newfoundland, Canada. American Association of Petroleum Geologists Bulletin 94, 1059-1078.

Twitchett, R. J., and P. B. Wignall, 1996. Trace fossils and the aftermath of the Permo-Triassic mass extinction: evidence from northern Italy: Palaeogeography, Palaeoclimatology, Palaeoecology, v. 124, no. 1, p. 137–151.

Twitchett, R. J. 2007. The Lilliput effect in the aftermath of the end-Permian extinction event. Palaeogeography, Palaeoclimatology, Palaeoecology, 252(1), 132-144.

Van Weering, T. C. E., and Van Iperen, J. 1984. Fine-grained sediments of the Zaire deep-sea fan, southern Atlantic Ocean. Geological Society, London, Special Publications, 15(1), 95-113.

Wentworth, C. K., 1922. A scale of grade and class terms for clastic sediments: The Journal of Geology, p. 377–392.

Wignall, P. B., and Hallam, A. 1992. Anoxia as a cause of the Permian/Triassic mass extinction: facies evidence from northern Italy and the western United States. Palaeogeography, Palaeoclimatology, Palaeoecology, 93(1-2), 21-46.

Wignall, P. B., and Twitchett, R. J. 1996. Oceanic anoxia and the end Permian mass extinction. Science, 272(5265), 1155.

Wignall, P. B., and Newton, R. 2003. Contrasting deep-water records from the Upper Permian and Lower Triassic of South Tibet and British Columbia: evidence for a diachronous mass extinction. Palaios, 18(2), 153-167.

Wilson, N., Zonneveld, J. P., and Orchard, M. 2012. Biostratigraphy of the Montney Formation: From the Alberta and British Columbia Subsurface to the Outcrop. Abstract GeoConvention 2012

Wood, J. 2013. Water distribution in the Montney tight gas play of the western Canadian sedimentary basin: significance for resource evaluation. SPE Reservoir Evaluation and Engineering, 16(03), 290-302.

Woods, A. D., Bottjer, D. J., Mutti, M., and Morrison, J. 1999. Lower Triassic large sea-floor carbonate cements: Their origin and a mechanism for the prolonged biotic recovery from the end-Permian mass extinction. Geology, 27(7), 645-648.

Woods, A. D., and Bottjer, D. J. 2000. Distribution of ammonoids in the Lower Triassic Union Wash Formation (eastern California): evidence for paleoceanographic conditions during recovery from the end-Permian mass extinction. Palaios,15(6), 535-545.

Wust, R., Kelly, D., Bonk-Richards, A., Offord, H., Collins, B., Nassichuk, B., and Nieto, J. 2016. The Middle Montney—A Dirty Old Carbonate Formation With a Secret Past?. In AAPG Annual Convention and Exhibition.

Zhang, S. 2015. Petrography, Lithology, Stratigraphy, Bioturbation, and Trace Fossil-permeability Relationship of the Montney Formation of Lower Triassic, in Barrick Puskwa, Alberta, Western Canadian Sedimentary Basin. Unpublished M.Sc. Thesis. University of Alberta.

Zonneveld, J.-P., 2001. Middle Triassic biostromes from the Liard Formation, British Columbia, Canada: oldest examples from the Mesozoic of NW Pangea: Sedimentary Geology, v. 145, no. 3, p. 317–341.

Zonneveld, J. P., & Pemberton, S. G. 2003. Ichnotaxonomy and behavioral implications of lingulide-derived trace fossils from the Lower and Middle Triassic of Western Canada. *Ichnos*, *10*(1), 25-39.

Zonneveld, J. -P., & Greene, S. E. 2010. Lingulide response to severe storms recorded in Middle Triassic strata of northeastern British Columbia. *Palaios*, *25*(12), 807-817.

Zonneveld, J. -P., Beatty, T. W., and Pemberton, S. G. 2007. Lingulide brachiopods and the trace fossil Lingulichnus from the Triassic of western Canada: implications for faunal recovery after the end-Permian mass extinction. Palaios, 22(1), 74-97.

Zonneveld, J.-P., R. B. MacNaughton, J. Utting, T. W. Beatty, S. G. Pemberton, and C. M. Henderson, 2010a. Sedimentology and ichnology of the Lower Triassic Montney Formation in the Pedigree-Ring/Border-Kahntah River area, northwestern Alberta and northeastern British Columbia: Bulletin of Canadian Petroleum Geology, v. 58, no. 2, p. 115–140.

Zonneveld, J.-P., M. K. Gingras, and T. W. Beatty, 2010b, Diverse ichnofossil assemblages following the P-T mass extinction, Lower Triassic, Alberta and British Columbia, Canada: Evidence for shallow marine refugia on the northwestern coast of Pangea: Palaios, v. 25, no. 6, p. 368–392

Zonneveld, J.-P., 2011a. Suspending the rules: unraveling the ichnological signature of the Lower Triassic post-extinction recovery interval. Palaios, 26(11), 677-681.

Zonneveld, J. -P., Golding, M., Moslow, T. F., Orchard, M. J., Playter, T., and Wilson, N. 2011b. Depositional Framework of the Lower Triassic Montey Formation, West-central Alberta and Northeastern British Columbia. In CSPG CSEG CWLS Convention p. 1-4

Zonneveld, J.-P., and T. F. Moslow, 2014, Perennial River Deltas of the Montney Formation: Alberta and British Columbia Subcrop Edge. Abstract GeoConvention 2014

Zonneveld, J.-P., and Moslow T.F., 2015a. The Geology of Resource Plays in the Montney Formation: Western Canada Sedimentary Basin. Unpublished short course notes.

Zonneveld, J.-P., and Moslow, T.F. 2015b. The Montney-Doig boundary and the 'Anisian Wedge' in northeastern British Columbia. British Columbia Unconventional Gas Technical Forum.

Zonneveld, J.-P., Furlong, C. M., Gegolick, A., Gingras, M. K., Golding, M., Moslow, T., Orchard, M., Prenoslo, D., and Sanders, S. 2015c. Stratigraphic Architecture of the Montney Formation, Peace District, Alberta and British Columbia. 2015 Gussow Conference.

Zonneveld, J.-P., Furlong, C.M., Gegolick, A., Gingras, M.K., Golding, M., Moslow, T., Orchard, M., Playter, T., Prenoslo, D. and Sanders, S.C. 2016. The Montney-Doig Boundary and the "Anisian Wedge". Canadian

APPENDIX I – BIOTURBATION INDEX

The bioturbation index (BI) was originally proposed by Reineck (1963) and then modified by Droser and Bottjer (1986), and Taylor and Goldring (1993). A table of the meaning and extent of each scale is summarized below:

Grade	Percent Bioturbated	Classification	Visual Representation
0	0	- bioturbation absent	
1	1-4	- sparse bioturbation - bedding distinct - few discrete traces	
2	5-30	- low bioturbation - bedding distinct - low trace fossil diversity	
3	31-60	- moderate bioturbation - bedding boundaries sharp - traces discrete - overlap rare	
4	61-90	- High bioturbation - bedding boundaries indistinct - high trace density - overlap common	
5	91-99	- intense bioturbation - bedding completely disturbed	
6	100	- complete bioturbation - total biogenic homogenization of sediment	

Modified from Bann et al. (2004).

APPENDIX II – DOUBLE INTEGRAL SAMPLE CALCULATION FOR SAMPLE 4

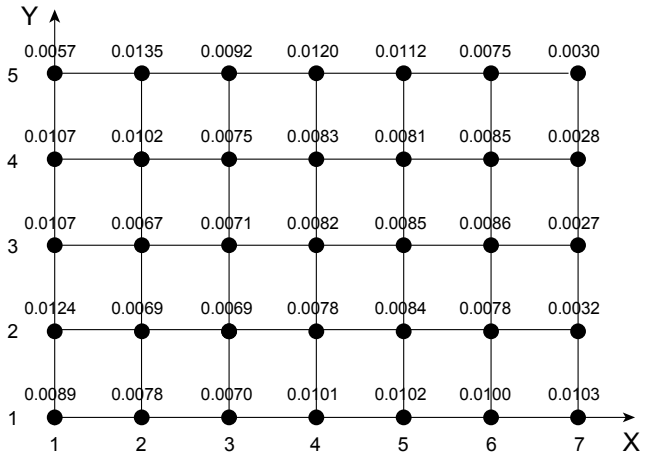

$$\bar{f} = \frac{\int_c^d \left(\int_a^b f(x,y)dx\right)dy}{(d-c)(b-a)}$$

$$\bar{f} = \frac{\int_c^d \left(\int_a^b f(x,y)dx\right)dy}{(d-c)(b-a)} = \frac{1}{(d-c)(b-a)}\int_c^d F dy$$

$$F = \int_a^b f(x,y)dx$$

where $c = 1, d = 5, a = 1, b = 7$

1. Calculate F1 for $y = 1$: $\Delta x = 1$

	x_1	x_2	x_3	x_4	x_5	x_6	x_7
K(x,y)	0.0089	0.0078	0.0070	0.0101	0.0102	0.0100	0.0103

$$F_1 = \frac{\Delta x}{2}[K_1 + K_7] + \Delta x \sum_{i=2}^{6} K_i = \frac{1}{2}[0.0089 + 0.0103] + 1[0.0078 + 0.0070 + 0.0101 + 0.0102 + 0.0100] = 0.0547$$

2. Calculate F2 for $y = 2$: $\Delta x = 1$

	x_1	x_2	x_3	x_4	x_5	x_6	x_7
K(x,y)	0.0124	0.0069	0.0069	0.0078	0.0084	0.0078	0.0032

$$F_2 = \frac{\Delta x}{2}[K_1 + K_7] + \Delta x \sum_{i=2}^{6} K_i = \frac{1}{2}[0.0124 + 0.0032] + 1[0.0069 + 0.0069 + 0.0078 + 0.0084 + 0.0078] = 0.0456$$

3. Calculate F3 for $y = 3$: $\Delta x = 1$

	x_1	x_2	x_3	x_4	x_5	x_6	x_7
K(x, y)	0.0107	0.0067	0.0071	0.0082	0.0085	0.0086	0.0027

$$F_3 = \frac{\Delta x}{2}[K_1 + K_7] + \Delta x \sum_{i=2}^{6} K_i = \frac{1}{2}[0.0107 + 0.0027] + 1[0.067 + 0.0071 + 0.0082 + 0.0085 + 0.0086] = 0.0458$$

4. Calculate F4 for $y = 4$: $\Delta x = 1$

	x_1	x_2	x_3	x_4	x_5	x_6	x_7
K(x, y)	0.0107	0.0102	0.0075	0.0083	0.0081	0.0085	0.0028

$$F_4 = \frac{\Delta x}{2}[K_1 + K_7] + \Delta x \sum_{i=2}^{6} K_i = \frac{1}{2}[0.0107 + 0.0028] + 1[0.0102 + 0.0075 + 0.0083 + 0.0081 + 0.0085] = 0.0494$$

5. Calculate F5 for $y = 5$: $\Delta x = 1$

	x_1	x_2	x_3	x_4	x_5	x_6	x_7
K(x, y)	0.0057	0.0135	0.0092	0.0120	0.0112	0.0075	0.030

$$F_5 = \frac{\Delta x}{2}[K_1 + K_7] + \Delta x \sum_{i=2}^{6} K_i = \frac{1}{2}[0.0057 + 0.0030] + 1[0.0135 + 0.0092 + 0.0120 + 0.0112 + 0.0075] = 0.0578$$

6. Calculate $\int_c^d F dy$, $\Delta y = 1$

	y_1	y_2	y_3	y_4	y_5
K(x, y)	0.0547	0.0456	0.0458	0.0494	0.0578

$$F_5 = \frac{\Delta y}{2}[K_1 + K_7] + \Delta y \sum_{i=2}^{4} K_i = \frac{1}{2}[0.0547 + 00578] + 1[0.0456 + 0.0458 + 0.0494] = 0.1970$$

$$K_{bulk} = \frac{0.1970}{4 \cdot 6} = 0.0082\ mD$$

APPENDIX IV – LITHOLOGY LOGS OF CORED INTERVALS

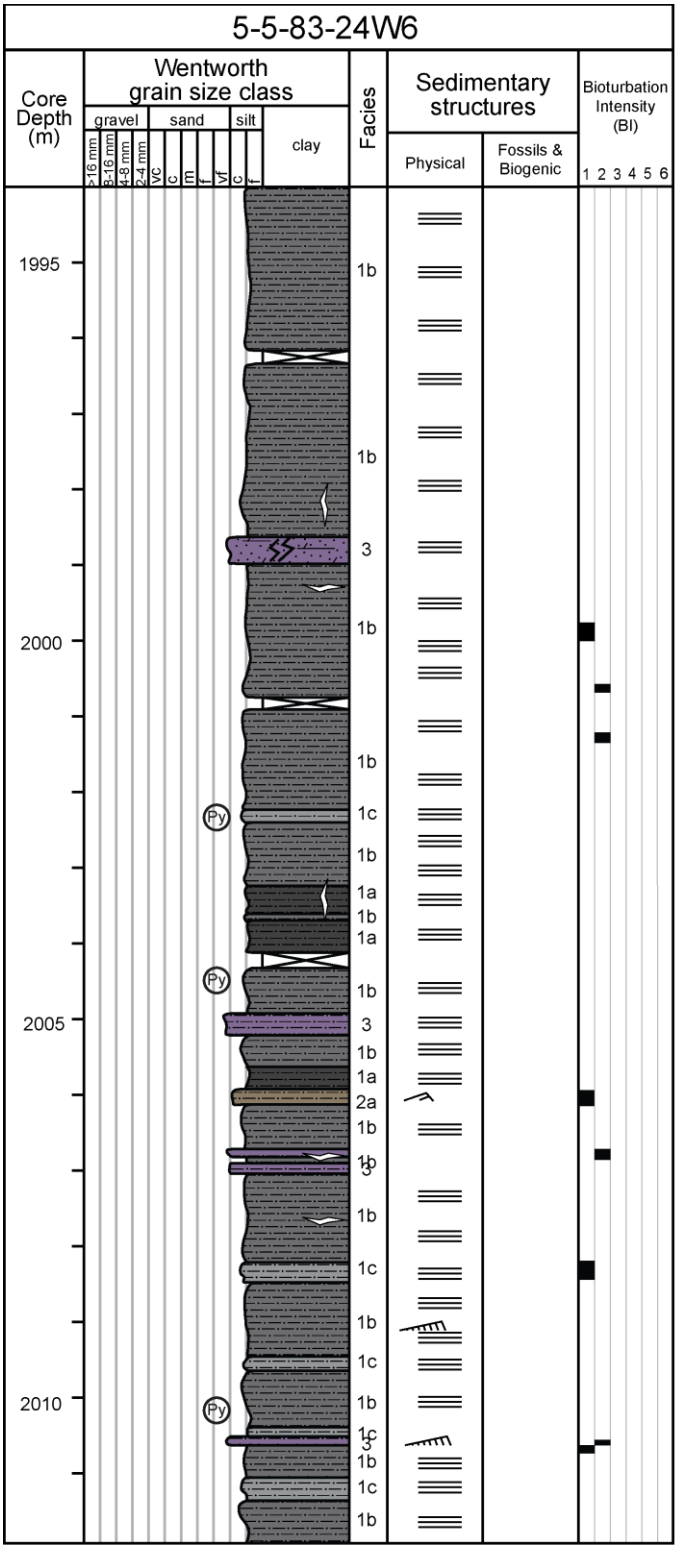

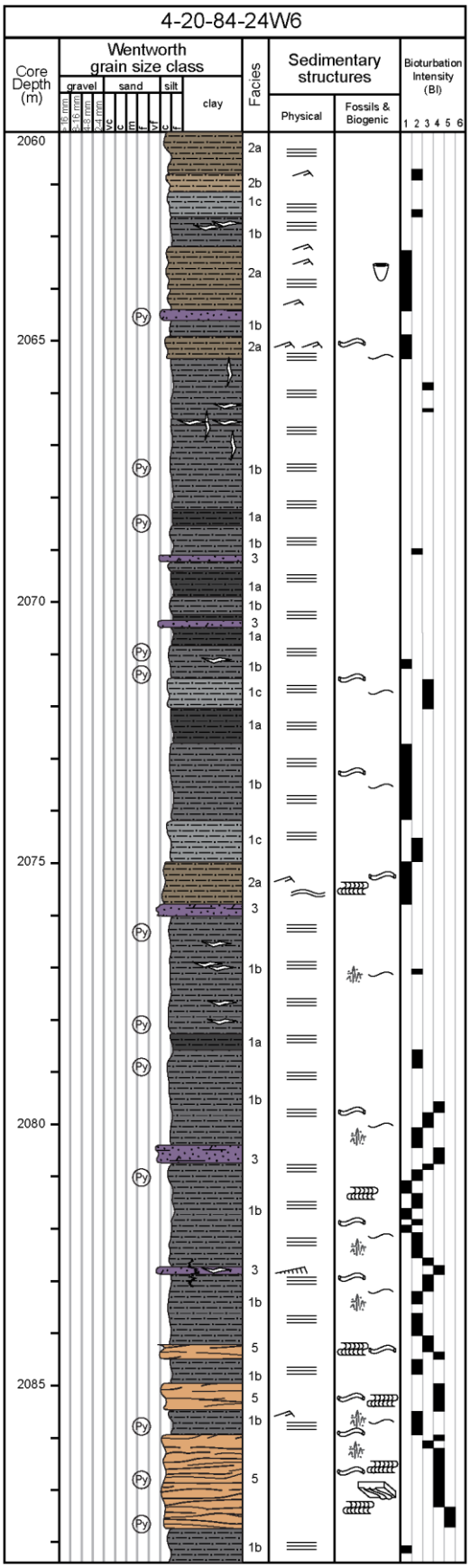
4-20-84-24W6
Core Depth (m)
Wentworth grain size class
gravel
sand
silt
clay
> 16 mm
5 - 16 mm
2 - 5 mm
1 - 2 mm
vc
c
m
f
vf
c
f
Facies
Sedimentary structures
Physical
Fossils & Biogenic
Bioturbation Intensity (BI)
1 2 3 4 5 6
2060
2065
2070
2075
2080
2085
Py

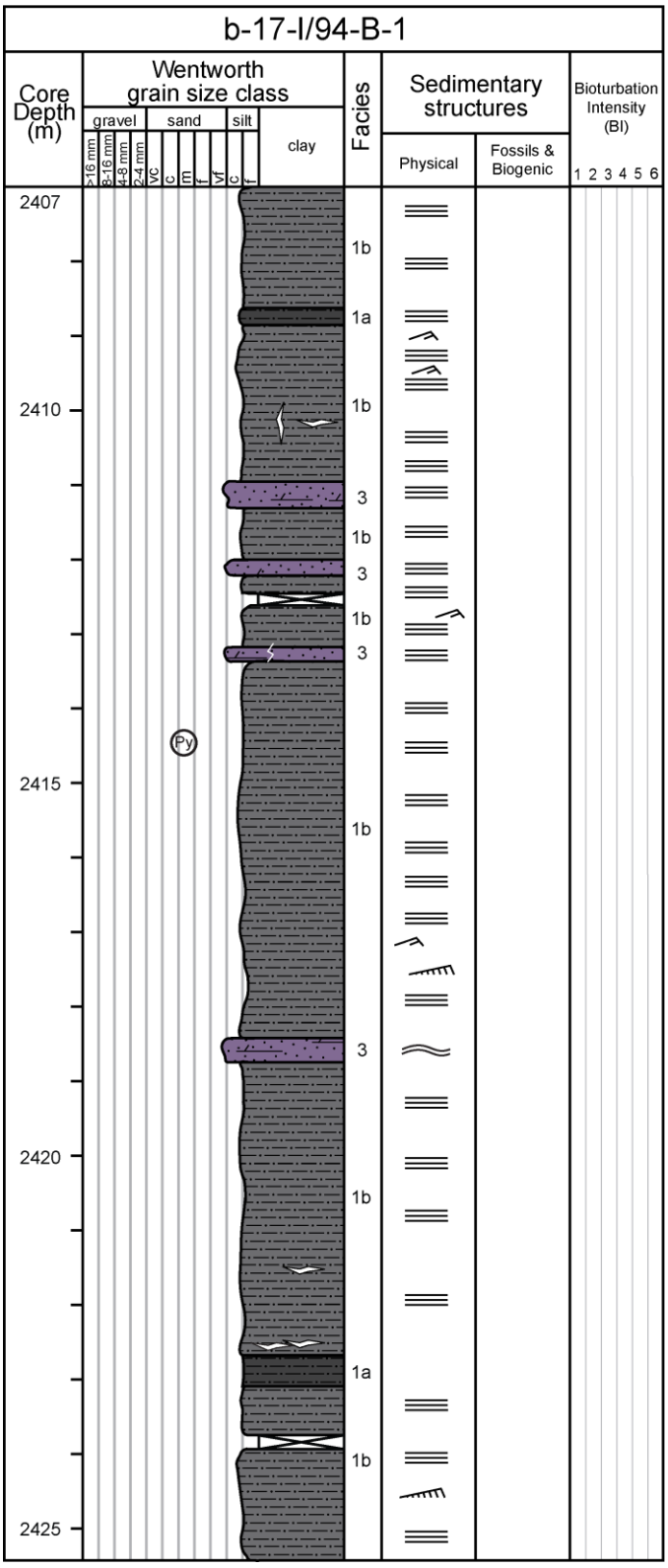
b-17-I/94-B-1
Core Depth (m)
Wentworth grain size class
gravel
sand
silt
clay
>16 mm
8-16 mm
4-8 mm
2-4 mm
vc
c
m
f
vf
c
f
Facies
Sedimentary structures
Physical
Fossils & Biogenic
Bioturbation Intensity (BI)
1 2 3 4 5 6
2407
2410
2415
2420
2425
1b
1a
3
Py

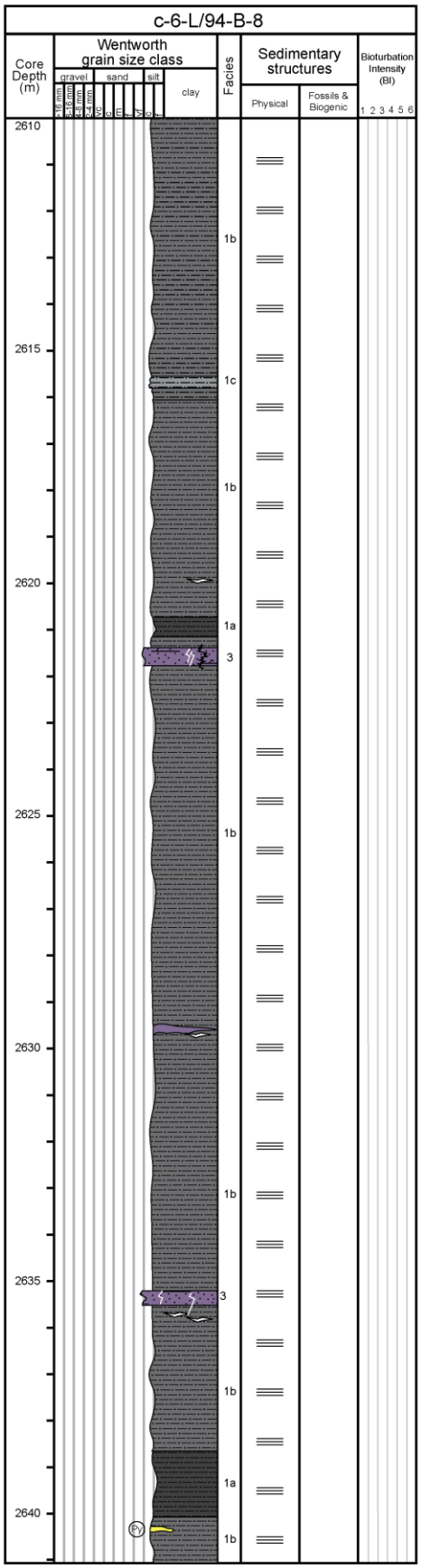
c-6-L/94-B-8
Core Depth (m)
Wentworth grain size class
gravel
sand
silt
clay
>16 mm
8-16 mm
4-8 mm
2-4 mm
vc
c
m
f
vf
c
f
Facies
Sedimentary structures
Physical
Fossils & Biogenic
Bioturbation Intensity (BI)
1 2 3 4 5 6
2610
2615
2620
2625
2630
2635
2640
1b
1c
1a
3
Py

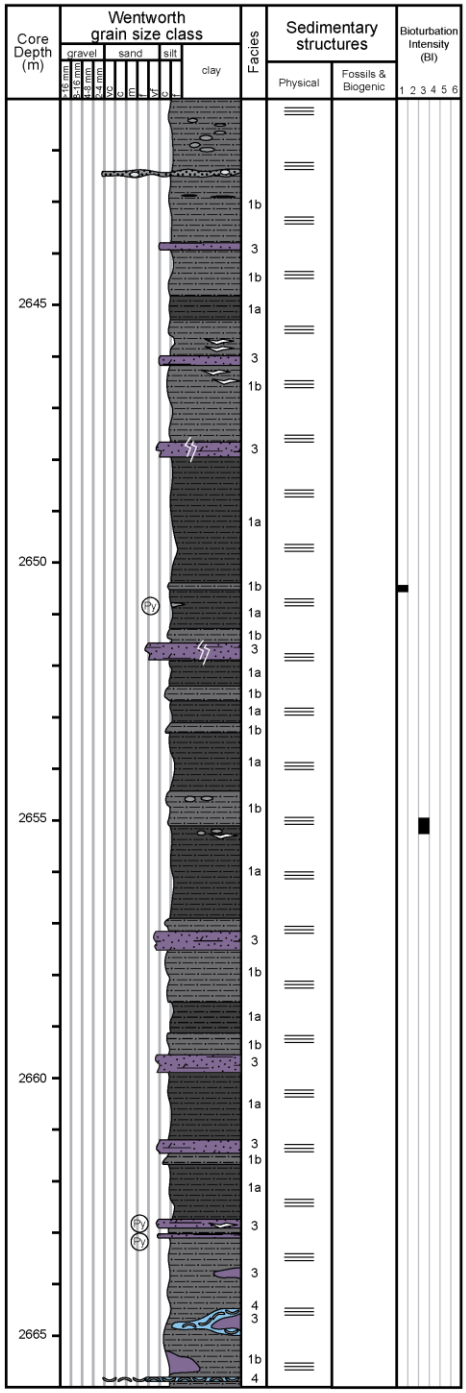
Core Depth (m)
Wentworth grain size class
gravel
sand
silt
clay
Facies
Sedimentary structures
Physical
Fossils & Biogenic
Bioturbation Intensity (BI)
2645
2650
2655
2660
2665
1b
1a
3
4
Py

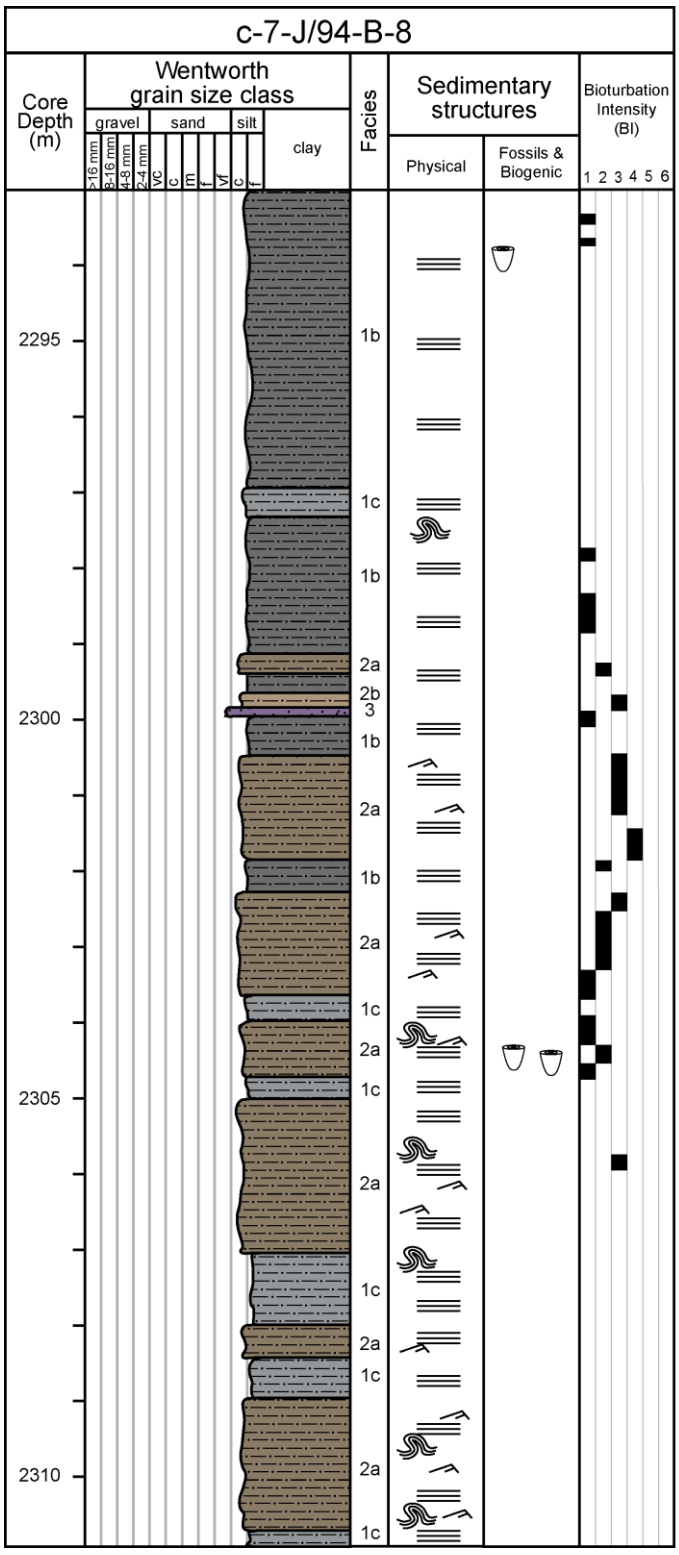
c-7-J/94-B-8
Core Depth (m)
Wentworth grain size class
gravel
sand
silt
clay
>16 mm
8-16 mm
4-8 mm
2-4 mm
vc
c
m
f
vf
c
f
Facies
Sedimentary structures
Physical
Fossils & Biogenic
Bioturbation Intensity (BI)
1 2 3 4 5 6
2295
2300
2305
2310
1b
1c
1b
2a
2b
3
1b
2a
1b
2a
1c
2a
1c
2a
1c
2a
1c
2a
1c

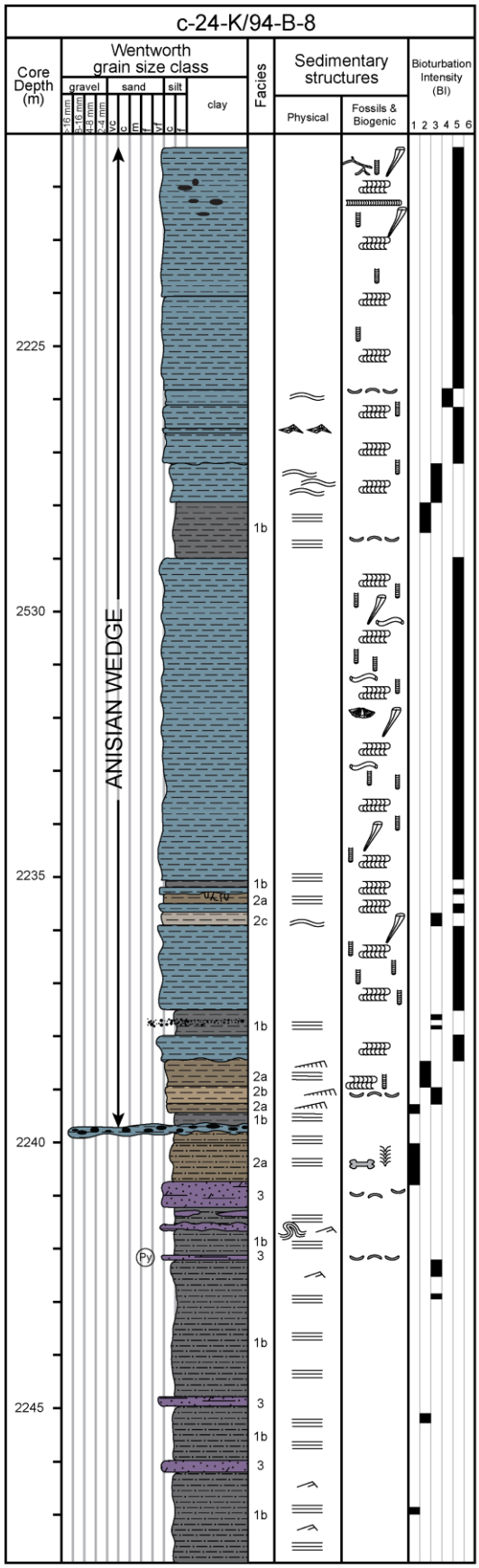
c-24-K/94-B-8
Core Depth (m)
Wentworth grain size class
gravel
sand
silt
clay
>16 mm
2-16 mm
1/16-2 mm
1/16-1/256 mm
<1/256 mm
c
m
f
vf
c
f
Facies
Sedimentary structures
Physical
Fossils & Biogenic
Bioturbation Intensity (BI)
1 2 3 4 5 6
2225
2530
2235
2240
2245
ANISIAN WEDGE
1b
2a
2c
1b
2a
2b
2a
1b
2a
3
1b
3
1b
3
1b
3
1b
Py

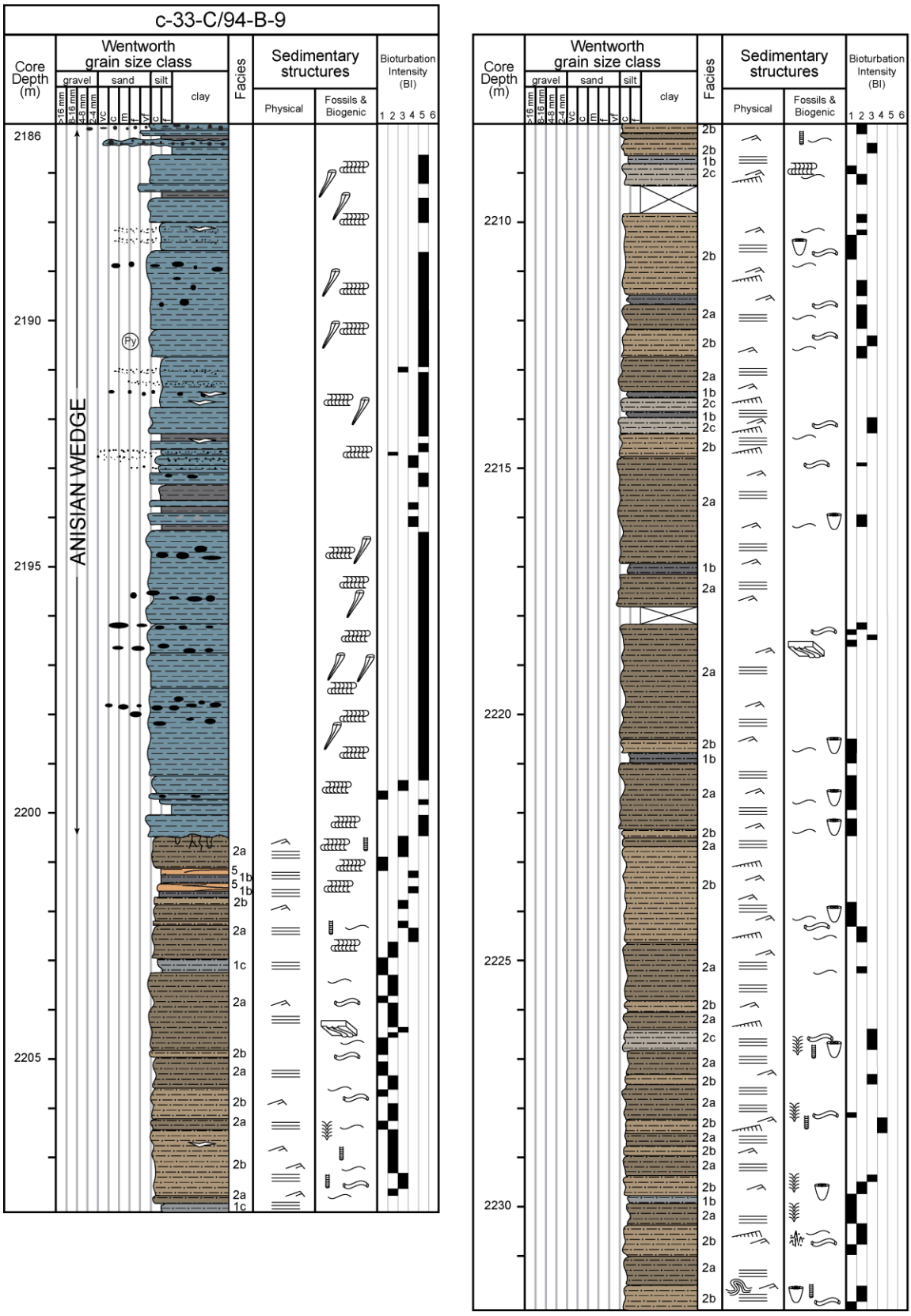
c-33-C/94-B-9
Core Depth (m)
Wentworth grain size class
gravel
sand
silt
clay
>16 mm
8-16 mm
4-8 mm
2-4 mm
vc
c
m
f
vf
c
f
Facies
Sedimentary structures
Physical
Fossils & Biogenic
Bioturbation Intensity (BI)
1 2 3 4 5 6
2186
2190
2195
2200
2205
2210
2215
2220
2225
2230
ANISIAN WEDGE
Fy
2a
1b
2b
1c

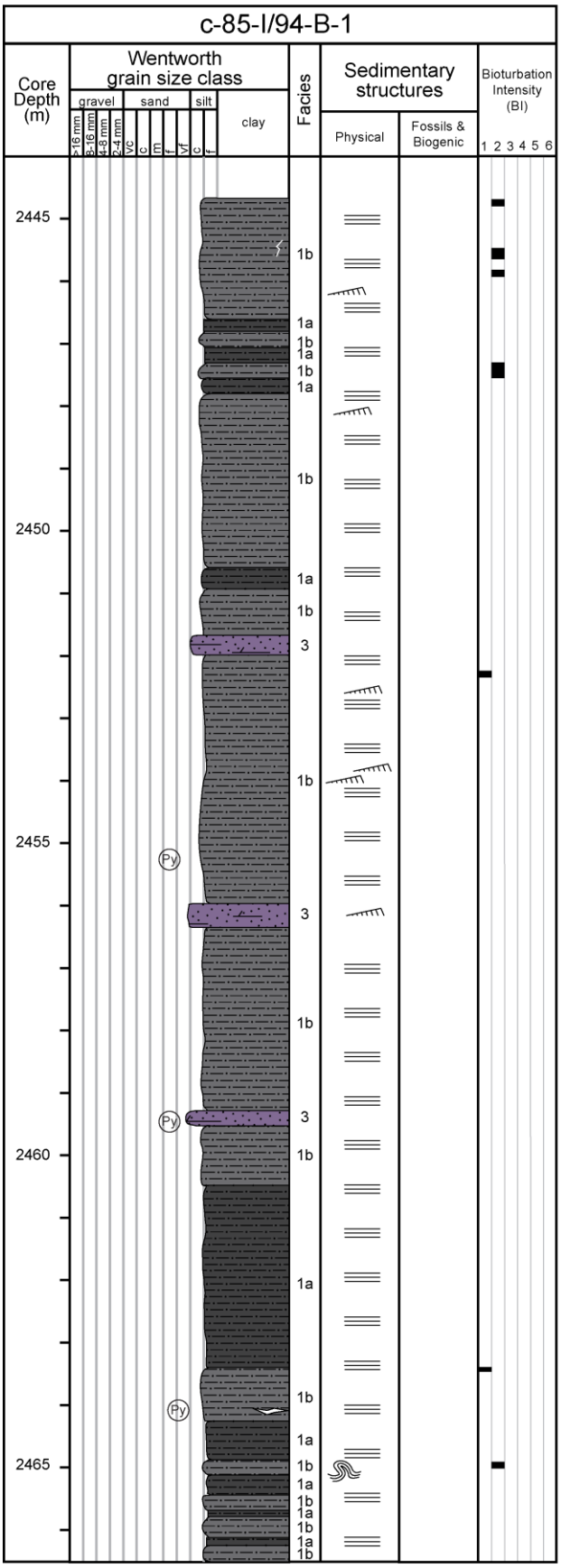
c-85-I/94-B-1
Core Depth (m)
Wentworth grain size class
gravel
sand
silt
clay
>16 mm
8-16 mm
4-8 mm
2-4 mm
vc
c
m
f
vf
c
f
Facies
Sedimentary structures
Physical
Fossils & Biogenic
Bioturbation Intensity (BI)
1 2 3 4 5 6
2445
2450
2455
2460
2465
1b
1a
3
Py

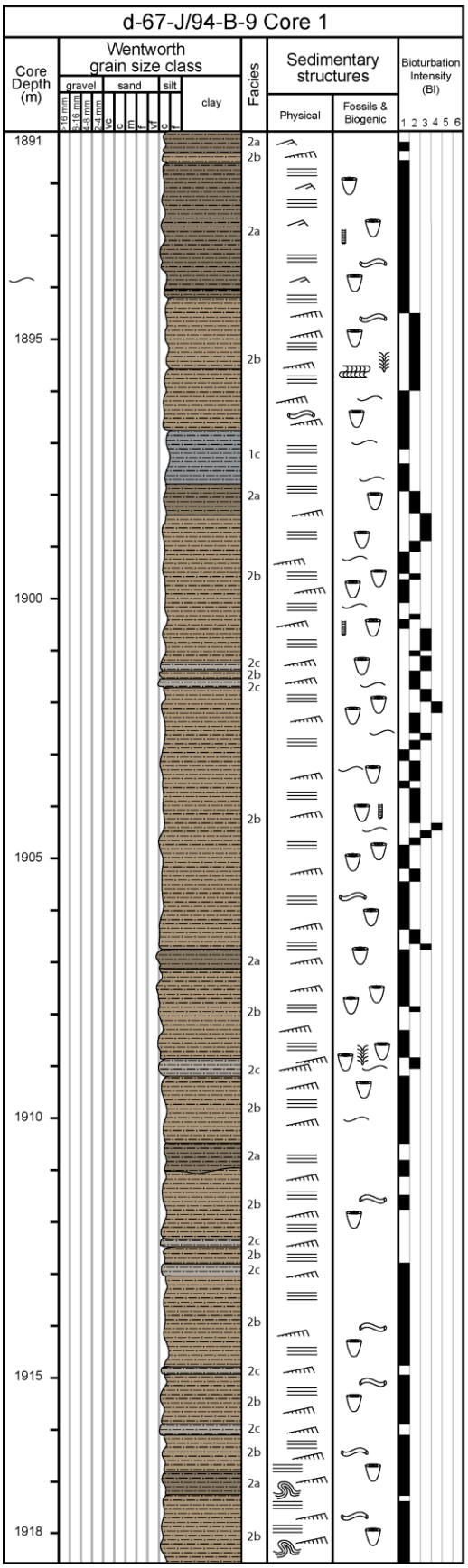
d-67-J/94-B-9 Core 1
Core Depth (m)
Wentworth grain size class
gravel
sand
silt
clay
>16 mm
2-16 mm
1-2 mm
vc
c
m
f
vf
c
f
Facies
Sedimentary structures
Physical
Fossils & Biogenic
Bioturbation Intensity (BI)
1 2 3 4 5 6
1891
1895
1900
1905
1910
1915
1918

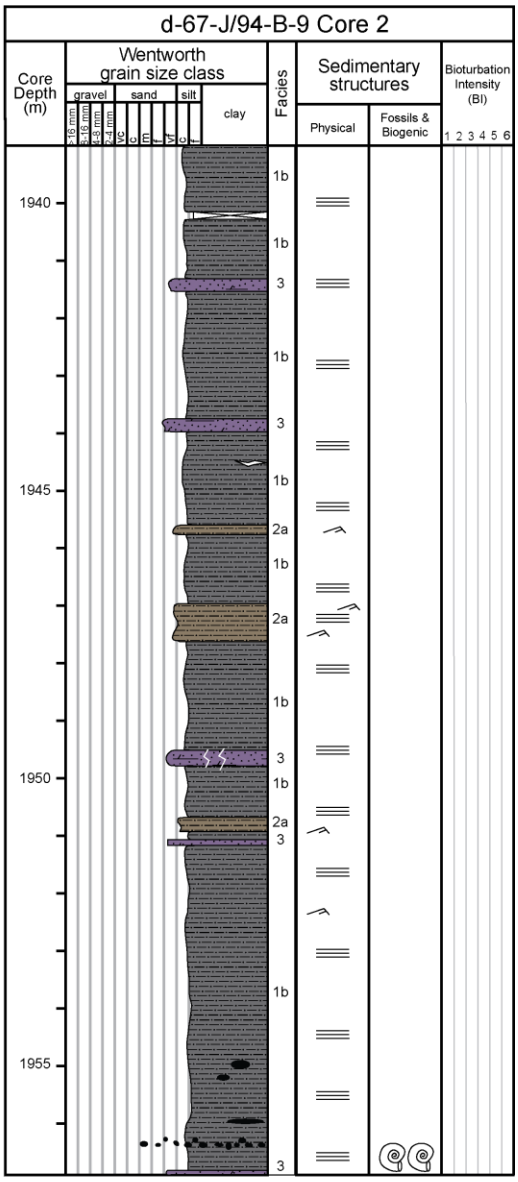
d-67-J/94-B-9 Core 2
Core Depth (m)
Wentworth grain size class
gravel
sand
silt
clay
Facies
Sedimentary structures
Physical
Fossils & Biogenic
Bioturbation Intensity (BI)
1940
1945
1950
1955